REPUBLIC OF TÜRKİYE

YILDIZ TECHNICAL UNIVERSITY

GRADUATE SCHOOL OF SCIENCE AND ENGINEERING

RADIATION SHIELDING PARAMETERS OF DY^{3+} DOPED CALCIUM ALUMINUM BARIUM SODIUM BORATE GLASS SYSTEM USED FOR RADIATION PROTECTION IN HOSPITALS

Ayşenur KÜTÜK

MASTER OF SCIENCE THESIS

Department of Biomedical Engineering

Program of Biomedical Engineering

Supervisor

Assoc. Prof. Osman GÜNAY

July, 2024

REPUBLIC OF TÜRKİYE

YILDIZ TECHNICAL UNIVERSITY

GRADUATE SCHOOL OF SCIENCE AND ENGINEERING

RADIATION SHIELDING PARAMETERS OF DY^{3+} DOPED CALCIUM ALUMINUM BARIUM SODIUM BORATE GLASS SYSTEM USED FOR RADIATION PROTECTION IN HOSPITALS

A thesis submitted by Ayşenur Kütük in partial fulfillment of the requirements for the degree of MASTER OF SCIENCE is approved by the committee on 29.07.2024 in Department of Biomedical Engineering, Program of Biomedical Engineering.

Assoc. Prof. Osman GÜNAY
Yıldız Technical University
Supervisor

Approved By the Examining Committee

Assoc. Prof. Osman GÜNAY, Supervisor
Yildiz Technical University
____

Assoc. Prof. İsmail CANTÜRK, Member
Yildiz Technical University
____

Prof. Dr. İskender AKKURT, Member
Suleyman Demirel University
____

I hereby declare that I have obtained the required legal permissions during data collection and exploitation procedures, that I have made the in-text citations and cited the references properly, that I haven't falsified and/or fabricated research data and results of the study and that I have abided by the principles of the scientific research and ethics during my Thesis Study under the title of "Radiation Shielding Parameters of Dy^{3+} Doped Calcium Aluminum Barium Sodium Borate Glass System Used for Radiation Protection in Hospitals" supervised by my supervisor, Assoc. Prof. Osman GÜNAY. In the case of a discovery of false statement, I am to acknowledge any legal consequence.

Ayşenur KÜTÜK

to my auspicious bird,

Hüma

ACKNOWLEDGEMENTS

Undoubtedly, certain individuals significantly enhance one's life, making it more manageable and enriching, and empowering one to undertake their endeavors with greater zeal, pursue their goals steadfastly, and find meaning in their efforts. I consider myself exceedingly fortunate to have been surrounded by such remarkable individuals throughout the process of writing my thesis.

First and foremost, I would like to express my deepest appreciation to Assoc. Prof. Osman GÜNAY, my thesis advisor, who has always encouraged me, believed in me from beginning to end, and was always there to share his expertise and enthusiasm, which kept me on track and happy.

I am indebted to my extended family, Rahime and Remzi KÜTÜK, who were the heroes of my dissertation process and provided me with a wealth of both physical and mental assistance.

Zeynep Nur KARAKUŞ, my dearest friend, was constantly available by phone, and for that, I am eternally grateful.

My siblings, Zeynep and Sadullah Yıldırım, Fatmanur and Halil İbrahim Çavuşoğlu, who anticipates my needs before I even recognize them, comprehends my emotions before I articulate them, and promptly comes to me, have my sincere gratitude.

Fatma and Eyüp Uğur Çavuşoğlu, I am immensely fortunate to have them as my parents. They continuously supported me every step of my life, sacrificed everything they could for our education, and dedicated their entire lives to their children.

Lastly, I want to express my profound admiration for my wonderful better half, Samet KÜTÜK, who believes in me more than I do, devotes his time and human-labor unconditionally, and endures me more than I can endure myself. To my little one, Hüma, whose existence brightens each and every day, I extend my heartfelt gratitude.

Ayşenur KÜTÜK

TABLE OF CONTENTS

LIST OF SYMBOLS

Al_2O_3	Aluminum Oxide
B_2O_3	Boron Trioxide
BaO	Barium Oxide
Bi_2O_3	Bismuth(III) Oxide
CaO	Calcium Oxide
CsI	Cesium Iodide
Dy	Dyprosioum
Dy_2O_3	Dysprosium(III) Oxide
Er_2O_3	Erbium(III) Oxide
Gd_2O_3	Gadolinium(III) Oxide
GdF_3	Gadolinium(III) Fluoride
GeO_2	Germanium Dioxide
Ho_2O_3	Holmium(III) Oxide
K_2O	Potassium Oxide
Li_2O	Lithium Oxide
MgO	Magnesium Oxide
MoO_3	Molybdenum Trioxide
Na_2O	Sodium Oxide
NaI	Sodium Iodide
Nd_2O_3	Neodymium(III) Oxide
P_2O_5	Phosphorus Pentoxide
Pr_6O_{11}	Praseodymium(III,IV) Oxide
SiO_2	Silicon Dioxide
SrO	Strontium Oxide
Tb_2O_3	Terbium(III) Oxide
ZnO	Zinc Oxide
ZrO	Zirconium Oxide
α	Alpha
β^-	Negatron Emission
β	Beta
β^+	Positron Emission
γ	Gamma

LIST OF ABBREVIATIONS

ACS	Atomic Cross Section
ALARA	As Low As Reasonably Achievable
C_{eff}	Effective Conductivity
CT	Computed Tomography
EABF	Energy Absorption Build-up Factor
EBF	Exposure Build-up Factor
ECS	Electronic Cross Section
E_{max}	Maximum Energy
HVL	Half-Value Layer
ICRP	International Commission on Radiological Protection
keV	Kiloelectron Volt
K_T	Total Energy
LAC	Linear Attenuation Coefficient
LOR	Line of Response
MAC	Mass Attenuation Coefficient
MeV	Megaelectron Volt
mfp	Mean Free Path
MSCT	Multislice Computed Tomography
mSv	Millisievert
N_{eff}	Effective Electron Densities
PET	Positron Emission Tomography
RE	Rare Element
SPECT	Single Photon Emission Computed Tomography
SSCT	Single-slice Computed Tomography
Sv	Sievert
TVL	Tenth-Value Layer
Z_{eff}	Effective Atomic Number
Z_{eq}	Equivalent Atomic Number

LIST OF FIGURES

LIST OF TABLES

ABSTRACT

Radiation Shielding Parameters of Dy^{3+} Doped Calcium Aluminum Barium Sodium Borate Glass System Used for Radiation Protection in Hospitals

Ayşenur KÜTÜK

Department of Biomedical Engineering
Master of Science Thesis

Supervisor: Assoc. Prof. Osman GÜNAY

Due to its harmful effects on human health, ionizing radiation and the investigation of the radiation protection capability of radiation-affected materials have become important for contemporary research. The damage caused to tissues by ionizing radiation varies, depending on the amount of radiation exposure and the radiosensitivity of the target. Radiation safety procedures (a.k.a. ALARA) include reducing the exposure time, increasing the distance between the radiation source and the target, and using radiation shielding materials. Lead and concrete, two extensively employed radiation shielding materials, have considerable disadvantages, including both being opaque, lead being toxic, and concrete breaking and losing its moisture. Glass, on the other hand, stands out as an alternative to lead and concrete with its transparency, high homogeneity, wide thickness range and relatively simple production. Glass modifiers can be added to the system to increase the absorption capacity of the glass and at the same time reduce the melting point and viscosity of the system without changing its chemical properties.

This thesis assesses the shielding properties of the $23CaO - 10Al_2O_3 - (50-x)B_2O_3 - 6BaO - 10Na_2O - xDy_2O_3$ (x=0.1, 0.3, 0.5, and 1.0% mol) glass system doped with the rare earth element Dysprosium(III) ion (Dy^{3+}) at various concentrations against ionizing radiation. To evaluate the system, linear attenuation coefficient (LAC), mass attenuation coefficient (MAC), half-value layer (HVL), tenth-value layer (TVL), mean free path (mfp), atomic cross section (ACS), electronic cross section (ECS), effective atomic number (Z_{eff}), effective electron densities (N_{eff}), effective conductivity (C_{eff}, equivalent atomic number (Z_{eq}), exposure build-up factor (EBF), and energy absorption build-up factor ($EABF$) radiation protection parameters are reviewed. All four glass samples were made using the standard melt-quenching technique. The glass samples were tested as a shielding material against ionizing radiation using Phy-X/PSD software. The findings in this study demonstrate that Dy^{3+} doped Calcium Aluminum Barium Sodium Borate glass system can be employed efficiently as a radiation shielding material since it has been proven to be a suitable, effective and good alternative.

Keywords: Calcium aluminum barium sodium borate glass system, Dy^{3+} ions, photon, radiation protection, ALARA, radiation shielding parameters, Phy-X/PSD.

ÖZET

Hastanelerde Radyasyon Koruması İçin Kullanılan Dy^{3+} Katkılı Kalsiyum Alüminyum Baryum Sodyum Borat Cam Sisteminin Radyasyon Zırhlama Parametreleri

Ayşenur KÜTÜK

Biyomedikal Mühendisliği Anabilim Dalı
Yüksek Lisans Tezi

Danışman: Doç. Dr. Osman GÜNAY

İnsan sağlığı üzerindeki zararlı etkileri nedeniyle, iyonize radyasyon ve radyasyondan etkilenen malzemelerin radyasyondan korunma kabiliyetinin araştırılması, çağdaş araştırmalar için önemli konular haline gelmiştir. İyonlaştırıcı radyasyonun dokulara verdiği hasar radyasyona maruz kalma miktarı ve hedefin radyosensitivitesine bağlı olarak değişir. Radyasyon güvenliği prosedürleri (aynı zamanda ALARA olarak da bilinir) arasında maruz kalma süresinin azaltılması, radyasyon kaynağı ile hedef arasındaki mesafenin artırılması ve radyasyon koruyucu malzemelerin kullanılması yer alır. Yaygın olarak kullanılan radyasyon koruyucu malzemelerden kurşun ve betonun faydalarının yanında opak olmaları, bu malzemelerden kurşunun zehirli olması ve betonun çatlayıp nem kaybetmesi gibi önemli dezavantajları vardır. Cam ise şeffaflığı, yüksek homojenliği, geniş kalınlık aralığı ve nispeten basit üretimi ile kurşun ve betona alternatif olarak öne çıkmaktadır. Camın emme kapasitesini artırmak ve aynı zamanda kimyasal özelliklerini değiştirmeden sistemin erime noktasını ve viskozitesini azaltmak için sisteme cam modifiye ediciler eklenebilmektedir.

Bu tezde, çeşitli konsantrasyonlarda nadir toprak elementi Disprosiyum (III) iyonu (Dy^{3+}) katkılı $23CaO - 10Al_2O_3 - (50 - x)B_2O_3 - 6BaO - 10Na_2O -$

xDy_2O_3 (x=0.1, 0.3, 0.5, and 1.0% mol) cam sisteminin iyonlaştırıcı radyasyona karşı zırhlama özellikleri incelenmektedir. Sistemi değerlendirmek için doğrusal zayıflama katsayısı (LAC), kütle zayıflama katsayısı (MAC), yarı değer katmanı (HVL), onda bir değer katmanı (TVL), ortalama serbest yol mfp, atomik tesir kesiti (ACS), elektronik tesir kesiti (ECS), etkin atom numarası (Z_{eff}), etkin elektron yoğunluğu (N_{eff}), etkin iletkenlik (C_{eff}), eşdeğer atom numarası (Z_{eq}), maruz kalma birikim faktörü (EBF) ve enerji soğurma birikim faktörü ($EABF$) radyasyondan korunma parametreleri incelenmiştir. Dört cam numunenin tamamı standart eriyik söndürme tekniği kullanılarak üretilmiştir. Cam numunelerin iyonlaştrıcı radyasyona karşı zırhlama kabiliyetleri Phy-X/PSD yazılımı aracılığıyla test edilmiştir. Bu çalışmadaki bulgular ile Dy^{3+} katkılı Kalsiyum Alüminyum Baryum Sodyum Borat cam sistemi uygun, etkili ve iyi bir alternatif olduğu kanıtlandığı için radyasyon koruyucu malzeme olarak verimli bir şekilde kullanılabileceğini göstermektedir.

Anahtar Kelimeler: Kalsiyum alüminyum baryum sodyum borat cam sistemi, Dy^{3+} iyonları, foton, radyasyondan korunma, ALARA, radyasyon zırhlama parametreleri, Phy-X/PSD.

1
INTRODUCTION

Since the discovery of the atom and nucleus model, the orientation towards studies in nuclear physics, which is one of the sub-units of physics, has increased, and the concepts of electron, neutron and proton have emerged. The discovery of alpha (α) and beta (β) particles by Ernest Rutherford following his studies on the nuclear model, Wilhelm C. Roentgen's finding of X-rays and Paul U. Villard's finding of gamma (γ) rays completed the discovery process, and the concept of radiation took its place in our lives. With the radioisotope studies of Becquerel and Curie, the concept of radioactivity, meaning that elements in an unstable state emit radiation rays around them in order to become stable, was found, and radiation sources were divided into two as natural and artificial. After Maxwell expressed the rays as electromagnetic waves, the electromagnetic spectrum was defined according to the wavelengths and frequencies of the rays with the discoveries made in this field and the classification of radiation was completed. There are two types of radiation: ionizing and non-ionizing. X and gamma rays are included in the ionized radiation type. The wavelength of X and gamma rays is electron-sized, which means that their wavelengths are even smaller than the size of atoms. As the wavelength decreases, the energy of the radiation beam increases, and in high energy regions, the photon can remove a part of the electron or nucleus from the orbit of the substance with which it interacts. This type of radiation is called ionizing radiation. Photons generally interact with matter in three different ways: photoelectric interaction, Compton interaction and pair formation. These types of interactions occur at low, medium and high energy levels depending on the energy of the incident photon. It is possible for ionizing radiation to change its structure when it interacts with matter and to have the ability to penetrate or to propagate in media such as gas, liquid and air. Therefore, ionizing radiation may have direct or indirect harmful effects on human health, the environment, and future generations. There are radiation protection principles (verification, optimization, and limitation) that are accepted and applied by the whole world in order to protect from these harmful effects or to minimize the damage. In addition, according to the ALARA (As Low

As Reasonably Achievable) principles published by ICRP for radiation workers and patient safety, there are three basic principles that should be considered to minimize the radiation dose exposure: minimizing the exposure time, increasing the distance between the radiation source and the target, and using radiation protective materials. Measures for time and distance restrictions are limited, but there is a wide range of measures that have been taken and can be taken for radiation protective materials. Shielding can be done with many materials such as protective goggles, gloves, walls, storage containers, and the materials that can be used in the production of these materials are also very diverse. The design and evaluation of the shielding material is carried out by studying the parameters based on the interaction of the photon with matter formulated by Beer-Lambert. Commonly used shielding materials are lead and concrete. These two materials, both of which have high density, have a high ability to attenuate incoming photon beams and greatly reduce their intensity. However, despite the advantage of being very high-quality shielding materials, they have significant disadvantages such as the toxicity of lead and its bulkiness due to its weight; the fact that the water in concrete evaporates and loses its moisture as the radiation exposure increases, thus losing its strength; and the opacity of both lead and concrete. For this reason, it has recently become necessary to search for alternatives that contain low lead and concrete ratios or that do not contain either of them at all or consist of other materials. Glass materials are a good alternative to lead and concrete due to their transparency, high homogeneity, large thickness cross-sections and simple production. At the same time, by including heavy metal components in the production stages of glass materials, their density can be changed, and their radiation attenuation capacity can be improved. This also allows the melting point and viscosity of the system to be reduced without any change in the chemical properties of the glass. In this sense, studies are being carried out on many different glass systems such as silica, bismuth, alumina silicate, barium, borate, phosphate, lithium, tellurite and germanate containing glasses with low or no lead and concrete content. The use of heavy metal oxide containing glasses as radiation shielding materials is becoming more and more widespread due to their stable chemical structure, corrosion resistance, mechanical properties, and outstanding optical properties.

This thesis work involves the doping of Calcium Aluminum Barium Sodium Borate ($23CaO - 10Al_2O_3 - (50 - x)B_2O_3 - 6BaO - 10Na_2O - xDy_2O_3$) glass system with different concentrations of Dy^{3+} rare earth element ions and the investigation of the system's ability to absorb photon energies and its transition properties, followed by the evaluation of its radiation shielding capabilities and its use as an alternative to lead-free glass systems. As an alternative to lead-free glass systems, Calcium Aluminum Barium Sodium Borate glass system draws attention as a glass system that is more chemically resistant with the calcium element in its content, more transparent with barium oxide, more strength and has high thermal stability thanks to aluminum, and soluble in rare earth element ions with borate.

2
OVERVIEW

2.1 History of Radiation

Radiation is a form of energy that can be spread from atoms in various ways and sent over a certain distance. This energy travels through space and can penetrate assorted materials. It can be found in many forms, including all electromagnetic waves which are radio waves, microwaves, infrared rays, visible light, ultraviolet light, X-rays, and gamma rays and also atom and subatomic particles which are alpha, beta, and neutron[1].

The discovery of X-rays by German physicist Wilhelm Roentgen in 1895 marked the beginning of knowledge regarding the existence of radiation. During his experiment on cathode-ray tubes, he saw sparkles around the plaque that close to the tube. After several following experiments, Rontgen observed green fluorescence light induced by activated tubes and the ray emitted from the tube easily able to pass through solid materials while but not for bone or metal. He named this ray as the "X" ray which he could not fully define[2]. Figure 1 shows his first experiment, the film of his wife's hand.

Figure 2.1 X-ray graph of Anna Bertha Ludwig's (Roentgen's wife) hand[3]

Radioactivity is the process of the spontaneous disintegration of atoms in which unstable atomic nuclei emit particles and energy in the form of electromagnetic radiation. The fission of the atomic nuclei causes radioactivity and the substance that emits radiation is called radioactive material[4]. Radioactivity and radioactive material experiments first began in 1896 with Henri Becquerel. He showed that uranium crystals spontaneously emit some rays by exposing potassium uranyl sulfate to sunlight. Madame Curie was the founder of the word radioactivity. After Becquerel, in 1898, Madame Curie and Pierre Curie discovered radioactive elements such as radium and polonium in their experiments with radioactive uranium ore. With these discoveries, radiation sources were divided into two types: natural and artificial. Natural radiation types are also divided into two groups. The first is cosmic radiation emitted from the sun, atmosphere and space; the other is the radiation emitted by unstable radioisotopes formed in the soil as a result of interactions over time to stabilize. Radiation emitted by destabilizing stable elements and isotopes by giving energy from outside in order to be used in the fields of medicine, security, nuclear power plants and communication is a source of artificial radiation[5].

The first studies on different types of radiation began with Herschel's discovery of infrared rays. Immediately after Ritter's discovery of ultraviolet rays, in 1867 James Clerk Maxwell defined rays as electromagnetic waves and suggested that there should be rays with longer wavelengths. Maxwell's propose was proven by Hertz's production of radio waves. Although X-rays were discovered much earlier, it was not until 1912 that it was discovered that X-rays were a form of light with short wavelengths. In 1914, gamma rays, which have even shorter wavelengths than X-rays, were included in this classification and the electromagnetic spectrum (Figure 2.2) was completed[6]. Meanwhile, Ernest Rutherford discovered that the rays emitted from radioactive elements are different from electromagnetic radiation he made the characterization of the radioactive particles as alpha, beta and gamma particles based on their ability to penetrate matter[7].

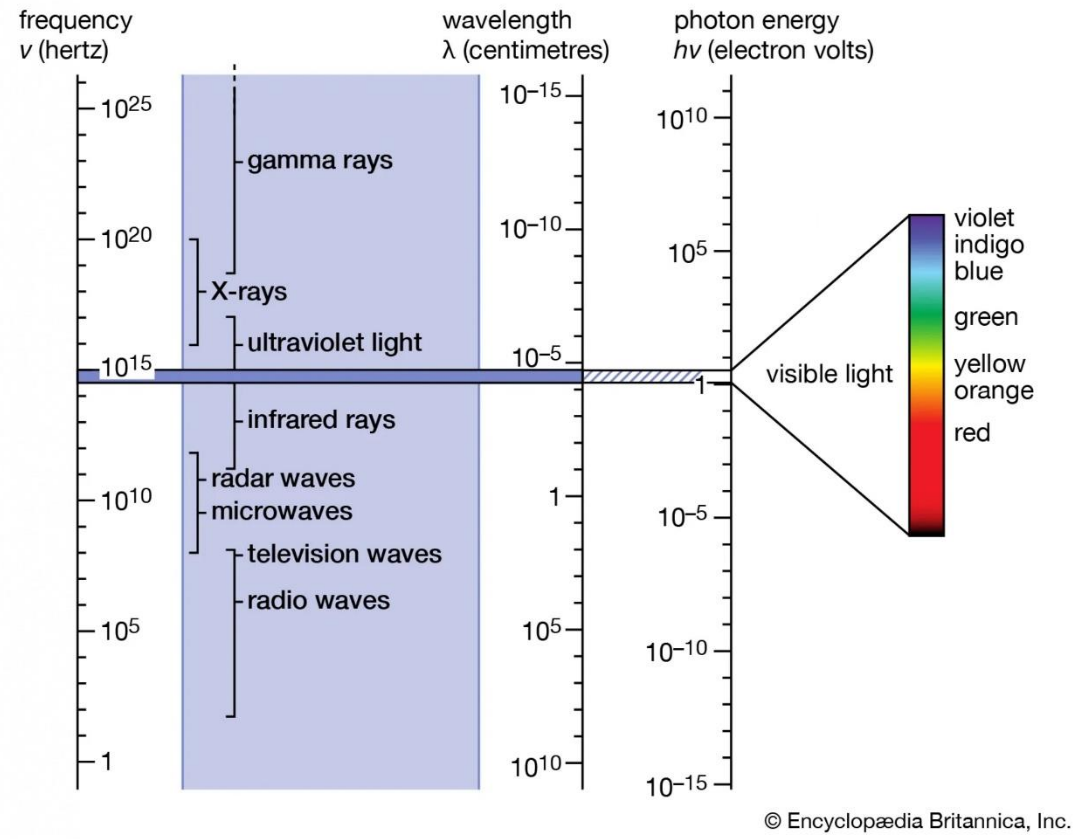

Figure 2.2 Electromagnetic spectrum[8]

Radiation is a powerful tool for both the diagnosis and treatment of a wide range of medical conditions, from cancer to cardiovascular diseases. It is used in radiology field to produce images of the body with X-ray devices, computed tomography (CT), fluoroscopy and scopy devices. Also, it is used in the field of nuclear medicine to destroy cancer cells with artificial radioactive substances and to give targeted radiation treatments to tumors with gamma cameras, positron emission tomography (PET) and single photon emission computed tomography (SPECT) devices[9].

2.2 Types of Radiation

Radiation is the emission of energy through matter as electromagnetic waves or particles. Electromagnetic radiation includes all waves in the electromagnetic spectrum: radio waves, microwaves, infrared rays, visible light, ultraviolet light, X-rays and gamma rays. Particle-type radiation includes all subatomic particles: alpha (α) particles, beta (β) particles and neutrons (Figure 2.3).

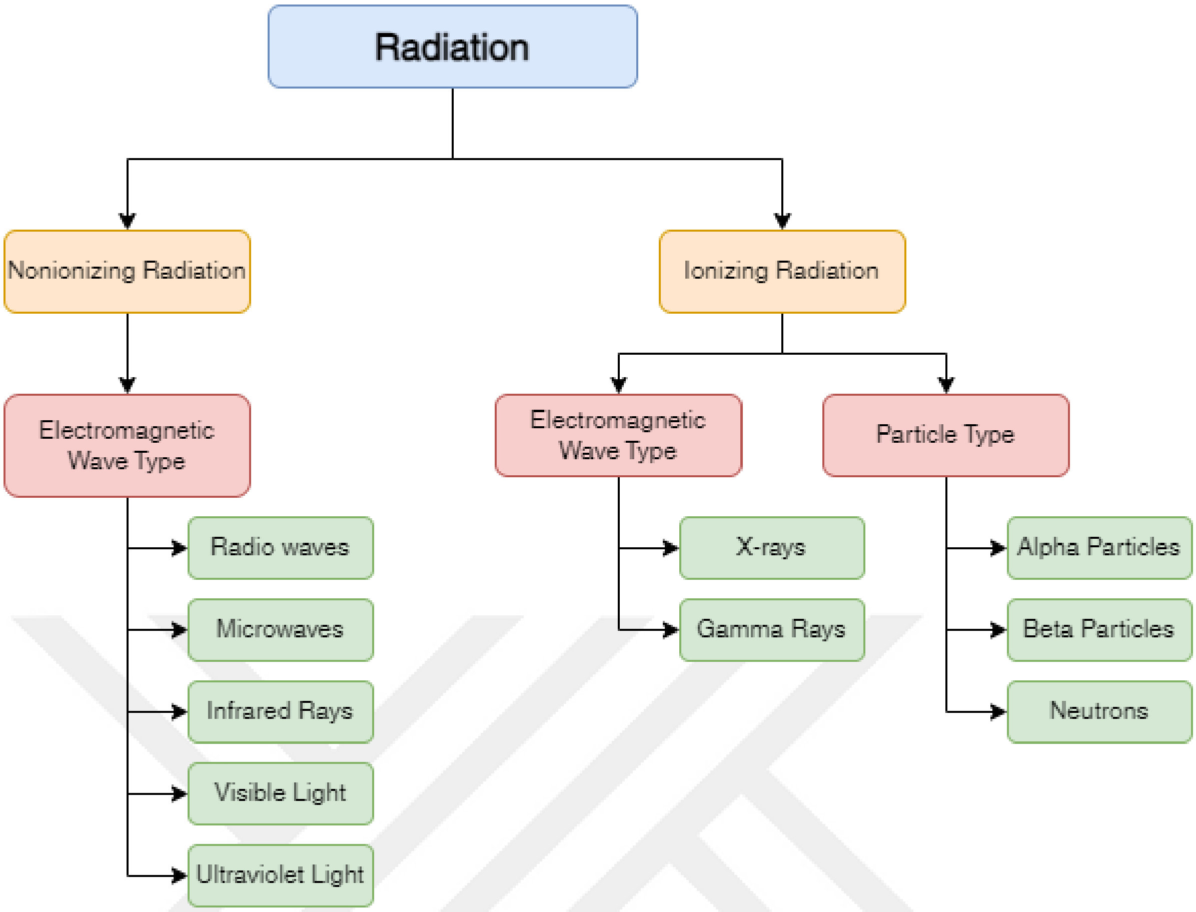

Figure 2.3 Types of radiation[10]

When a photon interacts with matter, it can extract electrons from the orbit or nucleons from the nucleus of the atom it interacts with. This feature of radiation called ionization is related to the frequency and therefore the energy of the incident photon (Figure 2.4). As the frequency of the photon increases, its energy also increases. The interaction and bond breaking force of the photon with matter increases with increasing energy. In the electromagnetic spectrum, the energy regions with ionizing power include the X-ray and gamma-ray regions. The remaining radiation types are not capable of ionizing because they do not have sufficient energy. At the same time, the fact that the wavelengths in the X-ray and gamma-ray regions are very short (about the size of an electron[5]) increases the ionizing ability of these regions.

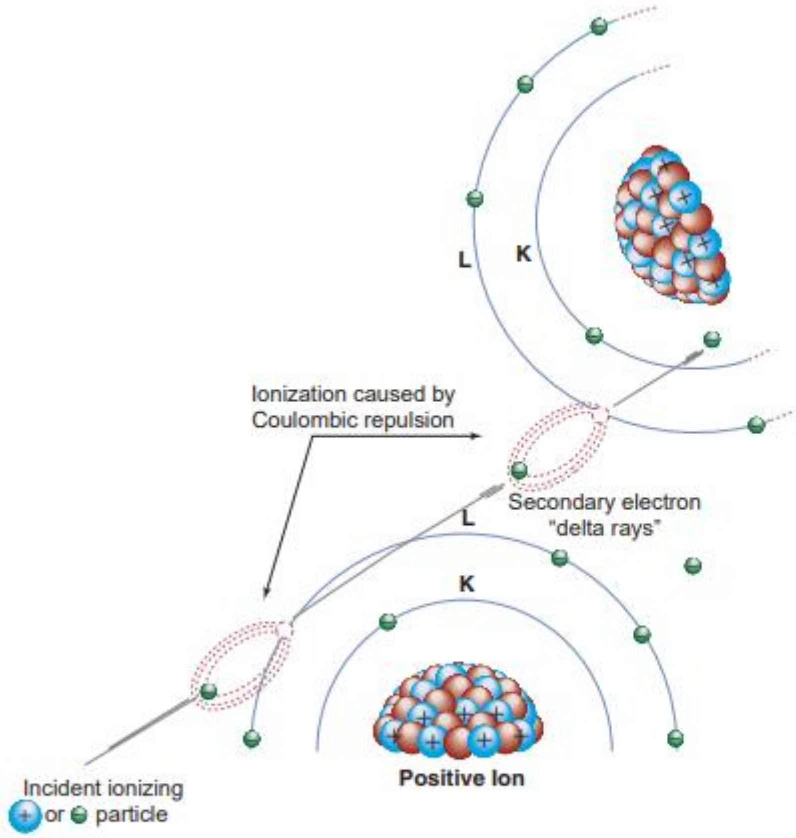

Figure 2.4 Ionization and the production of secondary electrons[11]

Ionizing radiation is also divided into charged and uncharged radiation. Charged radiation types are alpha and beta radiations, which are charged particles, while uncharged radiation types are X-rays, gamma rays and neutrons. Alpha and beta radiations can change the structure of the atom it interacts with. Uncharged ionizing radiation is divided into uncharged electromagnetic radiation (X-rays and gamma rays) and uncharged particle radiation (neutron) depending on the type of radiation[12].

2.2.1 Alpha Decay

The alpha particle is structurally equivalent to a helium nucleus, i.e. it consists of two protons and two neutrons, stripped of their electrons. It is denoted by the Greek letter α. It is very stable with its high proton/neutron ratio. Alpha decay occurs when the number of protons in the nucleus exceeds the number of neutrons. Radionuclides with energies ranging from 4 MeV-10MeV emit an alpha particle and product nuclides are formed[13]. Due to the loss of two protons and two neutrons from the parent nucleus, the atomic number of the product nucleus decreases by 2 and the mass number decreases by 4. Equation 2.1[14] gives the general equation for a nucleus undergoing alpha decay. According to the Geigere-Nuttall law, the range of motion and energy of the alpha particle are related to each other. Radionuclides emitting low-energy alpha particles have long half-lives, whereas high-energy ones have short half-lives.

$$ {}^{A}_{Z}X \rightarrow {}^{A-4}_{Z-2}Y + {}^{4}_{2}\alpha \qquad (2.1) $$

Here,

X, main (parent) core

A, mass number (number of protons + number of neutrons)

Z, atomic number (number of protons)

Y, product (daughter) core

He, the emitted alpha particles

Alpha particles have a positive electric charge due to its two protons. This causes a Coulomb interaction with the atomic electrons of the substance through which it passes and thus ionization occurs. Since the mass of the alpha particle is much larger than the electron, the atomic electrons are rapidly ejected by collision. Alpha particles, which lose their kinetic energy rapidly in this way, have very short effective distances. For the same reason, it is the easiest type of radiation to stop, even with a piece of paper of suitable thickness[5][15]. Figure 2.5 shows the illustration of the alpha decay.

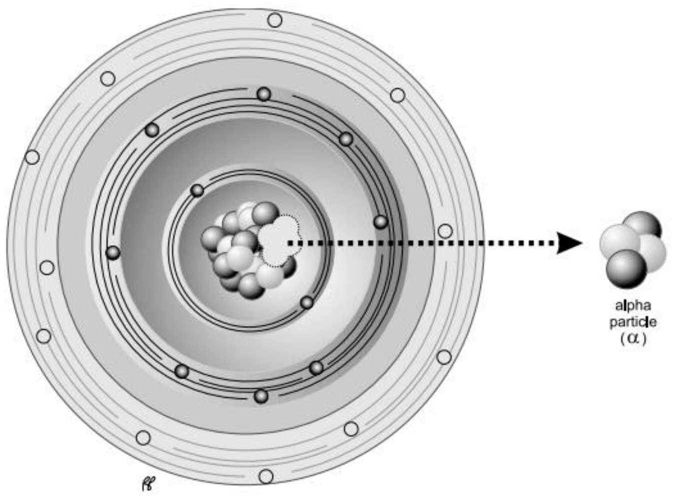

Figure 2.5 Alpha decay[16]

2.2.2 Beta Decay

Beta decay is the release of negatively charged electrons or positively charged electrons (positrons) from atomic nuclei with a high number of protons. During the decay, protons in the nucleus turn into neutrons or neutrons into protons. Therefore, while the mass number of the nucleus remains constant, the atomic number changes. It has 3 types: β^- (negatron) emission, β^+ (positron) emission and electron capture. Unlike alpha particles, they emit in a wide spectrum. Depending on the radionuclide emitting beta, the maximum energy (E_{max}) they can have varied, but in general they emit between 0 and E_{max}[17]. Since beta particles are lighter than alpha particles, they are less ionizing. For this reason, their travelling distances are longer than alpha particles. According to their energy levels, they can move centimeters in the air, while they can only move a few millimeters in the material. Therefore, while they cannot be stopped by a piece of paper like alpha particles, they can be stopped by aluminum and plastic plates[5][18]. Beta particles are used in the field of medical imaging with positron emission tomography (PET) to visualize cancerous cells by injecting a β^+ (positron) emitting substance into the patient before the imaging procedure.

β^- emission is the release of a negatively charged electron from the nucleus. The neutron in the nucleus is converted into a proton and the neutron/proton ratio in the nucleus decreases. The general expression of β^- emission is given in Equation 2.2[14].

$$ {}_{Z}^{A}X \rightarrow {}_{Z+1}^{A}Y + \beta^- + \bar{\nu} \tag{2.2}$$

Here, X is the beta radiating nucleus. Y is the daughter nucleus and there is no change in the mass number (A) of Y, since the decrease of the negative charge in the nucleus occurs by neutron-proton conversion. Z is the atomic number, an increase in the number of protons makes Y a different nucleus. β^- stands for the electron released from the nucleus, the beta particle and $\bar{\nu}$ is antineutrino. Due to the mass of the released electron and the high energy emission of the negatively charged electron, there is a slight decrease in the mass of the nucleus. The energy obtained due to this change in the radioactive nuclide is the maximum energy that the beta particle can have (E_{max}) and they are emitted in a wide energy spectrum from 0 to E_{max}[15][17][18]. Figure 2.6 shows the illustration of the β^- decay[16].

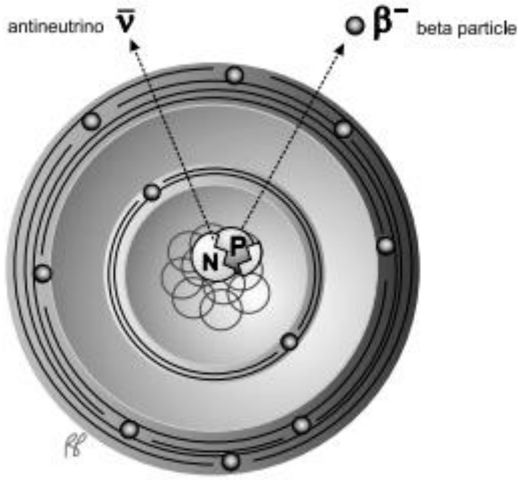

Figure 2.6 β$^-$ decay[16]

β$^+$ emission is the release of a positively charged electron from the nucleus. These nuclei are unstable due to their high number of protons. The proton cannot provide the necessary mass for both the neutron and the electron to be emitted. Therefore, in β$^+$ emission, a complete change in the nucleus occurs when the proton and neutron in the nucleus rearrange their bonding to obtain a neutron and release a positively charged electron. The neutron/proton ratio in the nucleus increases. The general expression for β$^+$ emission is given in Equation 2.3[14][15].

$$ {}^{A}_{Z}X \rightarrow {}^{A}_{Z-1}Y + \beta^{+} + \bar{\nu} \qquad (2.3) $$

Here X is the beta radiating nucleus. Y is the daughter nucleus and there is no change in the mass number (A) of Y, since the decrease of the positive charge in the nucleus occurs by neutron-proton conversion. Z is the atomic number, a decrease in the number of protons makes Y a different nucleus. β$^+$ stands for the electron emitted from the nucleus, the beta particle and $\bar{\nu}$ is antineutrino. For β$^+$ emission to occur, the radioactive nucleus X must be two electron masses heavier than the daughter nucleus Y. In other words, decay can only take place when the energy required to produce two electron masses is above 1.02 MeV. The beta particle is emitted in a broad energy spectrum from 0 to E_{max}[18][19]. Figure 2.7 shows the illustration of the β$^+$ decay.

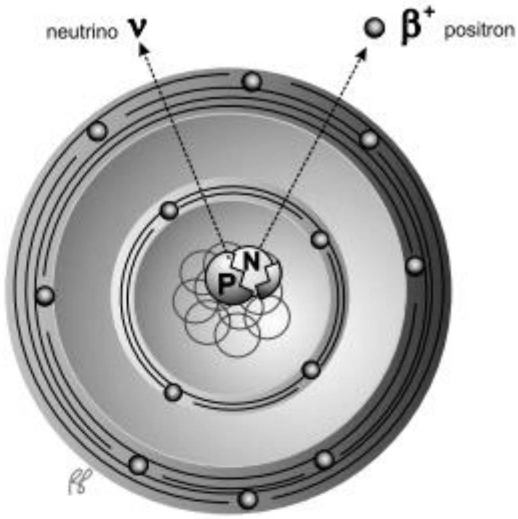

Figure 2.7 β^+ decay[16]

2.2.3 Electron Capture

Electron capture is the capture of electrons from the orbital shells of nuclei with excess protons to reduce the number of protons. In fact, there is no beta particle emission, but since it is an electron process and the proton/neutron ratio changes without changing the mass number, it is included among the beta emission types. Capture occurs when the energy required for β^+ emission is not available. Nuclei with insufficient mass can approach the unstable nucleus by the wave motion of the orbital electrons and capture electrons from the shell[16][18]. The general expression for the electron capture process is given in Equation 2.4[18].

$$ {}^{A}_{Z}X + e \rightarrow {}^{A}_{Z-1}Y + \nu + K_T \tag{2.4}$$

Here, X is the parent nucleus and Y is the daughter nucleus. e is the electron captured from the orbit and the captured electron causes the number of protons in the nucleus to decrease. As a result of the transformation, the mass number (A) does not change, the number of protons (Z) decreases by 1 and the number of neutrons increases by 1. ν is the neutrino and K_T is the total energy released. The K-shell electrons, the shell closest to the nucleus, contain 90 per cent of the electron capture electrons, while only 1 per cent are M-shell electrons. During electron capture, the vacancy of the captured electron is immediately filled with electrons from the outer shells, resulting in the production of X-rays characteristic of the daughter radionuclide. The produced X-rays and their associated Auger electrons are the only way in which electron capture transformations produce energy emission[15][17]19]. Figure 2.8 shows the illustration of the electron capture process.

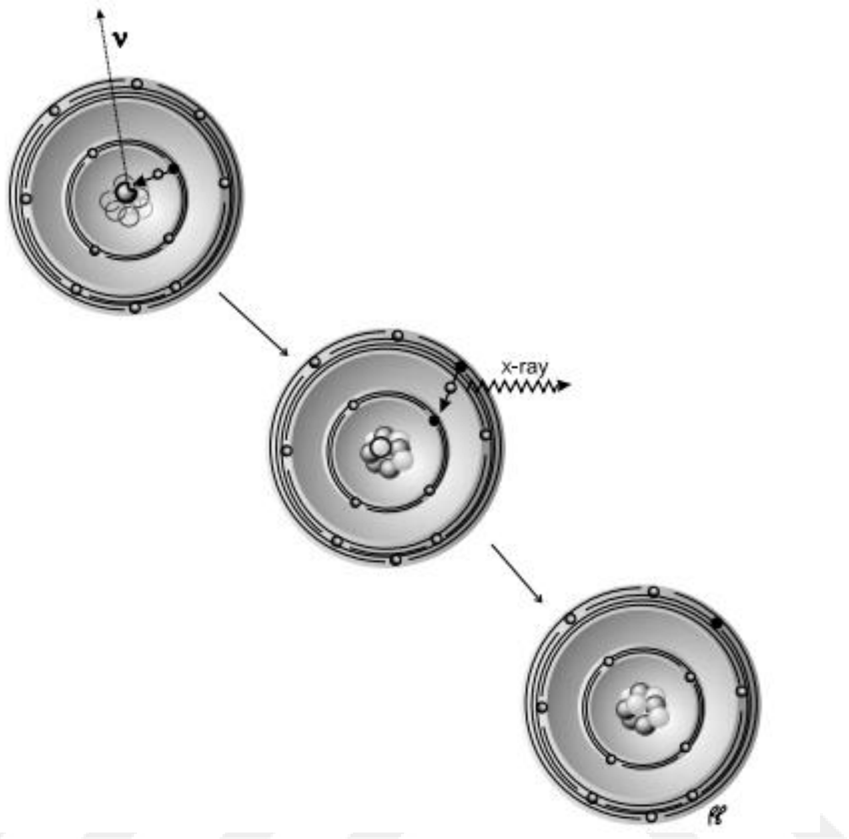

Figure 2.8 Electron capture[16]

2.2.4 Gamma Decay

Unstable atomic nuclei that undergo radionuclide decay sometimes do not fully release their energy and their protons and neutrons remain excited. In this case, the protons and neutrons in the nucleus reorganize themselves and emit high-energy electromagnetic waves to their surroundings and descend to lower energy states. These electromagnetic waves are called gamma rays. The nuclide in the unstable state is called a nuclear isomer and the transition from a high-energy state to a low-energy state is called an isomeric transition. Gamma rays are emitted at different energies since the energy transition states for neutrons and protons in the excited nucleus are discrete. The difference between the energy states of the nuclear isomers gives the gamma-ray energy. The general expression of the gamma ray is given in Equation 2.5[18].

$$ {}^{A}_{Z}X^{*} \rightarrow {}^{A}_{Z}X + \gamma \tag{2.5}$$

Here, X* is the excited nucleus, X is the stable nucleus and γ is the emitted gamma ray. Since the isomeric transition is the release of excess energy from the nucleus, the number of protons and neutrons in the stable nucleus and therefore the atomic number of the nucleus do not change. In other words, the product nucleus is characteristic of the parent nucleus, the atom remains the same atom. Gamma emission can only occur after alpha and beta decays have taken place. They have an ionizing effect like alpha and beta particles, but they have a low penetrating ability, whereas they have a high penetrating ability. Since it can pass through living tissue, it is used in medical imaging. Its travelling distance is very long, it spreads along a straight line in space. It can be blocked by high density materials such as lead, steel and concrete sheets[5][17][19]. Figure 2.9 shows the illustration of the gamma decay.

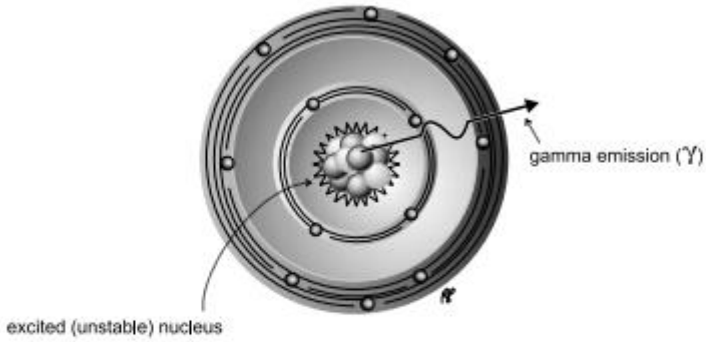

Figure 2.9 Gamma decay[16]

2.3 Radiation-Matter Interactions

Radiation is used in many fields such as medicine, industry, agriculture, and animal husbandry. In order to use radiation, it must first be detected. Detection of radiation is possible by interacting with matter. All types of radiation can interact with the atoms of the substance through which it passes. The result of the interaction with the detector is converted into an electrical signal and recorded. Radiation-matter interaction mechanisms vary depending on the type of particle, the energy it has, the number of protons and the density of the substance it interacts with. The distance travelled by charged and uncharged particles in matter, the path they follow, and their interaction mechanisms are different. Radiation-matter interaction mechanisms are evaluated under three different headings:

- Interaction of charged particles with matter
- Photon matter interactions
- Neutron matter interactions[20]

2.3.1 Interaction of Charged Particles with Matter

As charged particles (i.e. α particles, β particles, protons, heavy nuclei) pass through matter, they lose energy by interacting with the absorbing atoms. This interaction occurs with the shell electrons of atoms or rarely with the nucleus. As a result of the interaction, the charged particle with excitation transfers all or some of its kinetic energy to the shell electrons and causes these electrons to rise to higher energy shells. The interactions of charged particles with matter are categorized into two different categories: heavily charged particles with heavier mass, such as α-particles and heavy nuclei, and lightly charged particles such as electrons. Because the charges of the particles and the distance they travel in matter due to their charges and their scattering patterns are related[15].

2.3.1.1 Interaction of heavy charged particles with matter

Due to their mass, heavily charged particles lose a small amount of their kinetic energy when they interact with matter. The interaction is caused by the Coulomb force between the negative charges of the electrons in the medium and their positive charges. If the energy of the incoming substance is greater than the energy of the absorbing atom, it ionizes the electrons of the absorbing atom and transfers the excess energy. Energy loss occurs rapidly. Most of this energy loss occurs close to the stopping moment and more ionization occurs at the stopping moment due to their low energy. Since the energy loss in a single interaction is low, they produce many ion pairs until they lose all their energy. The path they take is short and in the form of a linear line travelling from the starting point. The shortness of this distance they take until they stop, which is called range, causes the formation of a large number of ion pairs due to the collisions occurring in a small area. The range quantity is also used for the characterization of charged particles. Charged particles also interact with matter by electron excitation and elastic scattering from the nucleus. Electron excitation is the phenomenon in which the incoming atom, when it does not have enough energy for ionization, is excited by the absorption of a part of its energy by the absorbing material and goes to a higher energy level, where it emits a photon and returns to the lower level. In the mechanism of elastic scattering from the nucleus, due to the effect of the Coulomb forces, the massive nucleus causes the heavily charged particles to change direction without causing any change in the atom[14][21].

2.3.1.2 Interaction of Light Charged Particles with Matter

Due to their weight, light charged particles are faster than heavily charged particles of the same weight and follow a highly dispersed path as they pass through matter. High-speed particles lose energy due to the Coulomb force when they approach the nucleus when interacting with matter. This energy appears as a continuous X-ray spectrum called bremsstrahlung radiation, which means braking in German. This radiation, which is produced by the acceleration of the electron, causes the particles to deviate from their path due to the coulomb force in the nucleus (Figure 2.10). The total distance travelled by the particle until it loses all its energy is longer than the actual range. This is called range dispersion. In the meantime, the particles follow a zigzag path, colliding with the orbital electrons in the neighborhood and thus losing their energy. Figure 2.11 shows the illustration of the path of light and heavy charged particles in matter. Bremsstrahlung radiation production increases as the energy of the particle and the atomic number of the absorbing atom increase. Therefore, bremsstrahlung production must be considered for heavy metals such as lead. For example, in the field of radiation protection, plastic containers should be preferred over lead as protective material for storage containers[14][21][22].

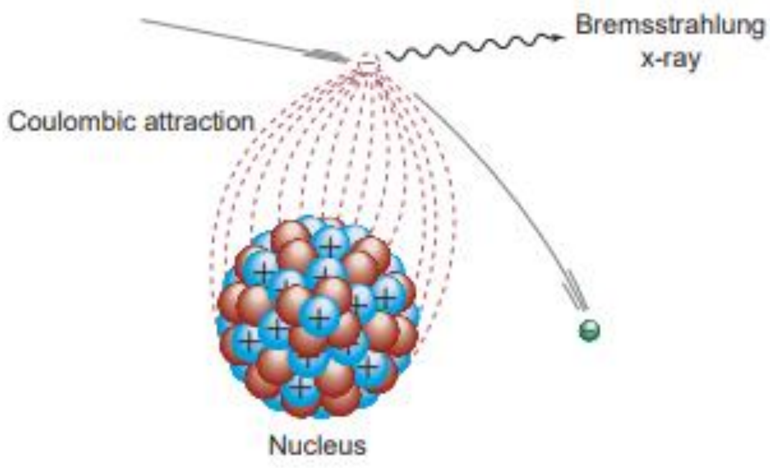

Figure 2.10 Bremsstrahlung radiation[11]

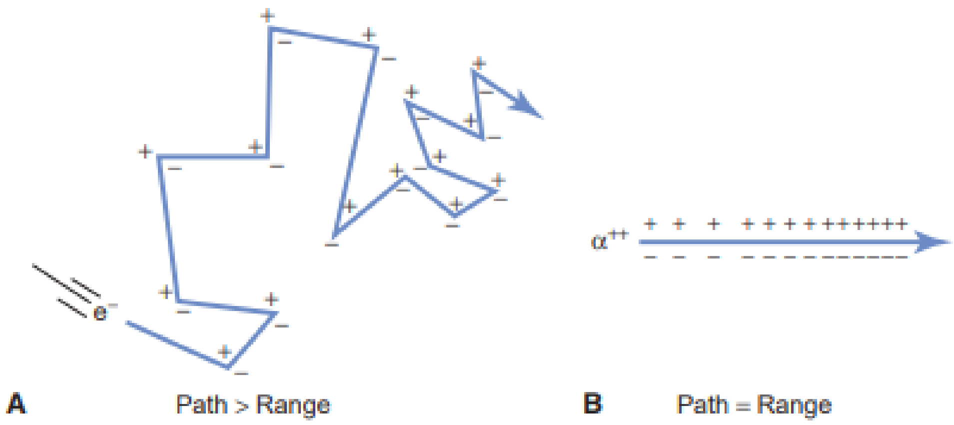

Figure 2.11 A. Light charged particles path in matter. B. Heavy charged particles path in matter[11]

2.3.2 Photon-Matter Interactions

Photons have no mass and electrical charge. Since they are uncharged, they are not subject to Coulomb force. In their interaction with matter, they can consume their energy by transferring it to the electrons in the matter and can be completely absorbed or they can store energy in the medium. They can also penetrate directly into the cross-section of matter. They do not have a specific range like charged particles. They can scatter over very long distances, deviate greatly from the initial direction or disappear completely. Types of photon-matter interactions are:

- Photoelectric phenomena
- Compton scattering
- Pair formation
- Rayleigh scattering
- Photodisintegration[14][15][22]

2.3.2.1 Photoelectric Phenomena

In the photoelectric phenomena, the photon transfers all its kinetic energy to one of the orbital electrons of the absorbing atom during its interaction with the matter and is lost. The energized electron (photoelectron) jumps out of its orbit and interacts with the surrounding atoms. The photoelectron rapidly loses its energy by ionization and moves to a distance not far from its initial position (Figure 2.12). The photoelectric effect, which occurs at low energies (<0.5 MeV), is inversely proportional to the energy of the incident photon and directly proportional to the atomic number of the absorbing atom. Since the photoelectric effect occurs with electrons tightly bound to the orbit, it occurs mostly with K-shell electrons. The vacancy of the electron leaving the K-shell is filled by the electron from the L-shell, and the vacancy of the electron leaving the L-shell is filled by the electron from the M-shell. These transitions often lead to characteristic X-ray emission[15][19][20][23][24].

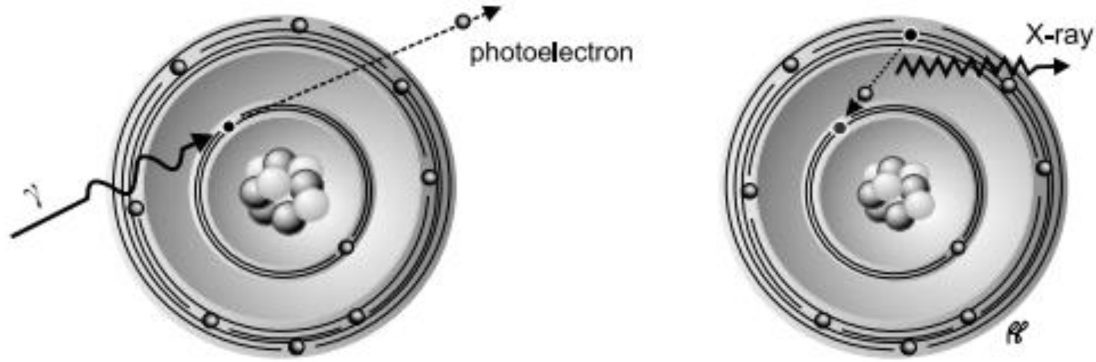

Figure 2.12 Photoelectric phenomena[16]

2.3.2.2 Compton Scattering

Compton scattering is a collision in which during the interaction of a photon with matter only a fraction of its energy is transferred to an electron with much lower energy and a new photon is produced with the reduced energy. As a result of the collision, the electron is ejected from the orbit and the scattered photon travels in a different direction from the original photon (Figure 2.13). For medium energy photons (0.5-1.0 MeV) both energy and momentum are conserved because of the Compton interaction, which is important. The higher the energy of the incident photon, the greater the scattering angle. For photons above a certain energy level, Compton scattering can turn into a secondary radiation source. This causes unwanted distortions in the image and excessive radiation exposure. Therefore, attention should be paid to Compton calculations in radiation applications[15][18][23][25].

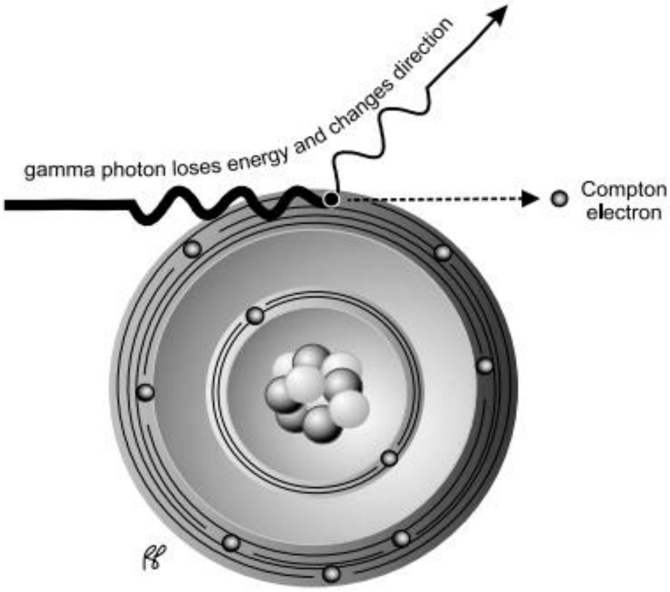

Figure 2.13 Compton scattering[16]

2.3.2.3 Pair Formation

When a photon of high energy (>1.022 MeV) enters the electromagnetic field around an absorbing atomic nucleus, it converts its energy into two particles, one positively charged (positron) and one negatively charged (electron). These two oppositely charged particles are called positron-electron pairs. Since the masses of the positron and electron are equal, they share the kinetic energy of the photon equally (0.511 MeV). The positrons in the medium then dissipate their kinetic energy by ionization. Nearly losing all of their energy, they interact with the surrounding free electron and disappear by producing two annihilation photons of 0.511 MeV each in opposite directions called the annihilation event (Figure 2.14)[15][16][18][23].

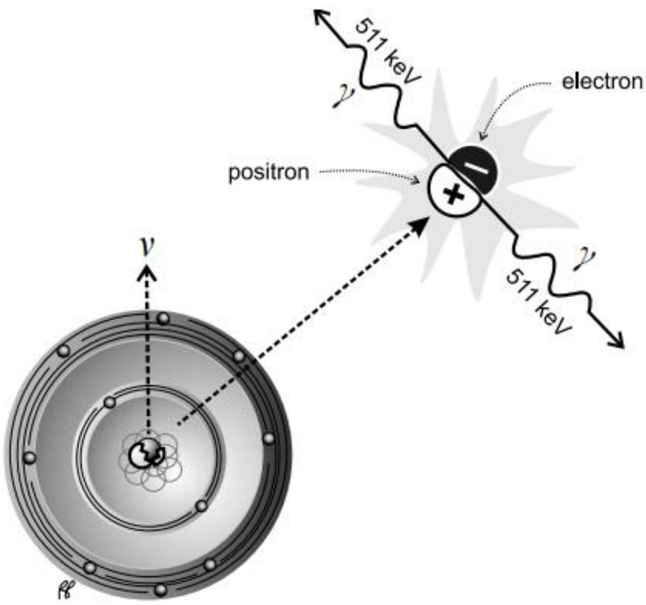

Figure 2.14 Annihilation event[16]

2.3.2.4 Rayleigh Scattering

Gamma rays do not interact with the orbital electrons of the atom through which they pass, but directly with the atom itself, and an energy is emitted in the same phase, but in a different direction (Figure 2.15). There is no energy transfer because of the interaction, only the direction of the atom has changed. In addition, since the probability of occurrence is low, it can be ignored in radiation procedures[11][15].

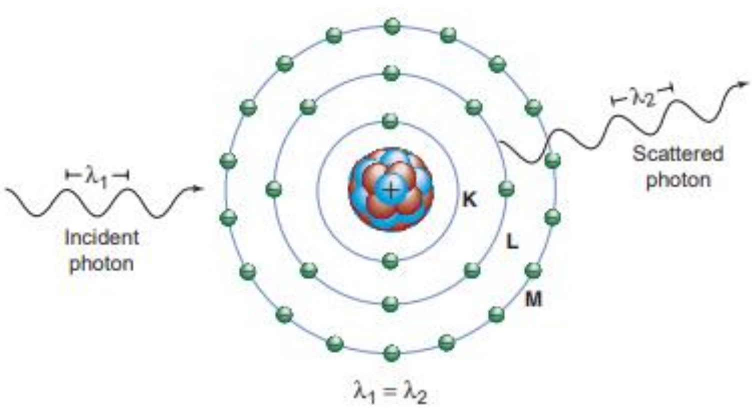

Figure 2.15 Rayleigh scattering[11]

2.3.2.5 Photodisintegration

Photodisintegration is a photon-matter interaction in which a photon with an energy greater than 10 MeV interacts with the nucleus of the absorbing atom, transferring enough energy to the nucleus to emit nucleons. It rarely occurs. For photon energies higher than 20 MeV the results are significant and important to consider in the design of radiation shielding materials[15][18].

2.3.3 Neutron-Matter Interactions

Since neutrons are uncharged particles, they are not subject to the Coulomb force as in photon interactions. They interact with nuclear reactions when the absorber is very close to the nucleus of the atom. They are very unlikely to interact with orbital electrons. Therefore, when neutron-matter interactions are evaluated, their interactions with the nucleus of the absorbing atom are considered. These interactions can take three different forms. These are elastic scattering, inelastic scattering and neutron capture. Elastic scattering is a collision in which the neutron hits the atomic nucleus and deviates in a different direction from its starting point after releasing some of its energy. As a result, the total kinetic energy of the colliding particles is conserved. Inelastic scattering is a type of collision in which a high-energy neutron leaves the atomic nucleus excited. The atom is then stabilized by decay. In neutron capture, the nucleus of the absorbing atom captures the neutron at a certain distance and an excited nuclide is formed. Depending on the magnitude of the energy, the excited nuclide radiates and radioactive nuclide is formed[16][21][22][25].

2.4 Medical Imaging Devices Using Radiation

2.4.1 Computerized Tomography

In the mechanism of the computerized tomography (CT) device, the X-ray tube and the detector located opposite to it are connected to the gantry, which rotates 360° around the patient continuously at a certain speed. The X-rays absorbed from the patient are detected and converted into a computerized image. Image acquisition with CT scanning takes place in 3 basic stages. In the first stage, X-rays generated by the X-ray tube are sent to the patient. X-rays, which are absorbed at different rates from different tissues, are detected by the detectors opposite to them and data are collected as electrical signals. In the second stage, these electrical signals are amplified in the computer system and the image is reconstructed. In the third and final stage, the image of the patient is generated by image processing (Figure 2.16). With the 360° rotation of the gantry, the image of the tissue is obtained from every angle. The resulting image is in slices. 2 and 3 dimensional images can be obtained with CT scanning[26][27].

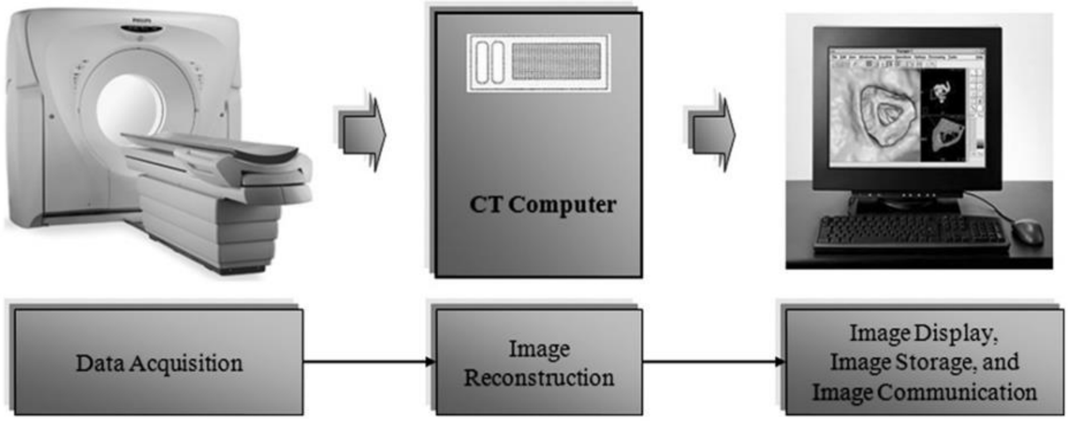

Figure 2.16 The three basic stages in the production of a CT image[26]

Until the CT device used today, the design and mechanism of CT devices have been continuously improved until the deficiencies of the previous one are eliminated. CT devices, which have undergone a series of developments such as improving image quality, reducing acquisition times and minimizing artefacts, have been grouped under 7 different generations until today[28].

The first generation CT was designed in 1979 by Dr. Godfrey Hounsfield called EMI, which was designed only for head scanning. It was designed using an X-ray tube and a single detector positioned opposite each other. The X-ray tube and detector rotate along a straight line called the pencil beam. The X-ray passes over the patient and the detector follows on the opposite side. When the scan on the pencil beam is complete, the X-ray tube and detector are rotated slightly for another section and the same process is repeated along a 180°arc (Figure 2.17). The processing time is quite long[27][29].

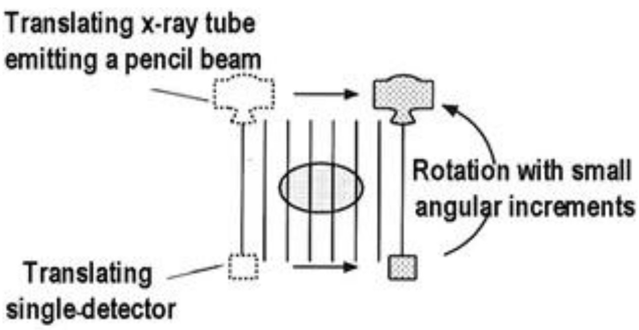

Figure 2.17 First generation CT scan design[30]

The second generation CT design includes an X-ray tube and detector as in the first generation design. The number of detectors is increased to 30 in the second-generation CT device and the X-ray tube is in the form of a fan-shaped beam. Scanning is done by moving the X-ray tube and detectors in a linear line. When the scanning along the line is completed, the X-ray tube and detectors are rotated by 10° and the same process is repeated along a 180°arc (Figure 2.18). The processing time is shorter than that of the first-generation device[27][28][29].

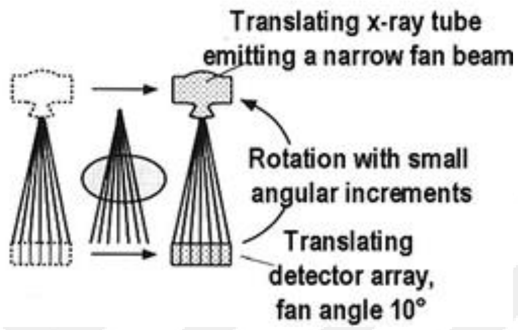

Figure 2.18 Second generation CT scan design[30]

Unlike the first and second generation, the third generation CT design scans the patient at a 360° angle. The X-ray tube is arranged in a fan shape and opposite the tube are many detectors (200 pcs to 900 pcs). The X-ray tube and detectors rotate together in an arc around the patient (Figure 2.19). The 360° detector array ensures a constant distance from the patient to the detector, which significantly improves the image quality compared to the first and second generation. Scan time is reduced to a maximum of 2 seconds[27][29][30].

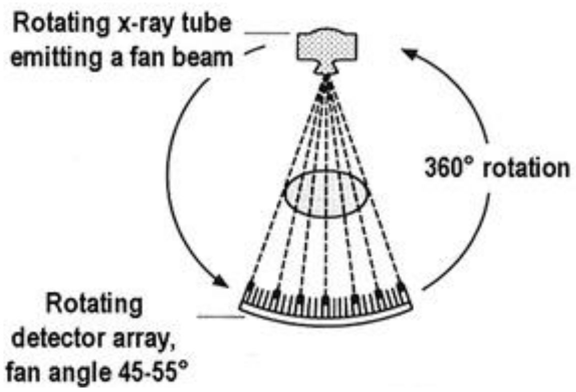

Figure 2.19 Third generation CT scan design[30]

The fourth-generation CT design differs from the first three in that it incorporates a fixed detector design. The detector ring consisting of approximately 5000 detectors surrounds the gantry gap where the patient is placed and is in a fixed position. The X-ray tube rotates through the detector ring at a 360° angle and an image of the patient is formed (Figure 2.20). Since the distance between the X-ray tube and the patient is narrower, it contains a higher level of radiation[27][28][30].

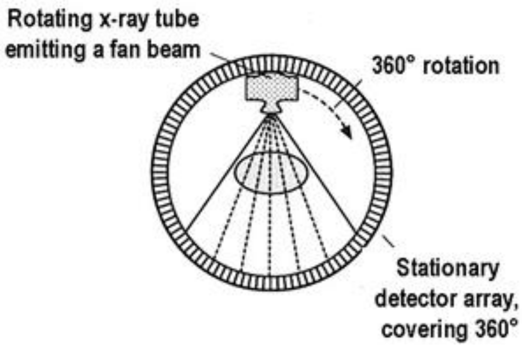

Figure 2.20 Fourth generation CT scan design[30]

The fifth generation CT design is a stationary system. In the fifth generation CT devices developed for cardiac tomography, the X-ray tube is placed as a large ring surrounding the patient. An electronic gun is used to detect electron beams travelling along the ring positioned in the gantry (Figure 2.21). The fact that the detector is also ring-shaped allows multiple simultaneous image sections to be taken[27][30][31].

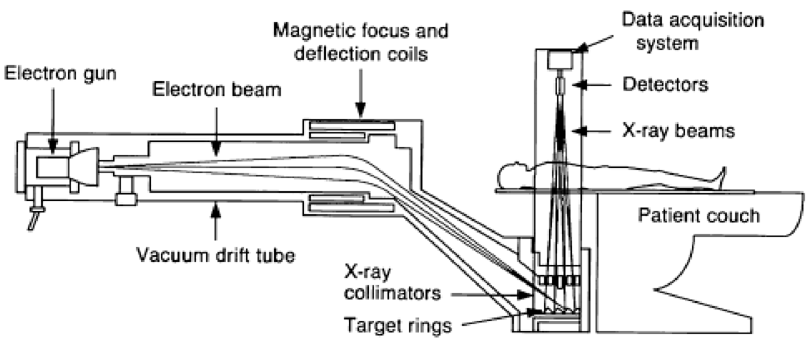

Figure 2.21 Fifth generation CT scan design[30]

The sixth generation CT design, which is still in use today, was developed by German physicist Dr. Willi Kalender. In addition to other generations, it includes a sliding patient bed. In this system, also called helical CT, the X-ray tube and detectors rotate 360° around the patient simultaneously. Together with the rotating detector ring, the sliding patient bed also moves back and forth (Figure 2.22). With this CT design, image sections were obtained in continuous time. At the same time, since the total rotation takes less than 1 second, artefacts caused by patient mobility are prevented[26][27][28].

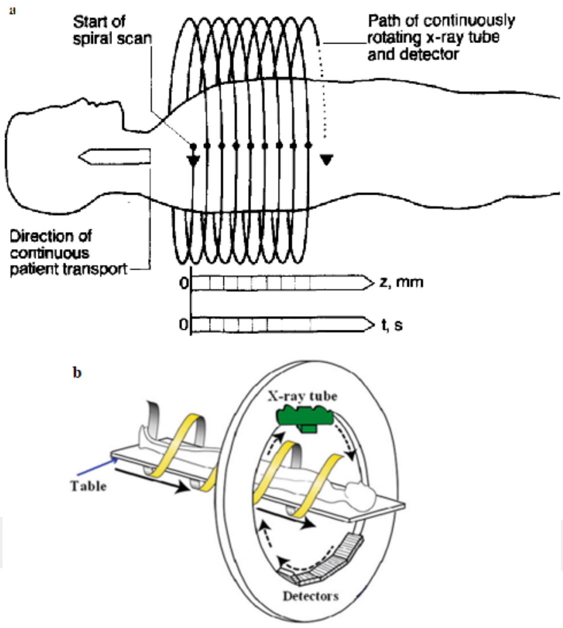

Figure 2.22 Sixth generation (also known spiral/helical CT or SSCT) CT design a. Spiral path of the scan, data is acquired continuously[32] b. Movement of the patient table, passes through the tube and detectors[27]

Developed in 1998, the seventh generation CT device design incorporates multiple detector arrays. The thickness of the image slice is determined by multiple detector arrays, which increases the slice thickness. By utilizing more of the X-rays produced, the image acquisition speed is increased[26][27][28].

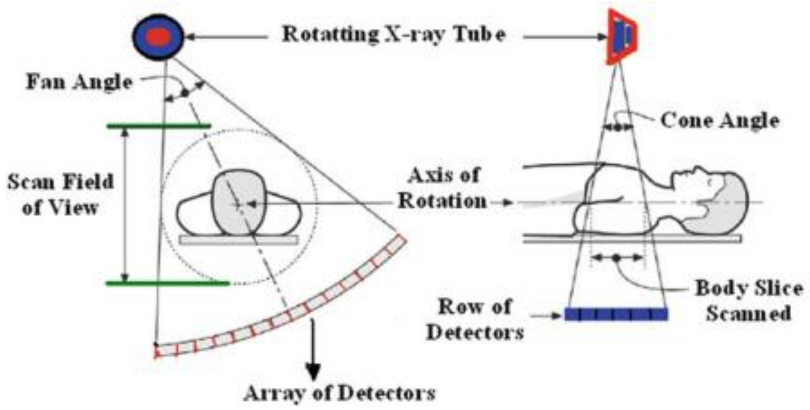

Figure 2.23 Seventh generation (also known MSCT) CT design[27]

2.4.2 Positron Emission Tomography

Positron emission tomography (PET) is a scan used in medical imaging for both diagnosis and treatment of disease, in which metabolic activity in the body is imaged using radioactive material. A positron-emitting substance (i.e. radioisotope) is injected intravenously into the patient. When positively charged positrons emitted from the patient collide with electrons in the environment, an annihilation occurs. The two opposite photons (gamma rays) produced as a result of an annihilation are detected by the detectors, and the image of the patient is taken by processing the received signals in the computer environment (Figure 2.24)[29].

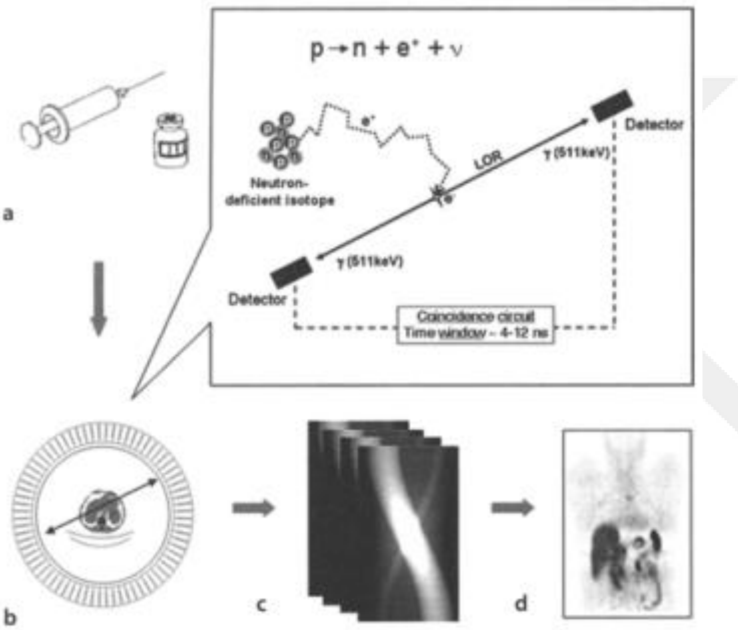

Figure 2.24 PET-CT imaging principles shown schematically. a Injection of labeled radiopharmaceutical into the patient b. Annihilation occurs between the positron and electron and the pair of annihilation photons measured by the coincidence detectors c. Data of collected positron annihilation events are stored in the form of sonograms d. A coronal section of the reconstructed image, it maps the utilization of the tracers throughout the patient[33].

Cancer cells are much more metabolically active than healthy cells[34]. Therefore, they are easily detected by PET scanning. PET scanning takes place in two stages: injection and imaging.

In the injection phase, the patient is injected intravenously with a pharmaceutical some time before the imaging and in an isolated room. The type of pharmaceutical varies according to the disease and the dosage is proportional to the age and weight of the patient. The pharmaceuticals are molecules labelled with a positron-emitting (β^{+}) radioactive isotope with a positive charge. The interaction with the cancer cell is thus monitored. They are usually labelled with fluorine-18 and carbon-11. The patient is kept in the injection room for a certain time to allow the pharmaceutical to be taken up and metabolized by the cells. The injection room is also a radiation-protected room, as the patient emits radiation for some time due to the injected pharmaceutical[35][36].

In the imaging phase, the radioactive patient is taken into the PET-CT device. The scanning device consists of a patient table where the patient lies, a gantry where the area to be imaged enters, a detector ring, a computer where the received signals are processed, and an imaging monitor. The detector ring is a ring that surrounds the patient 360° and rotates 360° and contains several detectors. Each detector contains a scintillator crystal and a photomultiplier tube. The detectors must simultaneously detect photons travelling in opposite directions. They are therefore positioned opposite each other[33][35][36].

A positron and an electron neutrino are emitted by β^{+} decay. When the positron is ejected, it loses its kinetic energy through ionization and scattering. When the positron loses almost all of its energy and becomes immobilized, it interacts with an electron in the environment. An annihilation event, which refers to the annihilation of the electron and positron, occurs and two photons are emitted in opposite directions, each with an energy of 511 keV due to conservation of momentum. These emitted photons are called gamma rays. These rays are captured by two detectors positioned opposite each other and a Line of Response (LOR) is formed between the detectors. In this way, the detector pair will only detect the desired annihilation pairs (Figure 2.25)[33][35][36].

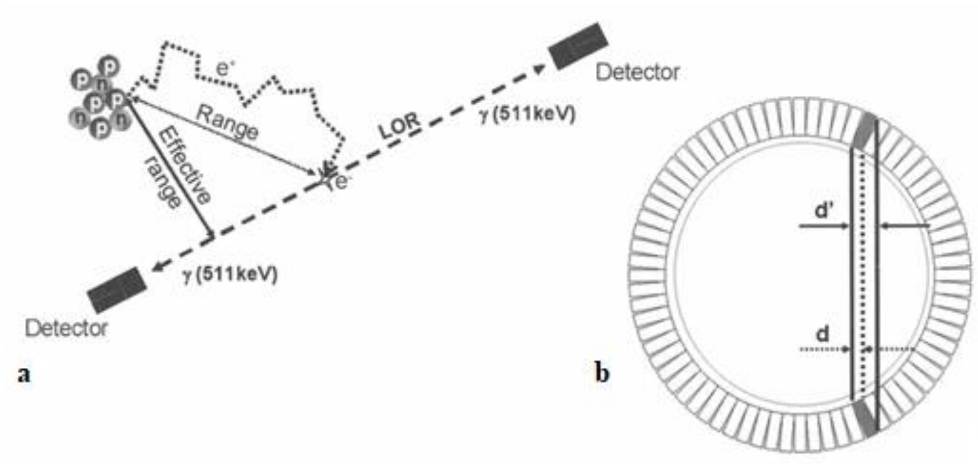

Figure 2.25 Annihilation event a. LOR b. Detection of paired annihilation photons[33]

The detectors (Figure 2.26) are scintillation detectors with the power to stop incoming photons. The power of the detector to stop the incident photon depends on the path of the photons in the detector. The progress of the photons in the detector is related to their atomic numbers and densities. Detector materials used in PET have high atomic number and density. When gamma rays strike the scintillator crystal in the detectors, a visible burst of light is produced, and an electrical signal is generated. These photons then strike the photocathode and detach electrons from the photocathode. The number of detached electrons is increased by photomultiplier tubes. Concave dynodes in the photomultiplier tubes accelerate the electron coming to the first dynode and increase its energy. It continues by removing more electrons while striking other diodes, so that the number of electrons removed increases exponentially. After these signals are amplified, they are sent to the synchronous counting unit. Since the collisions occur successively and rapidly, the interval of the synchronization window must be narrow for counting a single annihilation event. The electrical signals from the detectors are combined in a computerized environment and converted into images by amplifiers. Of the electrical signals passing through the amplifier, only electrical signals in the range of 350-650 keV are accepted. As a result of PET scanning, a three-dimensional image of the internal structures of the body is created and the distribution of the pharmaceuticals used in the body and metabolic activity are identified[33][35][37].

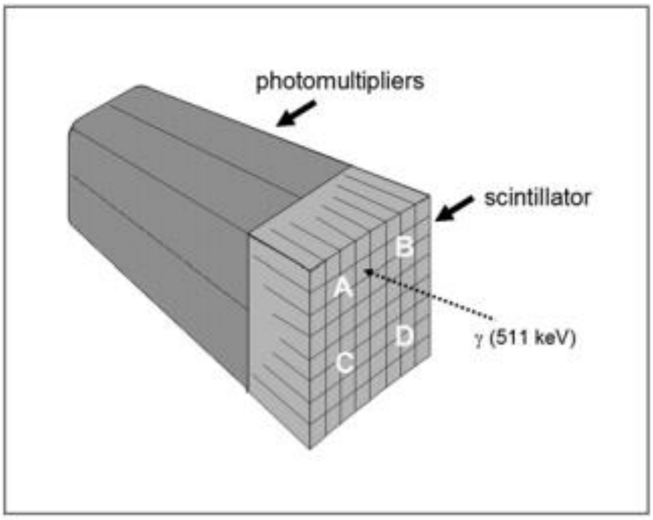

Figure 2.26 PET Detector Design[35]

Three different types of coincidence events can occur as a result of an annihilation: true, random, and scattered photon coincidence (Figure 2.27). For PET, the desired true overlap is the simultaneous detection of the annihilated photon pairs by the detectors placed opposite each other. The high-energy light output makes it easy to distinguish from other interferences, which results in high resolution in image quality. In random coincidence, the detectors detect two photons from different annihilations, resulting in a different LOR line. In scattered overlap, one of the annihilation photons is detected directly by the detector, while the other photon is scattered from the surrounding tissue and reaches the detector. These types of overlap are undesirable because they affect the image quality negatively at different rates[11][35].

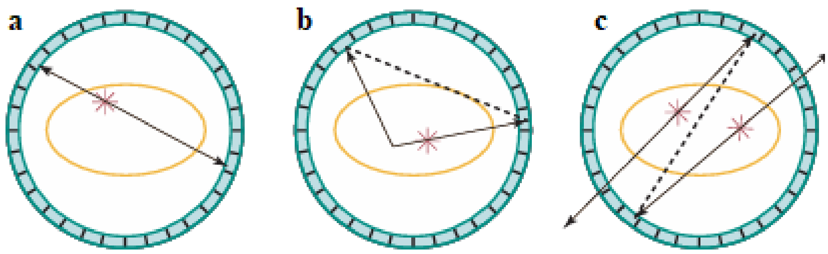

Figure 2.27 Types of coincidences a. true coincidence b. scatter coincidence c. random coincidence[11]

As a result of scanning, the image is obtained in sections. Cells/tissues showing activity with the labelled pharmaceutical appear as hot spots, while cells/tissues showing no or low metabolic activity appear as dark spots[33][38].

2.4.3 Single Positron Emission Computed Tomography

Single photon emission computed tomography is a medical imaging technique in which the activity of the pharmaceutical used as a radiation source in the body is shown. The pharmaceutical injected into the body intravenously, the photons emitted from the substance in a single direction are detected by the detectors and converted into an image by signal/image processing in the computer environment. First developed in 1963 by Kuhl and Edwards on the principle of a parallelized scanning detector[39], SPECT devices (Figure 2.28) are now commonly of two types: those using fixed detector arrays and those using rotating anger cameras. While the first design uses a single detector, two and three detector designs have been developed to shorten the acquisition time and improve image quality[40]. SPECT scanning takes place in two stages: injection and imaging. In the injection phase, as in PET scanning, the patient is injected with a pharmaceutical depending on the type of disease before imaging. After waiting for some time for the pharmaceutical to be taken up and metabolized by the cells, the patient is taken to the device for imaging[41][42].

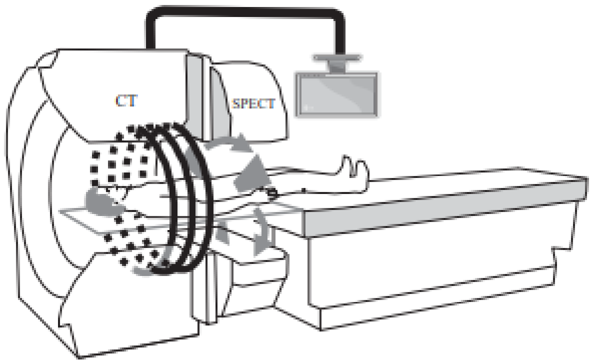

Figure 2.28 A SPECT Device[16]

The imaging device consists of a gantry in which gamma cameras and detectors are placed, a patient bed and a computer system for signal/image processing[43]. The patient injected with pharmaceuticals actively emits radiation around them. Gamma photons emitted from the patient are captured by collimators in gamma cameras and directed to the detector. Collimators are made of dense materials such as lead and tungsten, which have high interaction with photons. In SPECT scanning, the direction of the emitted photons must be recognized. The collimators transmit the emitted gamma photons to the detector through holes in them. Collimators are parallel and perpendicular to the detectors[44]. Due to their design and layout, only photons travelling parallel to the holes are transmitted to the detectors. The collimators block most of the gamma rays that would strike the detector, allowing only gamma rays travelling in the specified direction to pass through (Figure 2.29). The detectors used in SPECT are sodium iodide (NaI) crystals used as scintillation counters[45]. Due to the high atomic number of the iodine component of the NaI crystal, the photoelectric absorption is high. In this way, when gamma rays interact with photoelectric scattering, the pulses that will occur here are prevented. When gamma photons strike the detector crystal, they are stopped by the crystal. The NaI crystal emits scintillation photons proportional to the energies of the photons. Then, these photons strike the photocathode and extract electrons from it. The number of the detached electrons is increased by photomultiplier tubes located opposite the crystal and converted into electrical signals. The photomultiplier tubes are placed in large numbers directly opposite the crystal. The gamma ray travelling through the collimator channel and interacting with the scintillation crystal is distributed to the nearest photomultiplier tubes. In this way, the position of the gamma interaction is determined and recorded as a pulse counting rate. The signals are first slightly amplified in the computer environment and then converted into an image. Gamma cameras generate position signals in the XY plane for the output signals from the photomultiplier tubes. Therefore, while a 2-dimensional image is obtained, a 3-dimensional image of the patient is obtained as a result of the SPECT scan by rotating the detector around the patient[44][45][46].

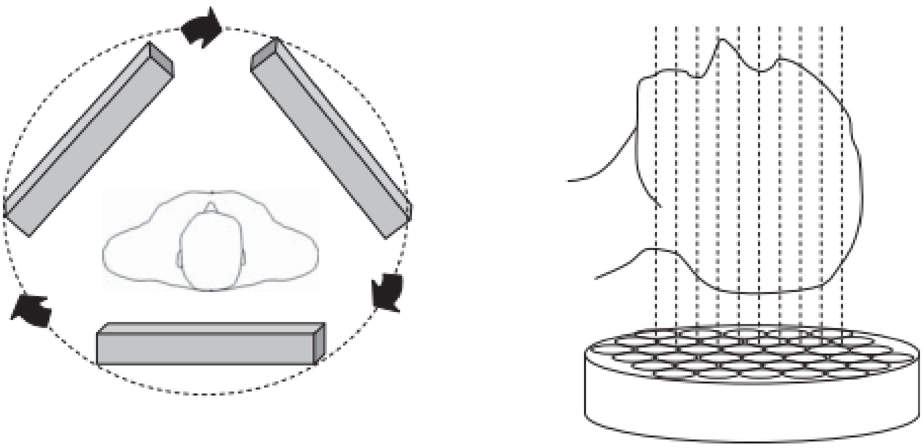

Figure 2.29 Three-head rotating gamma camera SPECT system(left) data acquisition (right)[46]

The quality of the SPECT scan image depends on the type of collimator, the number of projections, the distance between the detector and the patient (gantry diameter) and the scan time. Gamma rays are transmitted through collimators to the detectors. If gamma rays are scattered by photoelectric scattering, this will appear as undesirable scatter in the background of the image. The pharmaceutical injected into the patient normally emits one or two gamma-ray photons that can be adequately characterized. The energy of the photons emitted by diffuse scattering is considerably lower than the energy of these photons and therefore easily recognized. It is important that the collimators are selected from suitable materials to ensure that the photons of the desired magnitude are transmitted to the detectors and the undesired ones are blocked. For this purpose, collimators are made of high atomic number and high-density materials. The spatial resolution of the image is directly related to the projection images. Projection images should have similar widths. Since scanning is performed throughout the patient, images are taken in slices with a narrower range to increase sensitivity. The SPECT devices used today are designed with a slice thickness of 10-25 mm. The distance between the patient and the detector affects the discrimination power of the detector. A small distance increases the image quality. In addition, the image quality is improved by changing the angle between the detector and the patient in SPECT types with fixed camera and rotating anger camera. Increasing the scanning time may cause artefacts in the image as it may affect the movement of the patient[44][46].

2.4.4 Fluoroscopy

Fluoroscopy is the technique of real-time imaging of tissues using X-rays. Fluoroscopy device, which is widely used in the medical field, especially in orthopedic surgeries, is also used in many fields such as pain management, upper and lower gastrointestinal imaging, cardiology. Fluoroscopy device consists of X-ray tube, filter, collimator, anti-scattering grid, image intensifier or flat panel receptor and camera (Figure 2.30)[47].

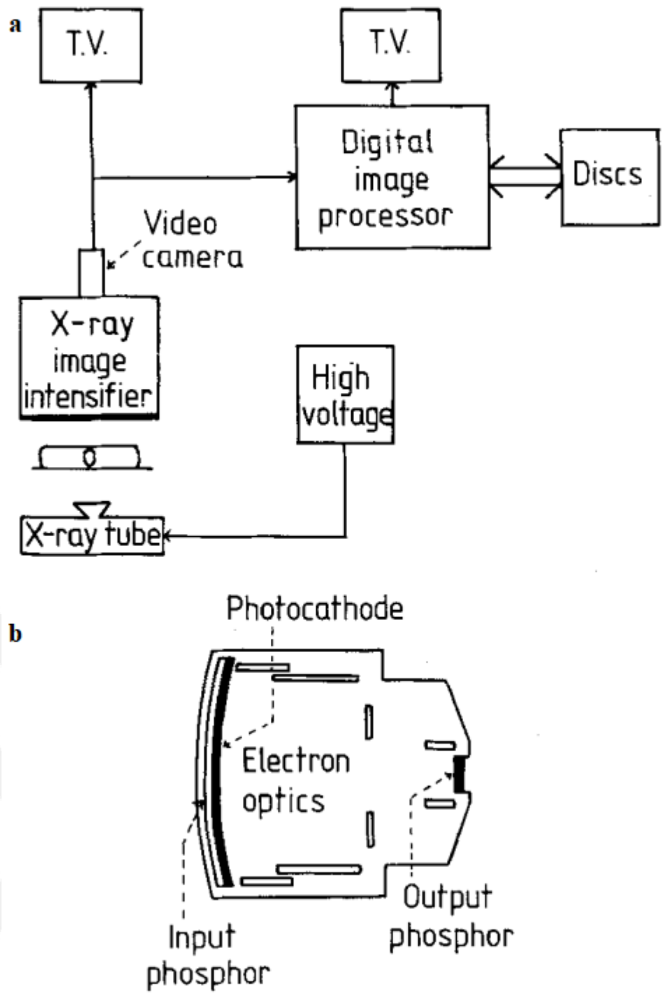

Figure 2.30 A fluoroscopy device a. Schematic diagram b. Image intensifier tube[48]

The radiation source is an X-ray tube that produces X-rays. X-rays are emitted in a wide spectrum from infrared rays to X-ray photons. The output port of the X-ray tube contains metal discs. These serve to filter out these low-energy undesired rays. Photoelectric absorption of photons occurs at low energies. Materials with low atomic numbers such as aluminum and copper are selected as disc materials. In this way, the filtering process is easily realized by taking advantage of photoelectric absorption. The collimator is located at the exit of the X-ray tube. The collimator, which can be controlled by the operator, serves to narrow the volume of X-rays emitted and to improve image quality by reducing Compton scattering. The X-rays passing through the patient reach the anti-scattering grid located between the patient and the image intensifier before the image received (Figure 2.31). The purpose of the grid is to ensure that photons travelling on direct lines between the X-ray tube and the image receiver are transmitted to the receiver. This prevents the transmission to the receiver of photons that are scattered in different directions as they pass through the patient or that are deflected by other interactions. The grid consists of radiopaque stripes placed at intervals. High atomic number materials such as lead are used for the stripe material, while low atomic number materials such as aluminum are used for the gaps between the stripes. Undesired photons are removed by photoelectric absorption. It is the imaging stage that distinguishes the fluoroscopy device from the conventional X-ray device. Two types of receivers are used in the device as image receiver: image intensifier and flat panel receptor[47].

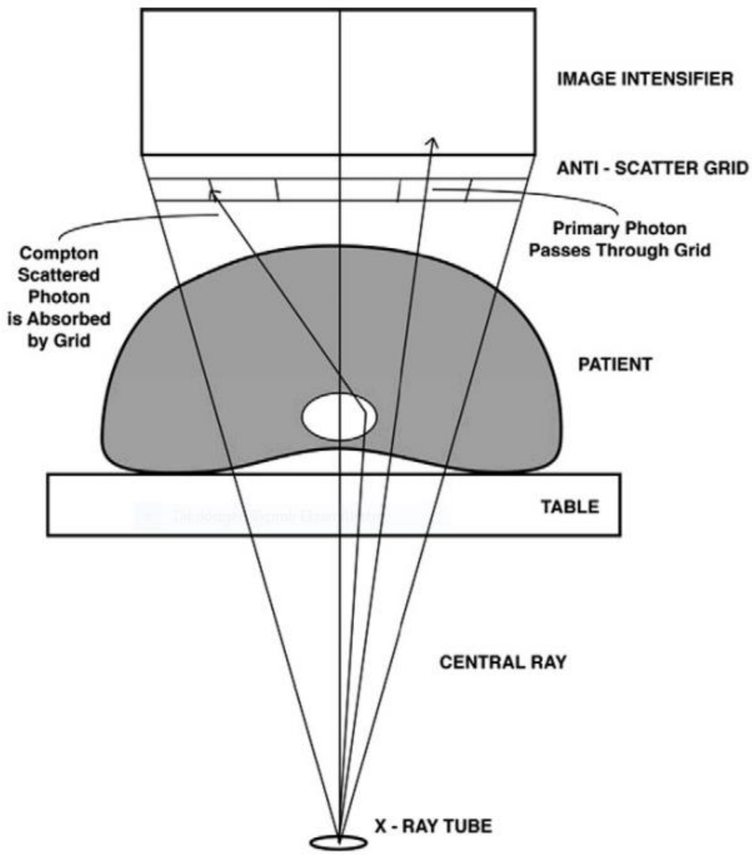

Figure 2.31 Location of the anti-scatter grid[47]

Image intensifier consists of an input phosphor and photocathode, focusing lens, accelerating anode and output photon. The input phosphor converts X-ray photons into visible light photons. A photocathode is placed at the end of a fluorescent screen coated with cesium iodide (CsI) crystals. The photocathode converts the low-visible light image from the crystal into an image of free electrons. These free electrons are then accelerated to high speeds and high energies by the accelerating anode. Since the accelerated electrons are pulled away from the focus by repulsive forces, this is prevented by the focusing lens. Due to the acceleration of the accelerated electrons and the reduction of the image area, an intensified image is obtained at the output phosphor[47][48].

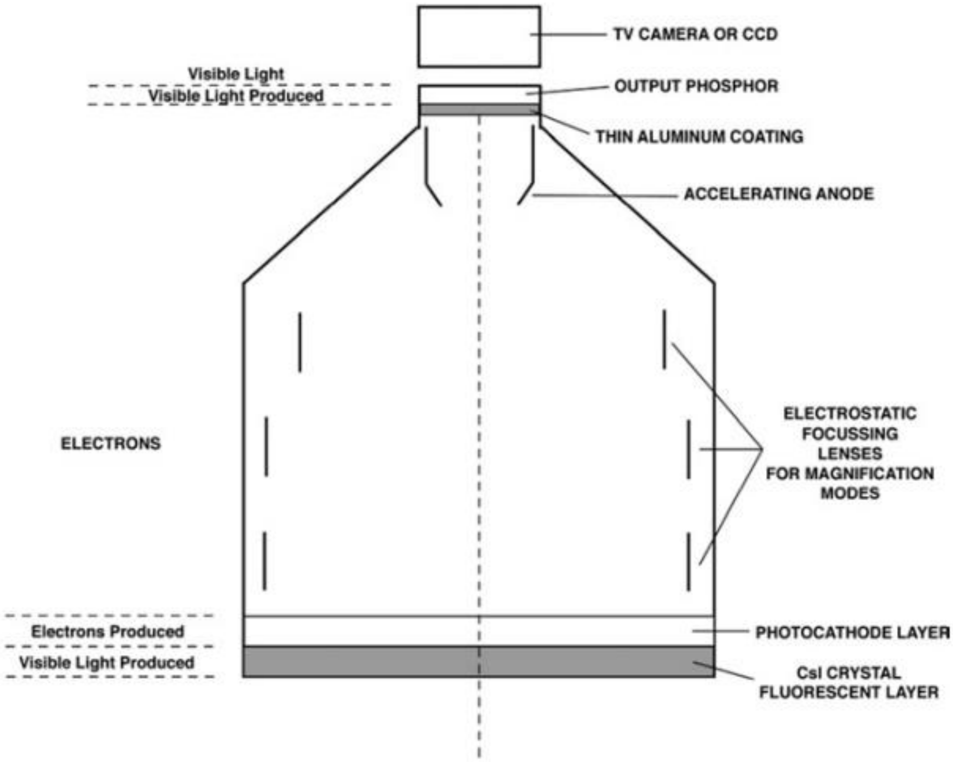

Figure 2.32 The image intensifier tube[47]

Flat panel receptors have been developed in recent years and are the preferred imaging tool instead of image intensifiers because of their great contribution to image digitization and storage. There are two types that convert X-rays into visible light images. Both types divide the image into a rectangular matrix. Each image element in the matrix is called a pixel. One type first converts X-rays into visible light, then interacts with the photocathode and collects electrons in pixels. In the second type, X-rays are converted into electrons directly in pixels[47].

In fluoroscopy devices, image quality is affected by factors such as grid ratio, camera-matrix resolution compatibility, appropriate collimator selection, pixel filling ratio[47][48].

Grid ratio is the slat height/spacing between slats. As this ratio increases, the number of both Compton scattering and primary photons increases. Blocking undesired energetic photons improves image quality, but on the other hand, the radiation exposure of the patient increases[47].

When a 525-line video image is divided into a 512x512 matrix, there is little loss of spatial resolution. The smaller the electrons are packed into pixels in the flat panel array, the higher the spatial resolution of the image. This also has a positive effect on factors such as storage space and image speed[48].

Pixel fill factor refers to the efficiency of radiation utilization. In order to obtain higher quality images, the pixel fill factor should be high[47].

2.4.4.1 C-arm Scopy

C-arm scopy is a variant of fluoroscopy commonly used in operating rooms. In conditions where the use of a CT device is not appropriate (e.g. during surgery), fluoroscopic imaging methods are used to obtain a real-time image of the patient. It consists of an X-ray tube that produces X-rays, an arc-shaped detector (C-arm) and a monitor on which the image is displayed. Since the C-arm can be moved horizontally, vertically and around the axes of rotation (Figure 2.33), the image of the patient can be obtained from many angles, but the image obtained is 2-dimensional[49][50].

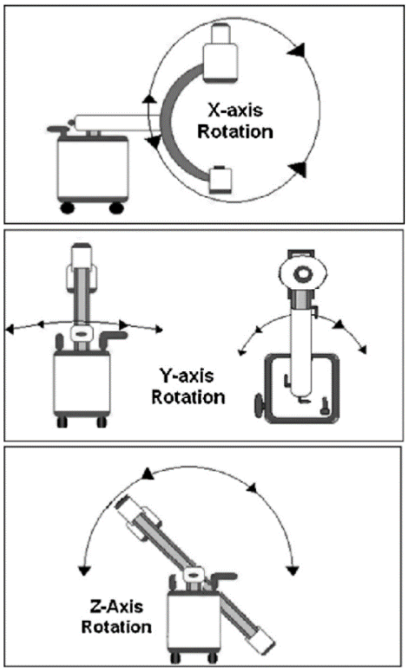

Figure 2.33 Mechanical axes of C-arm fluoroscopy[51]

2.5 Effects of Radiation and Radiation Protection

In addition to the benefits of radiation, which has applications in industry, food, medicine, materials, and many other fields, it is of great importance to protect against harmful consequences that affect even the next generations. The use of nuclear materials and radiation sources involves certain rules and safety measures to take precautions for the possible dangers of radiation and radiation accidents. Radiation has two types of effects on tissue, deterministic and stochastic. Deterministic effect occurs when the radiation dose exceeds the threshold value. It can affect the entire human body in a short time, or it can cause permanent damage by affecting only the contact site. In 1945, Hiroshima and Nagasaki atomic bomb attacks and 1986 Chernobyl Nuclear Power Plant accident caused instant and short-term deaths due to high dose radiation exposure. Acute Radiation Sickness (ARS) is a disease that occurs when exposed to very high doses of radiation in such a short time and results in death if left untreated. It starts with nausea and vomiting and continues with burns, bleeding, and severe infection. The diagnosis of ARS was reported for 237 people as a result of the Chernobyl Nuclear Power Plant accident. Radiation has various and dangerous deterministic effects such as burns on the skin, permanent damage such as loss of sensation, infertility for reproductive organs, cataract formation for the eye, depending on the area of contact. There is no threshold value for stochastic effects. The radiation dose exposed at different time periods or instantaneously triggers the stochastic effect. Not all organisms are affected at the same rate. The dose, type, duration, and speed of radiation affect the stochastic effect. Cancer is one of the most common stochastic effect results[52].

With the advancement of technology, it has become an obligation to take precautions against these effects, which have very severe consequences. For this purpose, The International Atomic Energy Agency first included radiation protection and safety principles in its publication "*Radiation Protection and Safety of Radiation Sources*" in 1996. In addition to these rules, which are accepted and implemented all over the world, the International Commission on Radiological Protection (ICRP) published recommendations for radiation exposure to workers in 1997 and 2007. Radiation protection and safety principles are grouped under 3 basic principles: *verification, optimization and dose limits*[53].

The results such as the shortening of the life span of individuals who are in direct or indirect contact with radioactive material and the reactions in the body have led to the need to draw a profit-loss table for the radiation to be used. The principle of verification of the application or, in simple terms, the determination of the net benefit of radiation is based on this principle. The benefit of the radiation to be applied must be greater than the harm. The ICRP statement states that the associated risk cannot be justified unless it is balanced against the expected medical benefit to the individual or to society[54].

The principle of optimization of protection is the dose-performance relationship. Established in 1954 by the ICRP, this principle, known as the "As Low As Reasonably Achievable (ALARA)" principle, aims to expose the patient to the lowest possible dose after evaluating all factors. Determining the ALARA dose requires optimization in a wide range of areas, from the design of the imaging screen to the knowledge and skills of the imaging operator. Healthy radiation does not mean low dose radiation. Image quality is directly related to radiation dose. If the target tissue cannot be reached with low dose radiation, a repeat scan is requested. In this case, the patient will have received higher intensity radiation. Therefore, it can be said that the ALARA principle represents the optimization between image quality and exposure dose. It is as important that the operator using the device has developed himself/herself both about the device and about the shooting techniques as it is that the device itself is advanced. The operator should know what to do in case of any malfunction and minimize the radiation exposure of the patient by minimizing the shooting time. Calibration follow-up of the shooting team and device vendors is also within the scope of the ALARA principle[54][55][56].

The principle of dose limits is based on limiting the radiation dose to which the patient or worker is exposed in the long term and thus preventing the stochastic effects of radiation. Since workers are regularly and continuously exposed to radiation, the limits for workers and the general public are different. The dose rate is expressed in millisievert/hour (mSv/h). The effective dose limit for workers was set by ICRP in 1991 as an average of 20 mSV for 5 years and an upper limit of 50 mSV for one year. For the public, these values are 1mSv and 5mSv respectively. The average radiation dose for a head CT scan is 2 mSV, while for nuclear medicine imaging these values range from 0.3-20 mSv. While 1 Sv radiation dose causes vomiting and nausea, 5 Sv causes 50 per cent death within months and 10 Sv causes direct death[17][53][57][58][59][60].

Apart from radiation protection and safety principles, there are also precautions that can be taken during radiation exposure. These are time, distance and shielding precautions[61].

The duration of exposure to the radiation source is directly proportional to the radiation exposure of the person. The longer this period, the higher the dose received[15]. Therefore, it is a precaution for the patient to leave the room/desk at the end of the procedure or to try to minimize this time for the employee.

By increasing the distance to the radiation source, the intensity of the radiation exposed decreases. Kara et al. measured the radiation dose exposed by changing the distance between the fluoroscopy device beam source and the patient in 2016. The maximum dose was measured in the setup with the shortest distance[62][63][64].

Some materials placed between the radiation source and the patient or used to limit the radiation emitted in a certain area (e.g., to ensure that it does not go outside the shooting room) affect the amount of radiation received. This process is called radiation shielding (Figure 2.34). The main purpose of shielding is to weaken the incoming X or gamma rays before they reach the target by using a shielding material. The choice of the material to be shielded may vary according to the type and amount of radiation and economic conditions. With the selection of the appropriate material, the dose received or exposed can be reduced or eliminated at a high rate[15][17][18].

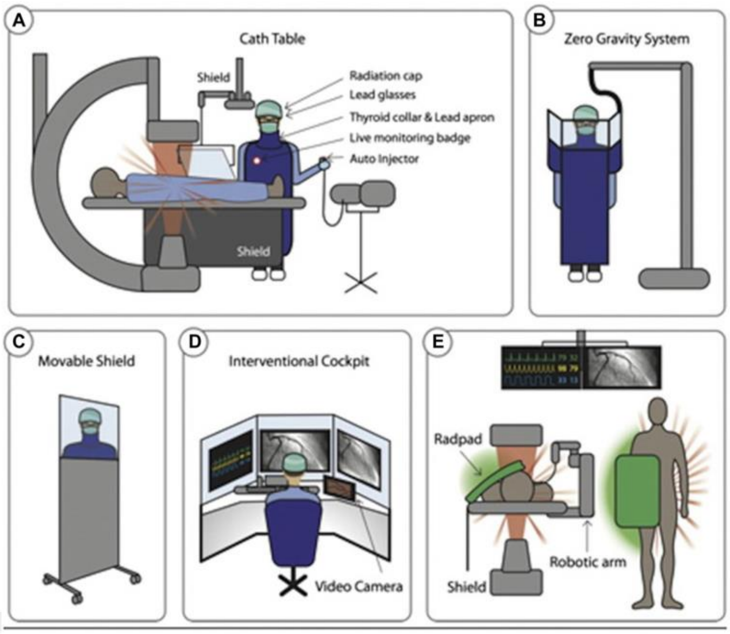

Figure 2.34 Shielding methods in an operating room a. Protection technique. For operator with cap, glass, and apron; for patient with the location of the radiation source b. Using zero gravity system c. A movable shield d. A glass shields between shooting room and operator room e. Using disposable shielding pads and robotic systems for shooting[65]

Alpha radiation has a short range and can be stopped even with paper, but for these reasons it is the most damaging type of radiation. Shielding in the form of fixing with paint is used to prevent the spread of radiation.

Beta particles are charged particles and distribute their energy to the environment during emission, but this distribution is also limited. While the air itself is a shielding material for beta radiation, they can be easily shielded with a media thickness selected in accordance with the range of the highest energy beta particle and exceeding this range (e.g. aluminum and plastic).

Compared to the interactions of charged particles, the shielding of photon-matter interactions is quite different. First, X and gamma rays are highly penetrating rays. In their interaction with matter, some rays pass directly through the matter, some are absorbed, some are scattered in different directions as low-energy photons. The scattered photons produce a radiation field to the patient and the surroundings. Due to its penetrating properties, materials with high absorbance ability should be selected when selecting shielding materials. Parameters such as thickness, conductivity, density, atomic number of the selected material are other factors affecting the quality of shielding[15][17][18][60].

2.5.1 Commonly Used Shielding Materials

2.5.1.1 Lead

Lead is a corrosion-resistant[66] and workable metal with a specific gravity of 11.34 g/cm3, much more heavier than other elements[67]. It has a high atomic number and is highly stable, which makes it inevitable as a shielding against X and gamma rays. It is easy to access and economically cost-effective. In addition to these properties, its disadvantages are their toxicity, low fusion temperature and being too heavy for use as wearable shielding material (Figure 2.35). Despite these, it is the most widely used shielding material[60][68][69].

Figure 2.35 A lead apron

2.5.1.2 Concrete

It is used as a protective layer for storage because it is sensitive to high pressure and has a long service life (Figure 2.36). It is resistant to high temperatures and can be processed. It is easy to access and quite cost-effective compared to other shielding materials. Since it can be mixed with different materials, its shielding properties can be improved. Its weight and loss of moisture resistance over time are important disadvantages[60][68][70].

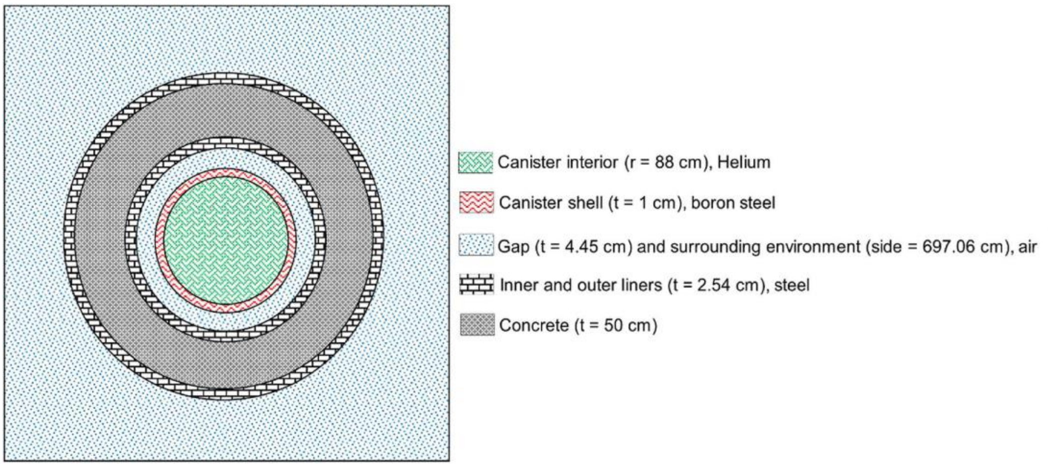

Figure 2.36 Dry storage barrel model with concrete base in sandwich design[71]

2.5.1.3 Steel

Steel with high mechanical resistance and heat resistance is used as shielding material especially in transport and storage barrels (Figure 2.37). Its surface is treated to increase its corrosion resistance. The absorption ability of steel, which has low radiation absorption ability compared to other materials, is increased in alloys with other elements. For example, by increasing the corrosion resistance of steel with nickel-steel alloy has been made into a better shielding material[60][72].

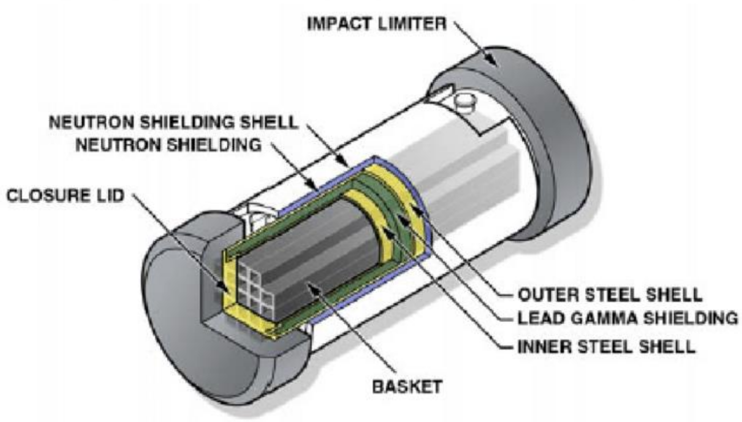

Figure 2.37 An example of transportation cask design[73]

2.5.1.4 Tungsten

Tungsten with high atomic number (74) has high density (19.25 g/cm3), high fusion temperature and very good shielding properties. However, it is not widely used because pure tungsten is very expensive. Unlike the widely used lead and concrete, it is a non-toxic material. This makes it attractive as a shielding material. Due to its high cost, it is used as shielding material in parts (Figure 2.38) such as caps and plugs[60][74][75].

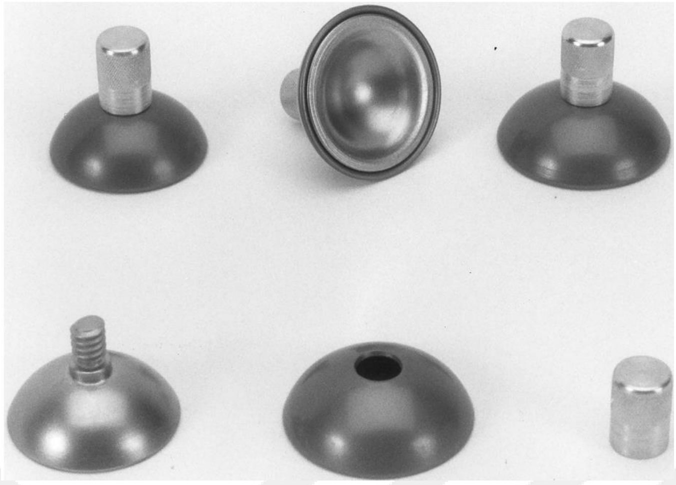

Figure 2.38 Tungsten eye shields[76]

2.5.1.5 Cast iron

Cast iron, like steel, is used as a shielding material for transport and storage casks. It is economically cost-effective and easy to supply. Cast iron alone has low effectiveness as a shielding material. It has been observed that its shielding ability increases when doped with concrete and hydrogen. Today, efforts are still being made to improve its shielding ability[60][77][78].

2.5.1.6 Glass

Glass is a protective material which has recently become widespread. The transparency of glass makes it attractive in contrast to the opacity disadvantages of concrete and lead. It is light, flexible, accessible and economical. The absorption cross-section value of glass systems to be used as shielding material should be high and irradiation should not affect the mechanical and optical properties of the glass[79][80].

Figure 2.39 Upper body protection with shielding glass material[81]

2.6 Use of Glasses as Radiation Shielding Materials

Due to their transparency, ease of production, processability, high homogeneity and optical properties, glass materials are a very promising alternative to lead and concrete, which are widely used as radiation shielding materials. The toxicity of lead, the structure of concrete, which is prone to cracking and losing moisture over time, and the fact that both materials are opaque and bulky materials due to their weight have led researchers to search for new materials as shielding materials[68][82].

2.6.1 Radiation Shielding Properties of Glasses

The prominent properties of glasses in the use of radiation shielding materials can be listed as follows:

- Glass materials provide protection from the harmful effects of radiation by absorbing X-rays, gamma rays and neutron radiations[83][84].
- Their structural hardness and optical properties can remain intact/unchanged even under radiation. This also means their long-lasting use[68].

- Glass materials have high homogeneity. This makes them suitable for the desired weight and composition for shield design[80].
- Glass materials are suitable for improving the radiation attenuation capacity by including heavy metal components in the production processes and changing their density. This also allows the melting point and viscosity of the system to be reduced without any change in the chemical properties of the glass itself[82].

2.6.1.1 Advantages of Glass as Radiation Shielding Material

The prominent advantages of glasses in the use of radiation shielding materials can be listed as follows:

- Homogeneity, transparency
- Wide thickness range
- Chemical composition can be changed during the production phase and mechanical and optical properties can be adjusted
- Low cost
- Ease of preparation, workability

2.6.1.2 Disadvantages of Glass as a Radiation Shielding Material

The disadvantages of glass as a radiation shielding material can be listed as follows:

- Some glass systems may have high costs.
- Special applications may be required to produce some glass systems.

2.6.2 Application Areas of Glass in Radiation Shielding

Glass materials are used as shielding materials in many fields such as medicine, industry, nuclear applications, dentistry. They are widely used as transparent radiation shields and protective barriers.

For instance, they are used as radiation shields in storage containers and bottles in laboratories and as radiation protective barriers between the room where the device is placed and the personnel room for high radiation emission imaging methods such as computerized tomography and PET-CT. These glasses absorb the incoming radiation and reduce the radiation dose exposed. At the same time, due to their hard structure, resistance to ambient temperature and longevity, they are preferred as storage containers and sealing materials in spacecraft. Due to the transparency and low effects of radiation rays on the optical properties of glass, it is used as an shielding material between the patient and the radiation source in the design of imaging devices. This may be in the form of adding a radiation shielding layer to the design of the device or directly selecting the lens of the camera used from the appropriate glass. In addition to their transparency and optical properties, due to their high absorption ability against photons, they are used as shielding materials in the form of a barrier or wearable accessory (e.g. glasses) between the operator and the device. Due to their transparency, they are preferred as shielding materials instead of lead or concrete, especially in imaging rooms to see inside[60][65][68][82][83][84][85].

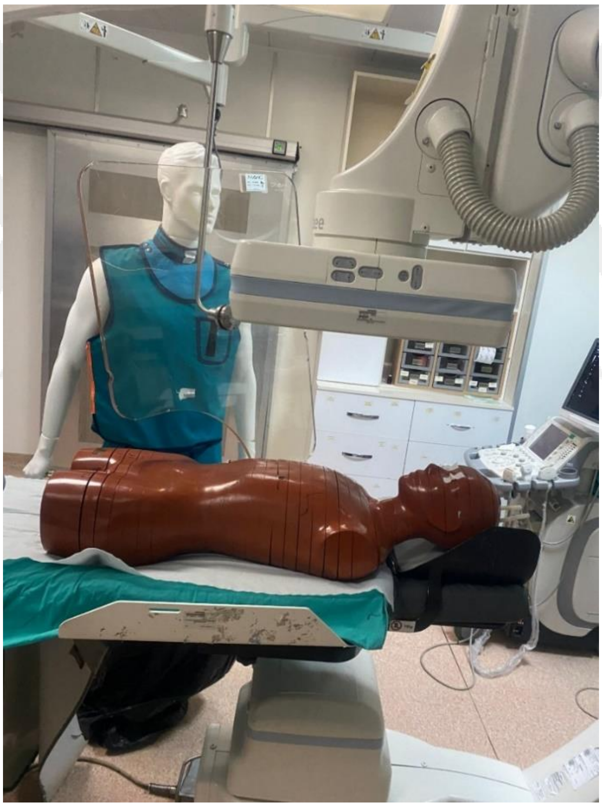

Figure 2.40 An example of the use of glass as a radiation protective barrier between the patient and the operator in a scopy device

2.6.3 Glasses Used as Radiation Shielding Materials

Unlike lead and concrete, glasses are used in shielding in the form of multi-component glass systems, so there are many types of glass systems that are currently being developed for use or have not yet emerged, as well as widely used glass systems.

Experimental studies on the use of glass systems in shielding began in 2004 with the studies of Singh et al.[80] examining the radiation shielding parameters of bismuth-borate and bismuth-lead-borate glass systems, and Fukuda et al. comparing the shielding capabilities of X-ray shielding and lead glass[86].

While lead can be used as a radiation shielding material on its own, by incorporating it into glass systems, the disadvantages of lead are transformed into the advantages of glass. However, the toxicity of lead has led researchers to develop lead-free glass systems.

Bismuth, silicate, barium, borate, lithium, tellurite and zinc are commonly used glass system components. Studies have been carried out to improve the shielding capabilities of the systems by changing the concentrations of metal components in the system or by doping with new components.

Singh et al. investigated the shielding parameters of barium-borate-flyash (BaO-B_2O_3-Flyash) glass system in 2008 and demonstrated that the system is a better shielding material than concrete and glass system containing only barium-borate due to its low mean free path value[87].

Dararutana et al. 2009 showed that the addition of high refractive index bismuth (Bi_2O_3) to the (Na_2O, K_2O)-SiO_2-CaO-Al_2O_3-B_2O_3 glass system increased the radiation shielding ability of the system and demonstrated that it is an environmentally friendly alternative to lead[88].

In 2012, Kaewjaeng et al. have shown that the optical properties of the system were improved by adding BaO at different concentrations to the SiO_2-B_2O_3-Al_2O_3-CaO-Na_2O glass system[89].

In 2016, Issa et al. developed a glass system with TeO_2 with high attenuation coefficient and ZnO, which increases the thermal stability of the system, and indicated that it is suitable for use as an shielding material[90].

In 2017, Shamshad et al. compared gadolinium-based oxide (Gd_2O_3) and oxyfluoride (GdF_3) doped Li_2O-SrO-B_2O_3 glass systems and showed that Gd_2O_3 is a better shielding material, fluoride has no effect on the optical spectrum and both glass systems are also better than concrete[91].

The comparative study of Kaky et al. in 2019 by doping 6 different types of heavy metal oxides (Li_2O, Na_2O, K_2O, MgO, CaO, SrO and BaO) separately into the B_2O_3-SiO_2-Al_2O_3-ZnO glass system is valuable in terms of evaluating these widely used metal oxides together. As a result of the study, the highest attenuation coefficient of radiation was observed in the BaO glass system and the lowest in the Li_20 doped glass system, while the best shielding characteristics were observed in K and Sr doped glass systems[92].

In 2019, Agar et al. characterized the shielding ability of BaO-P_2O_5 glass system doped with MoO_3, a transition metal, and showed that MoO_3 contributed greatly to the stability of the glass and improved the electrical and optical properties of the system[93].

In 2021, Alotaibi et al. evaluated the shielding ability of the P_2O_5-B_2O_3-Bi_2O_3-Li_2O_3-ZrO glass system according to the changing values of P_2O5 and ZrO. They have shown that the system has a higher LAC value in cases where ZrO is highly doped[84].

In 2023, Sayyed and Kaky investigated how the doping of 6 different types of rare earth elements (Ho_2O_3, Pr_6O_{11}, Er_2O_3, Nd_2O_3, Dy_2O_3 and CeO_2) into the GeO_2-B_2O_3-ZnO-P2O5-Tb_2O_3 glass system affects the shielding ability of the system. They have shown that the addition of rare earth elements to the system increases the LAC value of the system and decreases the HVL value, thus increasing the shielding ability of the system[94].

2.6.4 Dy^{3+} doped Calcium Aluminum Barium Sodium Borate Glass System

As an alternative to lead-free glass systems, Dysprosium doped Calcium Aluminum Barium Sodium Borate glass system is remarkable for its versatility, high refractive index, density, durability, thermal stability and electrical resistivity. Heavy metal components are preferred in glass systems since increasing the density of glass makes it a better radiation shielding material. The half-value layer value of the glass whose density increases decreases, thus reducing the thickness of the glass to be used. Reducing the thickness of the glass reduces the cost and provides an advantage for narrow area studies. Rare earth elements have unique physical and catalytic properties. When doped into glasses due to their phosphorescence properties, they increase the optical properties and shielding capabilities of glasses[82][95][96]. Dysprosium ion is the most suitable element to be doped into glasses because it has two dense emission bands in white light emission applications compared to other RE elements[98][99].

Barium oxide increases the shielding ability of the glass by reducing the energy of incoming photons. It accelerates heat transfer within the glass. It gives the system transparency in the infrared region[96]. Studies have shown that glass systems to which BaO is added cause an increase in MAC and Z_{eff} shielding parameters[100]. The use of barium oxide and borate oxide combination as an shielding material meets the desired shielding characteristics[101].

Borate glasses are frequently preferred in glass materials due to their low melting temperature, transparency, high optical transmittance, cost and solubility in ions of rare earth elements[96][102][103]. In contrast to these properties, it is suitable for use with other metal components due to its low chemical resistance and willingness to interact with water[99].

Aluminum oxide is a prominent material in glass systems with its thermal conductivity and moderate strength. It is expected to increase the chemical resistance and thermal stability of the system to which it is added and to contribute to the control of the solubility of the system. Also, it affects the compactness of the structure. Its low cost is one of the reasons why it is preferred. However, its addition to the borate-containing glass system at high rates causes both to show high bioactivity. Therefore, special attention should be paid to the material ratios in these systems[95][104][105][106].

Calcium metal oxides act as a network modifier in the glass system in which they are present. The addition of calcium ions to the glass system leads to a decrease in the crystallization temperature of the system and an increase in its chemical resistance (this ratio can be higher in borate-based glasses). It strengthens the thermophysical properties of the system. At the same time, since they show low decay and reactivity under nuclear irradiation, they have gained an important place in radiation applications. Due to its attractive K-absorption edge, it increases the shielding ability of the system to which it is added and stabilize it. The viscosity of the system containing calcium ions decreases at high temperatures. Strong covalent

Ca-O bonds lead to the strengthening of the glassy network[107][108][109][110][111].

Sodium metal oxides act as network modifiers in borate-based glass systems, thereby increasing the electrical resistivity, strength, optical transparency and chemical resistance of the glass system to which it is introduced. It also stabilizes the glass through its network modifying effect and allows the shielding capability to be easily investigated. With its addition to the glass system, the melting temperature and crystallization rate of the system decreases[107][110][111][112][113].

Doping of Dy^{3+} ions into glass gives it a wide emission range. The processing of the glass system doped with RE element becomes easier and its thermal stability increases. There are studies indicating that Dy^{3+} ion enhances the optical and electrical properties of the doped glass[93][96][98][99][114][115].

2.7 Radiation Shielding Parameters

Radiation shielding is a method applied to reduce the harmful effects of radiation on the environment and living things and to control radiation. Several parameters are considered to evaluate the properties, design and efficiency of the materials to be used for shielding. These parameters, called radiation shielding parameters, are used to measure and analyze the extent to which the applied radiation is absorbed, energy transfer transitions or chemical/physical properties of the material used. Linear attenuation coefficient (LAC), mass attenuation coefficient (MAC), half-value layer (HVL), tenth-value layer (TVL), mean free path (mfp), atomic cross section (ACS), electronic cross section (ECS), effective atomic number (Z_{eff}), effective electron densities (N_{eff}), effective conductivity (C_{eff}, equivalent atomic number (Z_{eq}), exposure build-up factor (EBF), and energy absorption build-up factor ($EABF$) are the radiation shielding parameters. It is desired that the material selected as shielding material should have low cost, high chemical/physical durability, and high density. With the correct values of the shielding parameters, it is possible to reach the material with the required properties. Therefore, understanding and application of the parameters is critical in the field of radiation protection[116].

3
MATERIALS AND METHODS

3.1 Properties of Glass Samples

For sample preparation and measurement, four different glass samples with the composition of $23CaO - 10Al_2O_3 - (50 - x)B_2O_3 - 6BaO - 10Na_2O - xDy_2O_3$ and x = 0.1, 0.3, 0.5, and 1.0 mol% were synthesized by classical melt-quenching technique, as outlined in the referenced research Gurav et al., 2024[95]. The components of the glass samples synthesized by the melt quenching method in the composition of $23CaO - 10Al_2O_3 - (50 - x)B_2O_3 - 6BaO - 10Na_2O - xDy_2O_3$ were ground in a mortar and pestle until weighed as 15g with an electronic balance and mixed until homogenized. It was heated in an electric furnace at 1150°C for three hours to melt completely. It was then annealed at 500°C for the whole day to avoid thermal stress and then allowed to cool gradually to ambient temperature. A portion of each of the cooled glass samples was ground into fine powder and used for characterization studies. Table 3.1 shows the coding and chemical compositions of four different glass samples[95]. The coding of the samples was done in the form of sample numbering.

Table 3.1 Sample codes and chemical compositions of glass sample components (Gurav et al., 2024)[95].

Chemical compositions (in mol%)						
Sample Codes	CaO	Al_2O_3	B_2O_3	BaO	Na_2O	Dy_2O_3
S1	23	10	50.9	6	10	0.1
S2	23	10	50.7	6	10	0.3
S3	23	10	50.5	6	10	0.5
S4	23	10	50.0	6	10	1.0

The density of the samples was measured using the Archimedes principle. Distilled water was used as immersion liquid. The density calculations of the samples were made according to Equation 3.1[117] and the calculated densities are given in Table 3.2[95]. The refractive indices of the samples were measured using a digital Abbe refractometer.

$$\rho = \frac{W_a}{W_a - W_l} \times \rho_l \, gm \, cm^{-3} \tag{3.1}$$

W_a and W_l are glass samples' weights in air and liquid respectively, ρ_l is density of the liquid and from the Equation 3.1 the molar volume (V_m) can be calculated with the Equation 3.2[117] below.

$$V_m = \frac{M}{\rho} cm^3 mol^{-1} \tag{3.2}$$

M: molecular mass of the sample.

The average boron-boron separation, which describes the effect of the dopant ion (Dy^{3+}) concentration in the glass composition, is calculated by Equation 3.3[117].

$$d_{B-B} = \frac{V^B{}_m}{N_A} \; ions \; cm^{-3} \tag{3.3}$$

N_A is the Avogadro's number and $V^B{}_m$ refers to the volume containing one mole of boron in the resulting network and calculated as

$$V^B{}_m = \frac{V_m}{2(1 - X_P)} \tag{3.4}$$

Here, X_P is the molar fraction of B_2O_3.

Table 3.2 Sample codes and densities (Gurav et al., 2024)[95].

Sample Codes	Density (g/cm^3)
S1	2.4738
S2	2.1746
S3	2.9603
S4	2.8424

The structural phase of four different glass samples was determined by X-ray diffraction (XRD) analysis. X-ray diffraction studies of the glass samples were carried out in the range of 2θ=10-100° and the glass samples obtained were found to be amorphous[95].

Structural and dynamic characterization of four different glass samples were carried out by Fourier Transform Infrared spectroscopy (FTIR) technique. FTIR analyses were performed in the wave number range 4000-500 cm^{-1} at room temperature[95].

The optical absorption spectra of four different glass samples were recorded at room temperature in the wavelength range 300-2000 nm using Shimadzu 3600 UV-VIS-NIR spectrofotometer.[95].

Photoluminescence (PL) measurements were performed using the Agilent Cary Eclipse spectrofluorometer. The photo-excitation spectra of the samples were recorded in the wavelength range of 250-550 nm, while for photo-emission the wavelength range of 400-700 nm was used [95].

For the determination of the radiation shielding parameters of the samples, ionising radiation shielding parameters were calculated using Phy-X/PSD software with the density values (Table 3.2) identified for four different glass samples. Phy-X/PSD software is a platform that enables fast and error-free simultaneous calculation of radiation shielding parameters for different material types in desired energy ranges[118].

3.2 Determination of Radiation Shielding Parameters of Glass samples

3.2.1 Linear Attenuation Coefficient

Linear attenuation coefficient (μ) is a radiation shielding parameter that indicates the rate at which radiation is attenuated as it passes through the material and is calculated by Lambert-Beer Law Equation[87]:

$$I = I_0 \; x \; e^{-\mu x} \tag{3.4}$$

The terms of

I_0 is the incident radiation intensity,

I is the attenuated radiation intensity after pass through an absorber of thickness x, and

μ (cm^{-1}) is the linear radiation attenuation coefficient.

LAC is related to the composition of the absorbing material and the energy of the incident photon. The LAC value increases with increasing density and atomic number of the absorber and decreases with increasing energy of the incident photon. Since the density of the material can vary greatly, its evaluation together with other parameters gives more favorable results[67][68][119][120][121].

3.2.2 Mass Attenuation Coefficient

MAC, μ_m (cm^2/g), is the absorption rate of the incident photon per unit mass of the medium[122]. According to Equation 2.7[87] it can be expressed as

$$\mu_m = \frac{\mu}{\rho} \tag{3.5}$$

where ρ is the density of the material.

Increasing the density of the material increases the amount of absorbed radiation. Therefore, higher MAC values mean that radiation is blocked more effectively[68][123][124].

3.2.3 Half-Value Layer

Half-value layer (HVL) is the absorber thickness parameter used to half the radiation intensity[75]. It is the value of the absorber thickness required to reduce the intensity of the incident photon beam to half of its initial value and from the Equation 2.8[18],

$$\frac{I}{I_0} = \frac{1}{2} = e^{-\mu x 1/2} \tag{3.6}$$

which can be solved for $x_{1/2}$ to yield

$$x_{1/2} = HVL = \frac{\ln 2}{\mu} = \frac{0.693}{\mu} \tag{3.7}$$

Therefore, the radiation exposure rate will also decrease by 50%. The HVL value increases as the energy of the incident photon increases, while the HVL value of materials with high atomic number is smaller[67][124].

3.2.4 Tenth-Value Layer

The tenth value layer (TVL) is the value of the absorber thickness required to reduce the intensity of the incident photon beam to one tenth of its initial value[68][123] and from the Equation 2.10[18] is equal to:

$$TVL = \frac{\ln 10}{\mu} = \frac{2.303}{\mu} \tag{3.8}$$

3.2.5 Mean-Free Path

The mean free path (mfp) is the average distance traveled by the photon as it interacts with the atoms of the material and calculated as shown in Equation 2.11[75].

$$mfp = \frac{1}{\mu} \tag{3.9}$$

The mfp value is directly related to the thickness of the absorber material. Increasing the thickness of the absorber means that fewer photons will pass through the material, thus increasing the effectiveness of the shielding[99][116][123].

3.2.6 Atomic Cross Section

Atomic cross section (ACS) is the parameter that indicates how much of the incident radiation is absorbed per atom per unit volume of absorber[123] and for any compound can be obtained by the Equation 2.12[116].

$$ACS = \sigma_a = \frac{N}{N_A}(\mu/\rho) \tag{3.10}$$

where,

N is the atomic weight and N_A is the Avogadro number.

3.2.7 Electronic Cross Section

Electronic cross section (ECS) is the parameter that indicates how much of the incident radiation is absorbed per electron per unit volume of the absorber[123] and calculated using the formula in Equation 2.13[116].

$$ECS = \sigma_e = \frac{\sigma_a}{Z_{eff}} \tag{3.11}$$

3.2.8 Effective Atomic Number

Effective atomic number (Z_{eff}) is an important parameter for radiation dosimetry[87][116][123] and is calculated using Equation 2.12 and Equation 2.13[124] as follows:

$$Z_{eff} = \frac{\sigma_a}{\sigma_e} \tag{3.12}$$

3.2.9 Effective Electron Densities

Effective number of electrons (N_{eff}), is the number of electrons of the interacting material[87][116][120][122] and calculated using the equation formulated as:

$$N_{eff} = \frac{\mu_m}{\sigma_e} \tag{3.13}$$

3.2.10 Effective Conductivity

Effective conductivity (C_{eff}) indicates how much free electrons are actualized in the material[123] and can be calculated by the following Equation 2.16[116].

$$C_{eff} = (\frac{N_{eff}\rho e^2 \tau}{m_e})10^3 \tag{3.14}$$

where e is the charge of the electron, τ is the average lifetime of the electron and m is the mass of the electron (kg).

The C_{eff} value is related to the absorber density, N_{eff} value and ambient temperature[116].

3.2.11 Equivalent Atomic Number

The equivalent atomic number (Z_{eq}), an energy-dependent parameter that describes the interaction properties of the selected glass system in terms of equivalent elements, is calculated by the following formula[120]:

$$Z_{eq} = \frac{Z1\,(\log R2 - \log R) + Z2\,(\log R - \log R1)}{\log R2 - \log R1} \qquad (3.15)$$

Here, R is the (μComp/μtotal) ratio. $R1$ and $R2$ are the (μComp/μtotal) ratios of samples with atomic numbers $Z1$and $Z2$, respectively[125].

3.2.12 Exposure Build-up Factor and Energy Absorption Build-up Factor

Exposure build-up factor (EBF) is an important parameter for correcting attenuation calculations due to the effects of scattered radiation or secondary photons accumulated in the material as a result of Compton scattering[125][126]. The EBF value is high at intermediate energies (about at 0.1 MeV) where the Compton scattering is effective[126].

The energy absorption deposition factor ($EABF$) is the amount of scattered photons deposited in the thickness of the glass material[125][126]. In addition to the energy of the incident photon and the glass composition, it is also related to the material penetration capacity (mfp) value[126].

For EBF and $EABF$ calculations, the geometric fitting parameters (GP) are first calculated[120][125].

$$C = \frac{C1(logZ2 - \log Z_{eq}) + C2\,(\log Z_{eq} - \log Z1)}{\log Z2 - \log Z1} \qquad (3.16)$$

where $C1$ and $C2$ are the GP parameters. Using the GP parameters and the equations below, EBF and $EABF$ of the glass system can be calculated with following Equations[120][125] (2.19 and 2.20).

$$B(E,X) = 1 + \left(\frac{b-1}{K-1}\right)(K^x - 1)\; for\; K \neq 1 \qquad (3.17)$$

$$B(E,X) = 1 + (b-1)x\; for\; K = 1 \qquad (3.18)$$

where K is the photon dose multiplication factor and E is the incident photon energy. x is the distance from the ambient source to the detector in mfp units, and b is the build-up factor at 1 mfp[126]. Where,

$$K\ (E,x) = cx^{a} + d\,\frac{\tanh\left(\frac{x}{X_K} - 2\right) - \tanh(-2)}{1 - \tanh(-2)}\ for\ x \le 40\ mfp \tag{3.19}$$

and

$$R_{dd} = \frac{\exp(-\mu x)\,(EBF)}{x^{2}} \tag{3.20}$$

$$R_{dd} = \frac{\mu_{abs}\exp(-\mu x)\,(EABF)}{4\pi\rho x^{2}} \tag{3.21}$$

Here, E is the photon energy, x is the penetration depth, (b, c, a , d, X_K) are GP fitting coefficients, R_{dd} is the relative dose distribution and μ_{abs} is linear absorption coefficient[120][125].

4
RESULTS

In this thesis, a comprehensive analysis of the gamma ray shielding properties of four different glass samples has been performed. This chapter presents the Phy-X/PSD results and the analysis of the shielding parameters of the glass system represented as $23CaO - 10Al_2O_3 - (50 - x)B_2O_3 - 6BaO - 10Na_2O - xDy_2O_3$ (where x =0.1, 0.3, 0.5, and 1.0%mol).

4.1 LAC

The LAC values of the glass samples were analyzed against photon energies ranging between 10^{-3}-10^{5} MeV as shown in Figure 4.1. Photons lose their energy by interacting with the orbital electrons of the absorbing atom. The result of these interactions can be either complete absorption of the photons or absorption of some of them and scattering of the rest.

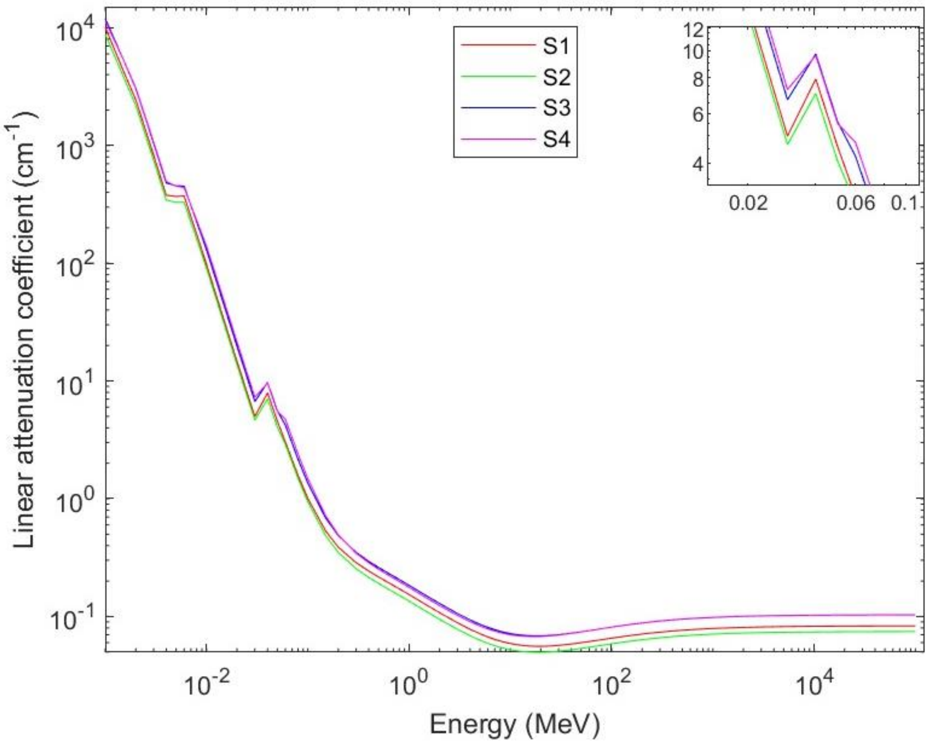

Figure 4.1 The changes of LAC values of glass samples as a function of incident photon energy

Low energy photons (e.g 0.1 MeV) show a marked sensitivity to the photoelectric effect and the probability of interaction increases with increasing atomic number. For medium and high energy photons, this interaction is replaced by Compton scattering. At photon energies exceeding 1.02 MeV, pair formation is also observed. Based on all these interactions, it is possible to assume that the LAC will show changes at different energy levels depending on the photon energy.

Figure 4.1 shows the change in the linear attenuation coefficients in response to the energy of the incident photon. From the graph, it can be said that all glass system samples show similar LAC fluctuations with increasing photon energy. For all systems, a sharp decrease in the LAC value is observed in the 0.001-0.1 MeV region where the photoelectric effect is dominant. In the 0.1 MeV-1 MeV energy region (Compton region), this sharp decrease is replaced by a gradual and smoother decrease. At energies exceeding 1.02 MeV, pair formation occurred, and LAC values started to increase.

In this study, there are two important factors for the LAC. One of these factors is the concentration differences of substances within the glass samples, and the other is the density of the glass samples. As the density of the material increases, the LAC value is expected to increase because the probability of photon interactions within the material is higher for denser materials. When comparing the S3 and S4 glass samples, it is observed that S3 has a higher density (2.9603 g/cm^3) than S4 (2.8424 g/cm^3), while S4 has a higher Dy^{3+} concentration than S3. Therefore, in some energy ranges, the LAC value of the S3 glass sample is higher (e.g., around 1 MeV), while in some energy ranges (e.g., around 0.01 MeV), the LAC value of S4 is higher.

When comparing the S1 and S4 samples, it is observed that the S4 glass sample has both a higher density and a higher Dy^{3+} concentration than S1. Due to the higher values of both these properties, the LAC of S4 is observed to be higher than that of S1 across all energy ranges.

From the results, it can be said that the LAC value for the $23CaO - 10Al_2O_3 - (50-x)B_2O_3 - 6BaO - 10Na_2O - xDy_2O_3$ glass system decreases when the energy of the incident photon is increased and rises when the density of the system is raised. At the same time, since different LAC values are obtained at different Dy^{3+}

concentrations, the gamma photon attenuation ability of Dy^{3+} can be mentioned. Doping the system with Dy^{3+} increases the LAC value, making the system a better shielding material.

4.2 MAC

The radiation attenuation rate is related to the mass of the material, but the determinant here is the mass of the material in relation to the entire cross-sectional area rather than the mass of the material. While the LAC value is related to the material density, MAC is a density independent shielding parameter. Figure 4.2 shows the change in the mass attenuation coefficients as a function of varying energies of the photon in the energy range 10^{-3}-10^{5} MeV.

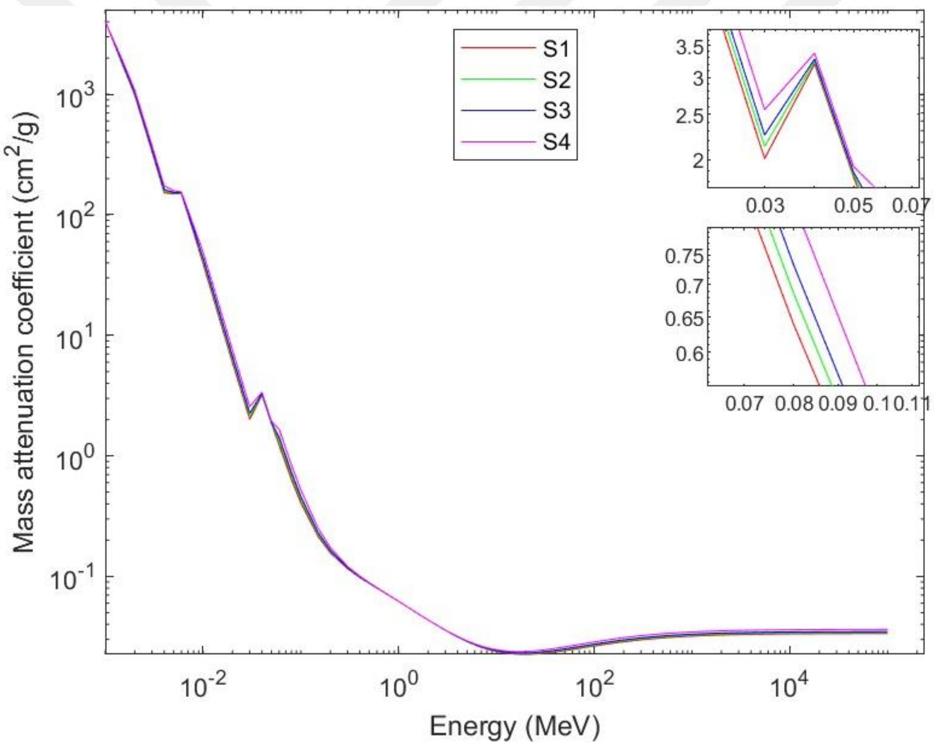

Figure 4.2 The changes of MAC values of glass samples as a function of incident photon energy

The MAC value obtained by dividing the LAC values by the density of the material is similar to the LAC graph. For all glass samples, there is a sharp decrease in the MAC value in the low energy region where the photoelectric effect is dominant. When it is replaced by Compton interactions at medium energy levels, a decrease in MAC value is observed with a smoother decrease due to the increase in energy. In high energy regions, an increase in MAC values were observed as a result of pair formation. The highest MAC value in most energy ranges in the glass samples examined was observed in the S4 glass sample, which had the highest Dy^{3+} concentration.

The results show that the MAC value is related to both the incident photon energy and the chemical composition of the glass samples. As can be seen in Figure 4.2, high MAC values are observed in low energy regions for all glass samples. The increase in the mass per unit of the material allows it to absorb radiation better. The increase in the MAC value with increasing Dy^{3+} concentration in the samples can be attributed to the large mole fraction of another material (here Dy^{3+}) with a higher atomic number than the mole fraction of the material components.

In conclusion, the addition of Dy^{3+} to the $23CaO - 10Al_2O_3 - (50 - x)B_2O_3 - 6BaO - 10Na_2O - xDy_2O_3$ glass system increased the shielding ability of the glass system.

4.3 HVL

HVL is the parameter that indicates the minimum thickness of the material to be used for radiation shielding in order to reduce its intensity by half the amount of incoming photon radiation. Figure 4.3 shows the change in HVL values of four different glass samples examined in response to the energy of the incident photon (10^{-3}-10^{5} MeV).

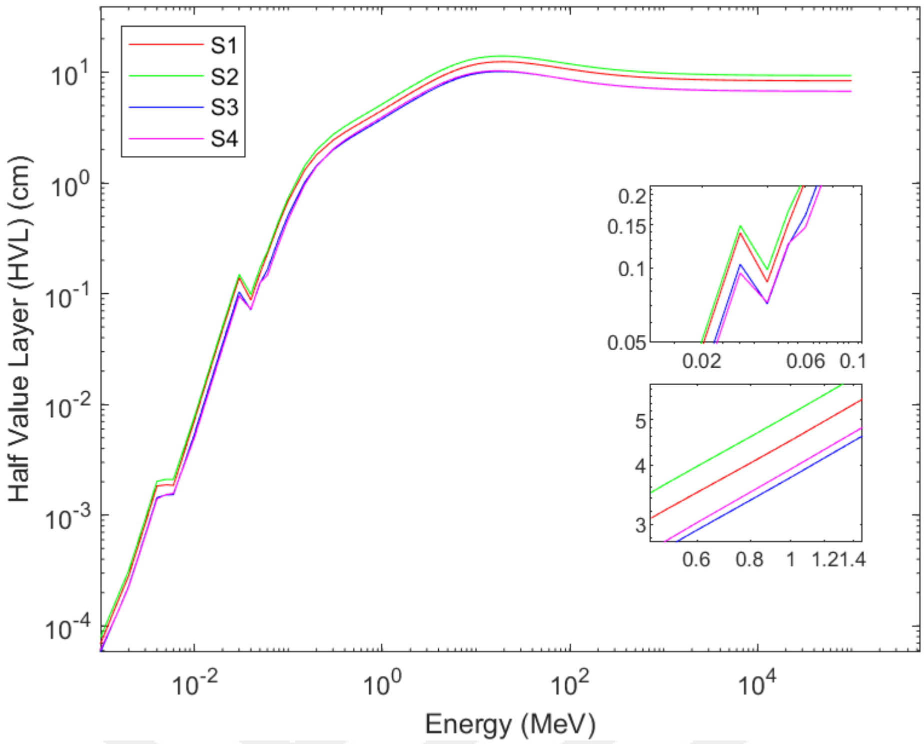

Figure 4.3 The changes of HVL values of glass samples as a function of incident photon energy

From the graph (Figure 4.3), it can be said that all glass system samples show similar HVL fluctuations with increasing energy of the photon. At low energy levels, HVL values have small thicknesses for all glass systems, while these values increase with increasing energy level. This means that as the energy of the photon increases, the radiation can penetrate the glass samples more easily. For the HVL shielding parameter, which has an inverse relationship with the LAC parameter, it is predicted that a low value at high energy levels will be a better shielding material. It can be said that increasing concentrations of Dy^{3+} cause a decrease in the HVL value.

The results show that the S4 glass sample with the highest Dy^{3+} concentration shows the highest LAC value although it has the lowest HVL value. For example, at 0.1 MeV, the HVL values for S1, S2, S3 and S4 glasses are 0.688, 0.736, 0.511, 0.469 cm, respectively.

Since the HVL is related to attenuation, both the density of the glass sample and the concentration of Dy^{3+} within the material affect the HVL value. When comparing the S3 and S4 glass samples, it is observed that S3 has a higher density, while S4 has a higher Dy^{3+} concentration than S3. Consequently, in some energy ranges, the

HVL value of the S3 sample is higher (e.g., around 100 MeV), while in other energy ranges (e.g., around 3 MeV), the HVL value of S4 is higher. When comparing the S1 and S4 samples, it is noted that the S4 glass sample has both a higher density and a higher Dy^{3+} concentration than S1. Due to the higher values of both these properties, the HVL of S4 is observed to be less than that of S1 across all energy ranges.

As a result, the addition of Dy^{3+} to the $23CaO - 10Al_2O_3 - (50 - x)B_2O_3 - 6BaO - 10Na_2O - xDy_2O_3$ glass system increased the shielding ability of the glass system.

4.4 TVL

TVL is the parameter that shows the minimum thickness required to reduce the intensity of the material to be used for radiation shielding by reducing the amount of incoming photon radiation to one-tenth. Figure 4.4 shows the change in TVL values of four different glass samples examined in response to the energy of the incident photon (10^{-3}-10^{5} MeV).

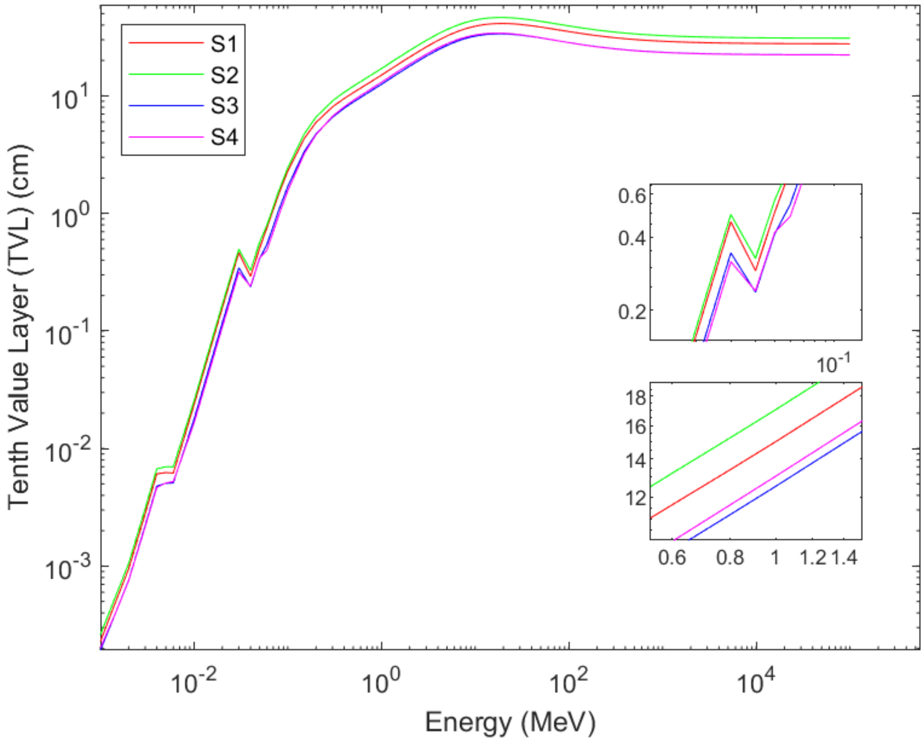

Figure 4.4 The changes of TVL values of glass samples as a function of incident photon energy

From the graph (Figure 4.4), it can be said that all glass system samples show similar TVL fluctuations with increasing photon energy. While TVL values at low energy levels have small thicknesses for all glass systems, these values increase with increasing energy level. This means that as the energy of the photon increases, radiation can penetrate the glass samples more easily. The TVL parameter, which shows similar shielding properties with HVL, has an inverse relationship with the LAC parameter. For the TVL value, it is predicted that a low value at high energy levels will be a better shielding material. It can be said that increasing concentrations of Dy^{3+} cause a decrease in the TVL value.

As a result, the addition of Dy^{3+} to the $23CaO - 10Al_2O_3 - (50 - x)B_2O_3 - 6BaO - 10Na_2O - xDy_2O_3$ glass system increased the shielding ability of the glass system.

4.5 MFP

mfp refers to the distance travelled by the radiation in the material during interactions. Therefore, a decrease in the mfp value means a shorter distance during successive interactions. Figure 4.5 shows the change in the average free path value of the glass samples as a function of the photon's energy ranging from 10^{-3}-10^{5} MeV.

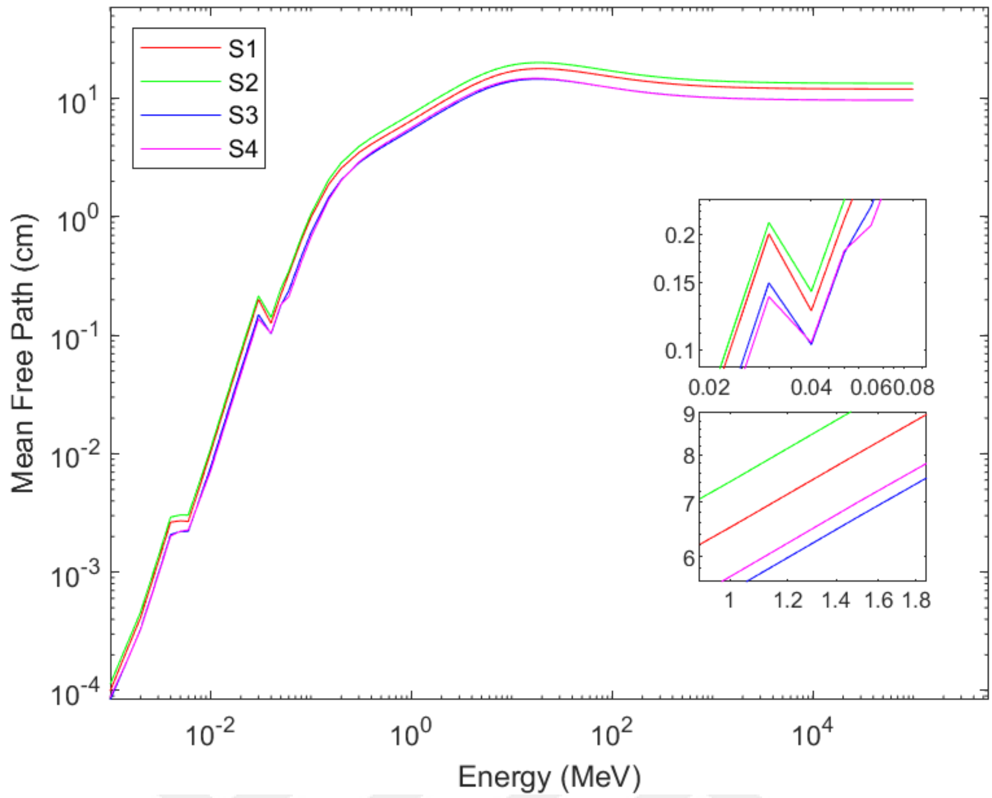

Figure 4.5 The changes of mfp values of glass samples as a function of incident photon energy

It is seen from the graph (Figure 4.5) that the mfp values increase similarly with the increase in photon energy for all glass system samples. While mfp values at low energy levels have short distance values for all glass systems, these values increase with increasing energy level. This can be attributed to the fact that low energy photons lose their energy over a short distance, while high energy photons lose their energy over a longer distance. The scattering probability of the photon increases as it moves from medium energy levels to high energy levels. Therefore, thicker materials will be needed for shielding since their absorption probability will also be low. The response of mfp as a function of incident energy in relation to HVL and TVL values is similar to that of HVL and TVL (see Figure 4.3 and 4.4). For a better shielding material, a low value of mfp at high energies is desirable. The figure also shows that the mfp values of the glass samples decrease significantly with increasing Dy^{3+} concentration.

As a result, the smaller the mfp value, the shorter the distance between two consecutive interactions, and the radiation attenuation ability becomes important for the material of equivalent thickness. Among all glass samples, S4 glass sample with high Dy^{3+} concentration showed lower mfp value than other glass samples at most energy levels. mfp value alone can give information about the shielding ability of the material. The addition of Dy^{3+} to the $23CaO - 10Al_2O_3 - (50 - x)B_2O_3 - 6BaO - 10Na_2O - xDy_2O_3$ glass system increased the shielding ability of the glass system.

4.6 ACS

The ACS value expresses the probability of photon interaction per atom per unit volume of the shielding material. Therefore, it is directly related to the atomic weight of the material. Figure 4.6 shows the change in ACS values of four different glass samples examined in response to the energy of the incident photon (10^{-3}-10^{5} MeV).

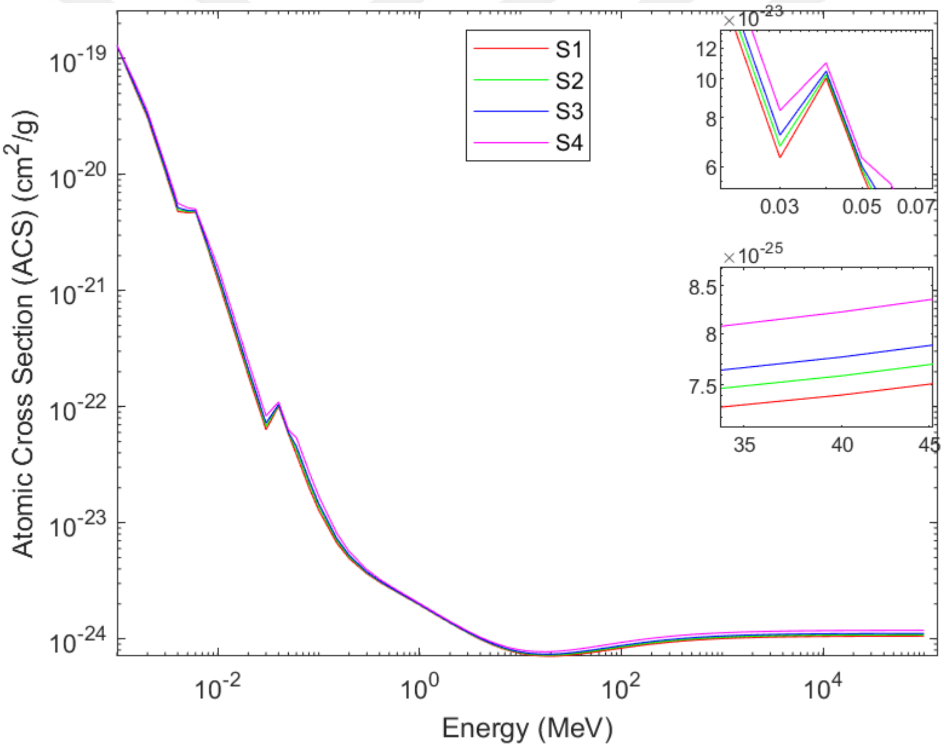

Figure 4.6 The changes of ACS values of glass samples as a function of incident photon energy

It can be seen from the graph (Figure 4.6) that for all glass system samples, while the incident photon energy increases, the ACS values are decreasing. Higher ACS value means that the material can absorb more rays per unit area and therefore the shielding ability of the material is better. The highest ACS values for all glass samples are observed at low energy levels (≤0.1 MeV) where the photoelectric effect is intense. Since the photoelectric effect depends on the atomic number of the element, it can be said that the shielding materials have higher ACS values by containing components with high atomic numbers. As can be seen from the graph, the decrease in the ACS value at medium energy levels, which is the Compton region, is smoothed compared to the sharp decrease at low energy levels. This is because the scattering in the Compton region has an inverse relationship with the photon energy.

As a result, it can be said that the ACS value is related to the energy of the incident photon and the chemical composition of the glass material, and the S4 glass sample with the highest Dy^{3+} concentration among all can samples shows higher ACS value than other glass samples at all energy levels. The addition of Dy^{3+} to the $23CaO - 10Al_2O_3 - (50 - x)B_2O_3 - 6BaO - 10Na_2O - xDy_2O_3$ glass system increased the shielding ability of the glass system.

4.7 ECS

The ECS value expresses the probability of photon interaction per electron per unit volume of the shielding material. Figure 4.7 shows the change in ECS values of four different glass samples examined in response to the energy of the incident photon (10^{-3}-10^{5} MeV).

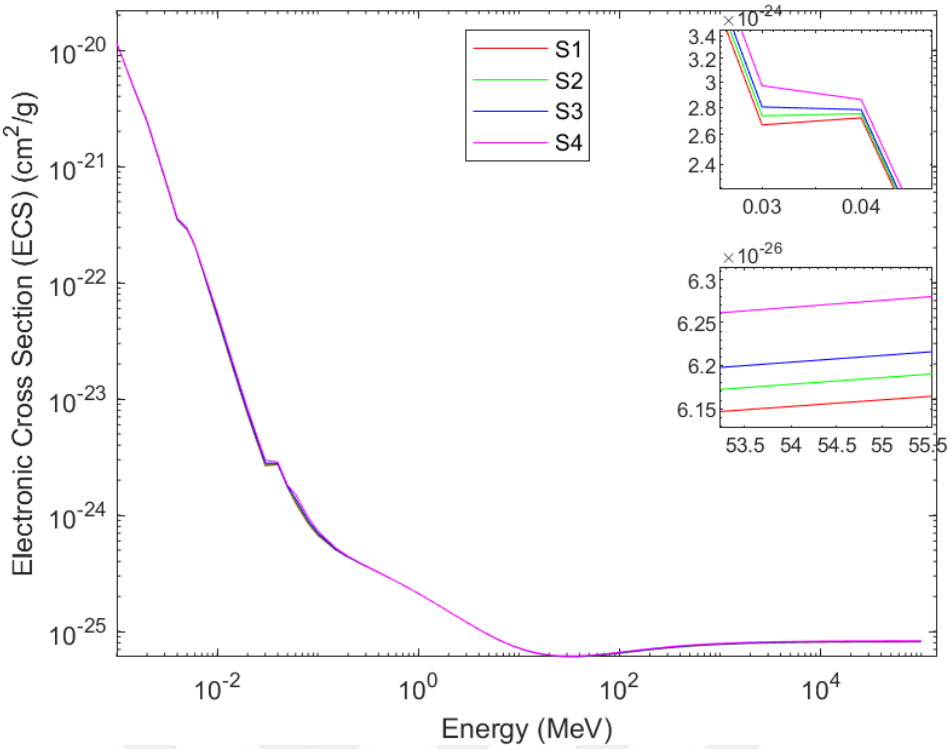

Figure 4.7 The changes of ECS values of glass samples as a function of incident photon energy

It is seen from the graph (Figure 4.7) that for all glass system samples, while the incident photon energy increases, the ECS values decrease. This is because the ECS value depends on the mass attenuation coefficient. The atomic number and density of the material do not directly affect the ECS value. However, as seen in the graph, the ECS value of the sample with the highest Dy^{3+} concentration in Dy^{3+} doped glass samples were the highest since the photoelectric effect at low energy levels and the pair formation at very high energy levels prefer elements with higher atomic numbers.

As a result, it can be said that the ECS graph is consistent with the MAC graph in Figure 4.2 as expected and the ECS value varies depending on the energy of the incident photon. It is seen that the S4 glass sample, which has the highest Dy^{3+} concentration among all glass samples, shows a higher ECS value than the other glass samples at all energy levels. The addition of Dy^{3+} to the $23CaO - 10Al_2O_3 - (50 - x)B_2O_3 - 6BaO - 10Na_2O - xDy_2O_3$ glass system increased the shielding ability of the glass system.

4.8 Z_{eff}

The change in the Z_{eff} values of the glass samples evaluated as a function of the incident photon energy (10^{-3}-10^{5} MeV) is shown in Figure 4.8.

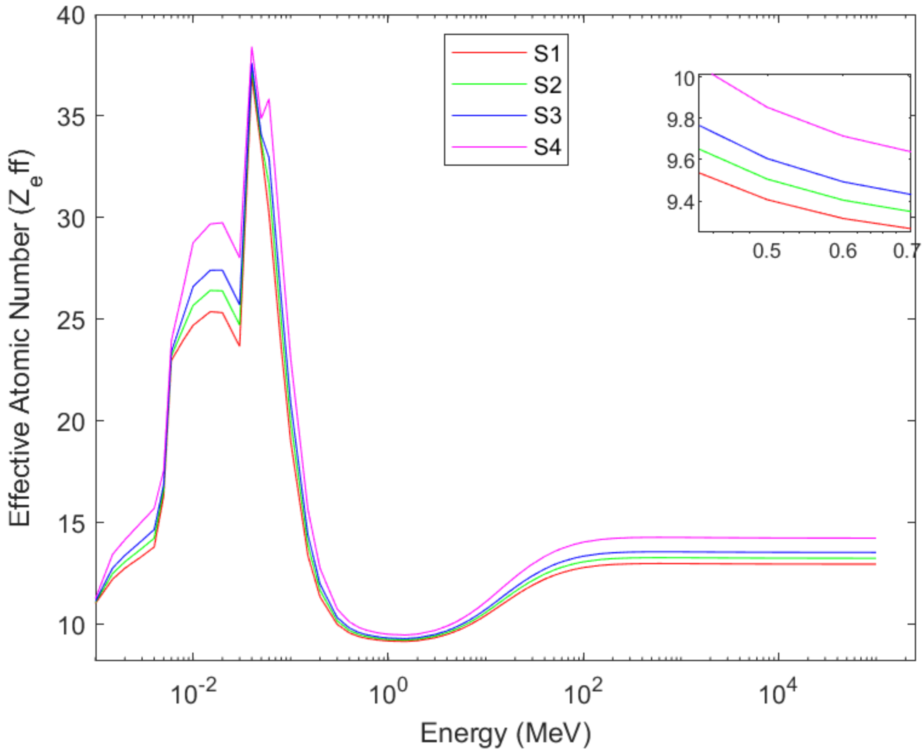

Figure 4.8 The changes of Z_{eff} values of glass samples as a function of incident photon energy

It is seen from the graph (Figure 4.8) that there are similar fluctuations in Z_{eff} values with the increase in photon energy for all glass system samples. According to the graph, the S4 glass sample has the highest Z_{eff} values, while the S1 sample with less Dy^{3+} doping has the lowest Z_{eff} value. This can be attributed to the fact that increasing the Dy^{3+} concentration leads to an increase in the Z value. For all glass samples, the energy region where Z_{eff} is highest is the low energy region (0.01-0.08 MeV) where the photoelectric effect is dominant. In the energy region where the photon is active (0.1-4 MeV), there are very small differences in the Z_{eff} values of the glass samples due to Compton interactions. As the energy of the incident photon increased further, the Z_{eff} values of the glass samples started to show large differences again since pair formation occurred.

As a result, it can be said that the Z_{eff} value depends on the energy of the incident photon and the chemical components of the glass material. Higher Z_{eff} values are observed at lower energy levels. When all glass samples were compared for all energy levels, S4 glass sample with the highest Dy^{3+} concentration was found to be the most suitable sample for shielding. The highest Z_{eff} value for S4 was measured as 38.40 at 0.04 MeV.

The addition of Dy^{3+} to the $23CaO - 10Al_2O_3 - (50 - x)B_2O_3 - 6BaO - 10Na_2O - xDy_2O_3$ glass system increased the shielding ability of the glass system.

4.9 N_{eff}

N_{eff} value shows the number of electrons interacting in the material. The change in the N_{eff} values of the studied glass samples as a function of the incident photon energy (10^{-3}-10^{5} MeV) is given in Figure 4.9.

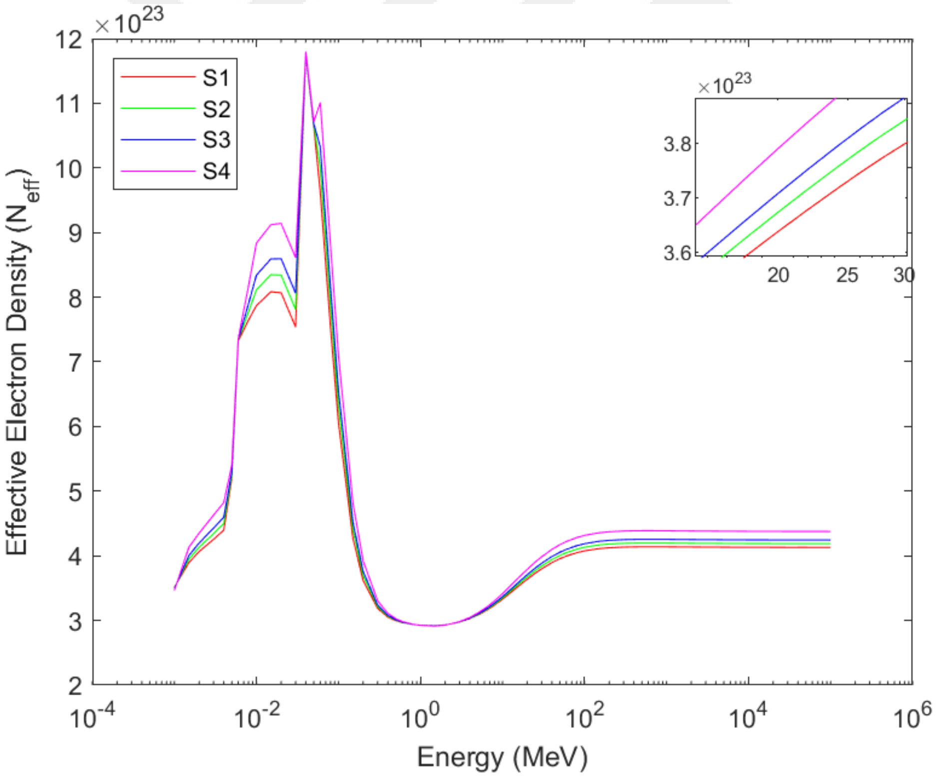

Figure 4.9 The changes of N_{eff} values of glass samples as a function of incident photon energy

It can be seen from the graph (Figure 4.9) that there are similar fluctuations in N_{eff} values with increasing photon energy for all glass system samples. The N_{eff} values of the glass samples at different concentrations are less pronounced compared to the Z_{eff} fluctuations, as the results are closer to each other. According to the graph, the S4 glass sample has the highest N_{eff} value, while the S1 sample has the lowest N_{eff} value. For all glass samples, the low energy region (0.01-0.08 MeV) where the photoelectric effect is dominant is the energy region with the highest N_{eff}. It is seen that there is a slight difference in the N_{eff} values of the glass samples in the energy region (0.1-4 MeV) where the Compton is effective due to Compton interactions. This situation reverses again when the energy of the incident photon increases further, and the pair formation region is reached. As a result, it can be said that the N_{eff} value depends on the energy of the incident photon. For all energy values, the N_{eff} value of the S4 glass sample with the highest Dy^{3+} concentration is higher than the other samples, and a sharp decrease is observed in all glass samples at the energy level exceeding $6x10^{-2}$ MeV. The high N_{eff} value of the glass sample means that the radiation shielding ability of the sample is better.

The addition of Dy^{3+} to $23CaO - 10Al_2O_3 - (50 - x)B_2O_3 - 6BaO - 10Na_2O - xDy_2O_3$ glass system increased the shielding capabilities of the glass system.

4.10 C_{eff}

The C_{eff} value expresses the number of free electrons produced in the glass material. The C_{eff} value varies proportionally to the number of effective electrons per gram at room temperature. Figure 4.10 shows the C_{eff} values of glass samples at 300K depending on the energy of the incident photon (10^{-3}-10^{5} MeV).

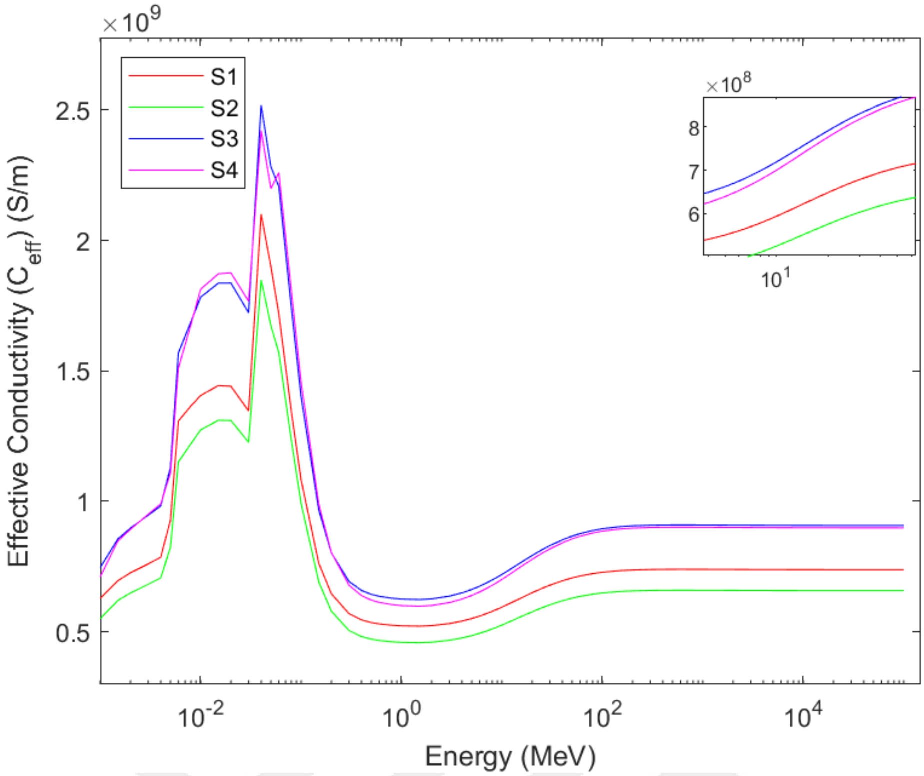

Figure 4.10 The changes of C_{eff} values of glass samples as a function of incident photon energy

It is seen from the graph (Figure 4.10) that there are similar fluctuations in C_{eff} values with increasing photon energy for all glass system samples. At all energy levels, the S3 glass has the highest C_{eff} values and S4 glass sample has very close results with S3 sample. This is because C_{eff} value is directly related to the system's density. S3 has a higher density (2.9603 g/cm^3) than S4 (2.8424 g/cm^3), while S4 has a higher Dy^{3+} concentration than S3. C_{eff} value also related to N_{eff} value. When the C_{eff} plot is compared with the N_{eff} plot in Figure 4.9, it is seen that the C_{eff} and N_{eff} fluctuations are similar for energy and concentration changes, but the C_{eff} values are smaller than the N_{eff} values. C_{eff} values show a sharp decrease in the middle energy level due to the dominance of Compton scattering. In addition, it is observed that C_{eff} values increase with the increase in Dy^{3+} concentration.

As a result, it can be said that the C_{eff} value varies depending on the energy of the incident photon and system's density. The C_{eff} value varies depending on the N_{eff} value, the effective electron number per gram, the density of the system and the ambient temperature. The higher C_{eff} value of the glass sample means that it is a better radiation shielding material. The addition of Dy^{3+} to the $23CaO -$

$10Al_2O_3 - (50-x)B_2O_3 - 6BaO - 10Na_2O - xDy_2O_3$ glass system increased the shielding ability of the glass system.

4.11 Z_{eq}

The change in Z_{eq} value of four different glass samples against increasing energies of the incident photon (10^{-3}-10^{5} MeV) is shown in Figure 4.11.

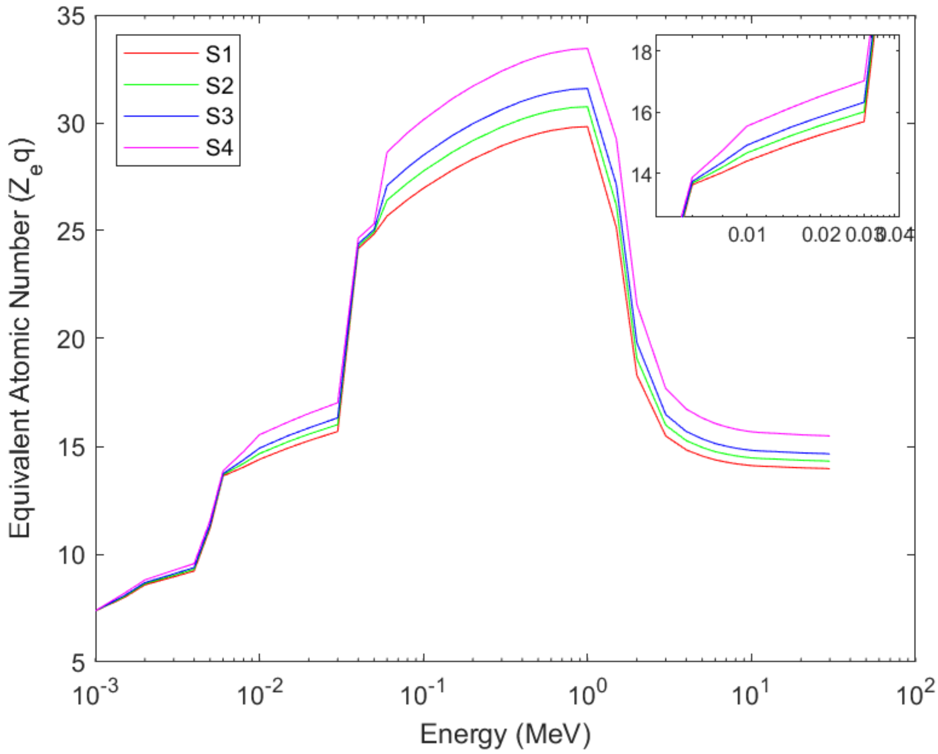

Figure 4.11 The changes of Z_{eq} values of glass samples as a function of incident photon energy

As seen from the graph (Figure 4.11), there is a sharp increase in the Z_{eq} value at low energy levels (0.006-0.06 MeV). This increase is followed by a slight decrease in the compton region and a sharp decrease at high energies. At the same time, with the addition of Dy^{3+} to the glass system, the highest Z_{eq} value was observed in the S4 sample with the highest Dy^{3+} concentration at all energy levels. As a result, it can be said that Z_{eq} is proportional to the atomic numbers of the material components and materials with high Z_{eq}values are better radiation shielding materials. At $4x10^{-2}$ MeV, the highest Z_{eq}values measured for S1, S2, s3 and S4 glass samples are 36.93, 37.27, 37.60 and 38.40 respectively. The S4 sample with the highest Dy^{3+} concentration consistently exhibited the largest Z_{eq} at various photon energies. The addition of Dy^{3+} to the $23CaO - 10Al_2O_3 - (50 - x)B_2O_3 - 6BaO - 10Na_2O - xDy_2O_3$ glass system enhanced the shielding ability of the glass system.

4.12 EBF and EABF

EBF is the number of scattered or secondary-energy photons deposited in the material as a result of the interaction of photons with the material, while $EABF$ is the number of photons deposited in the thickness of the glass being used. Both EBF and $EABF$ are important parameters that provide information about the interaction of photons with the material and surrounding atoms.

Exposure build-up factor (EBF) and energy absorption build-up factor ($EABF$) values for six different glass samples at different penetration depths (0.5mfp to 40mfp) were calculated using the GP fitting method. The EBF and $EABF$ values for glass samples containing different concentrations of Dy^{3+} examined against the energy of the incident photon (10^{-3}-10^{2} MeV) are shown separately in Figure 4.12 to Figure 4.15.

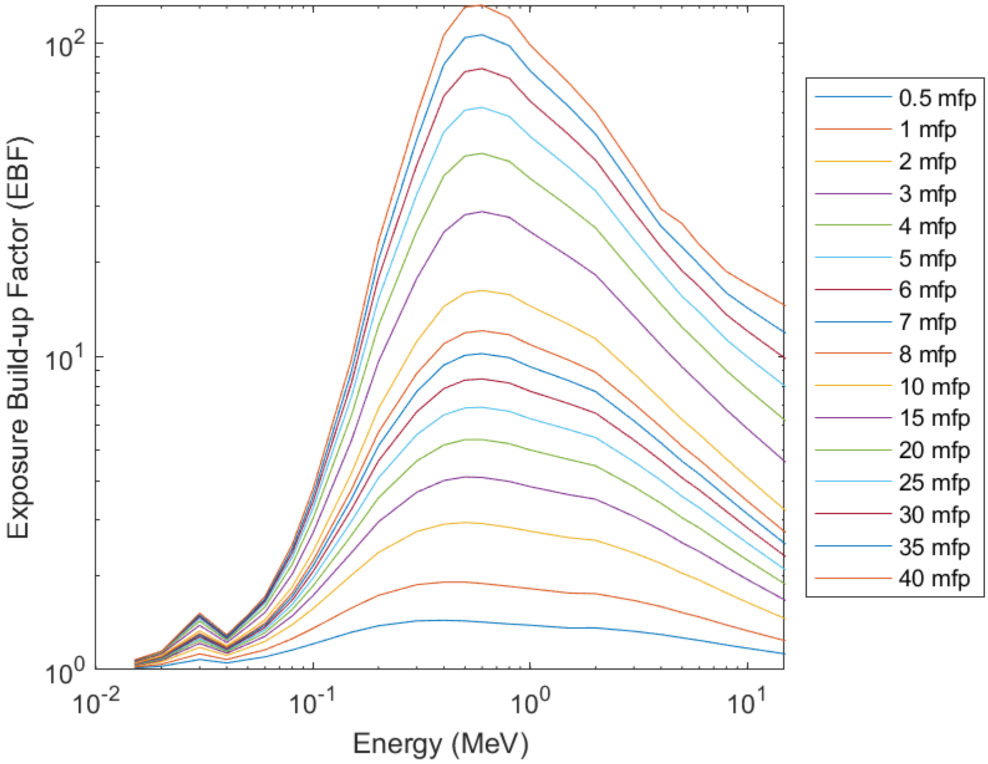

a

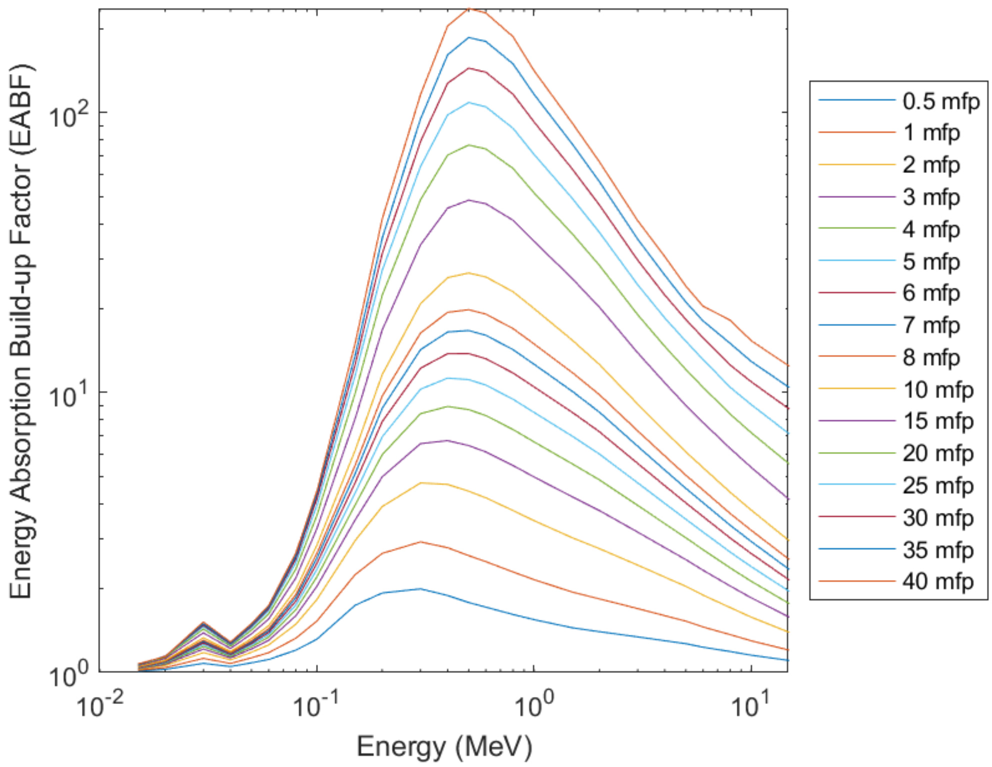

b

Figure 4.12 Variations of EBF (a) and $EABF$ (b) with photon energy at different mean free paths for S1 glass sample

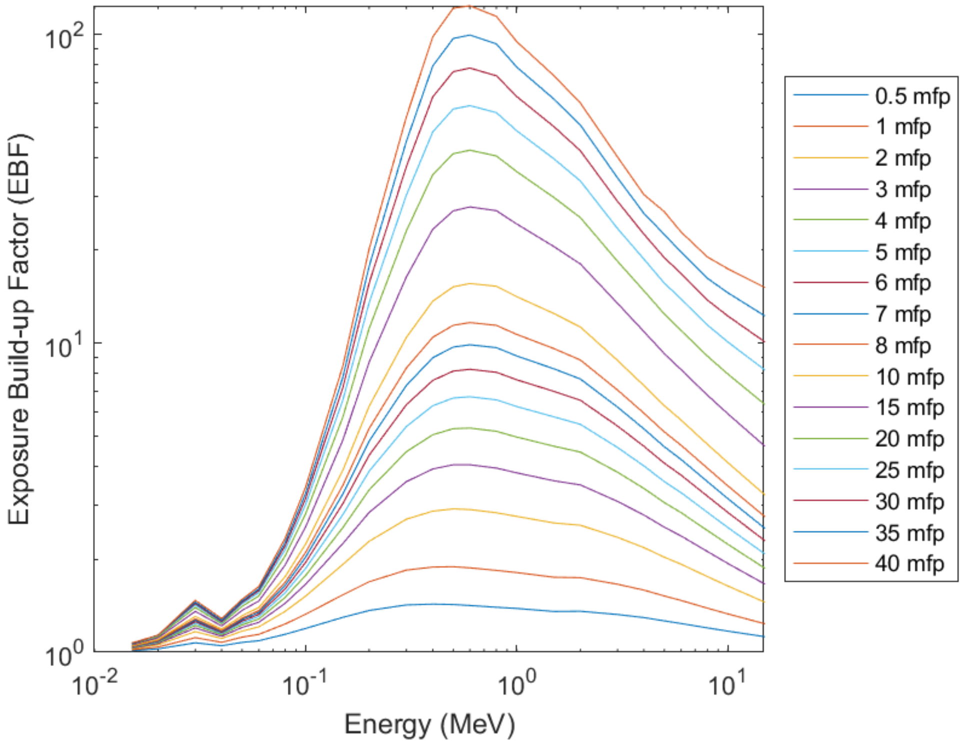

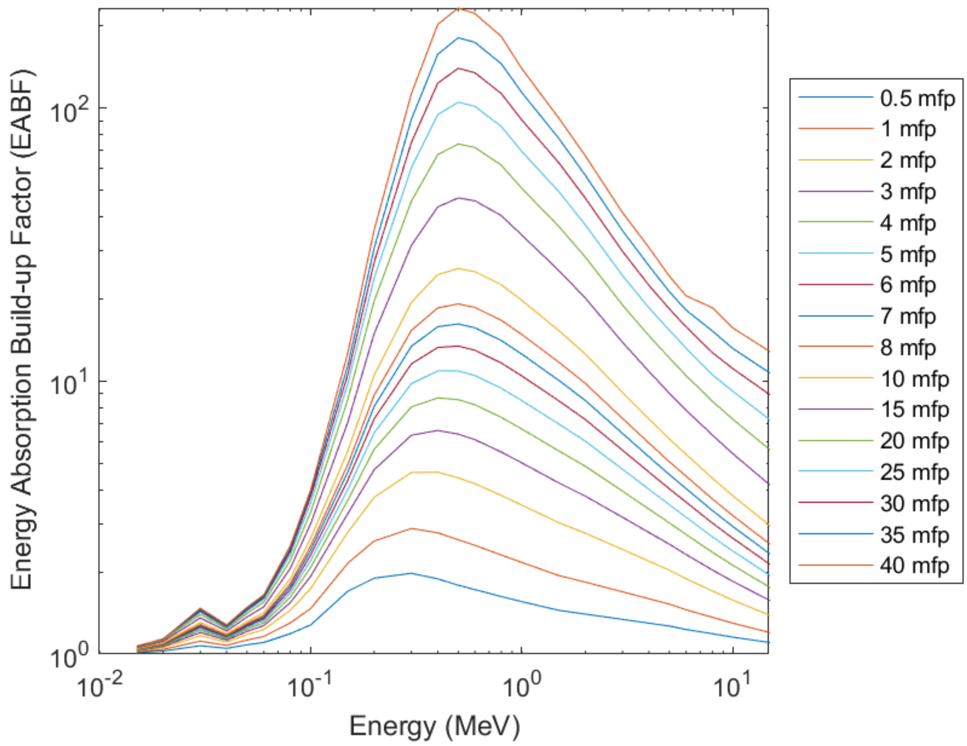

b

Figure 4.13 Variations of EBF (a) and $EABF$ (b) with photon energy at different mean free paths for S2 glass sample

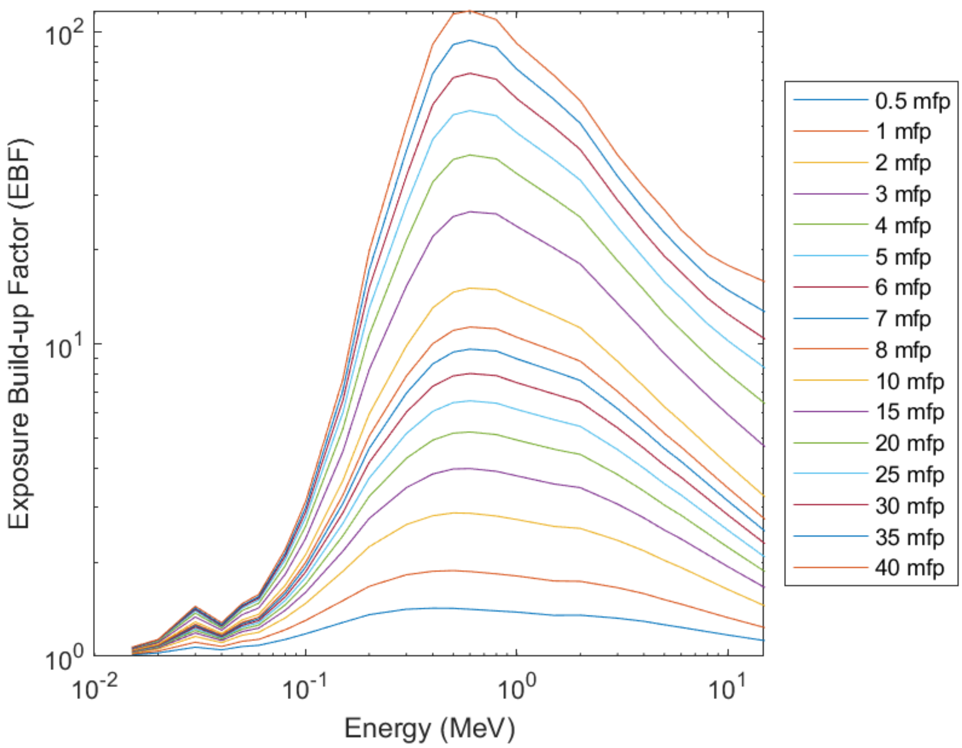

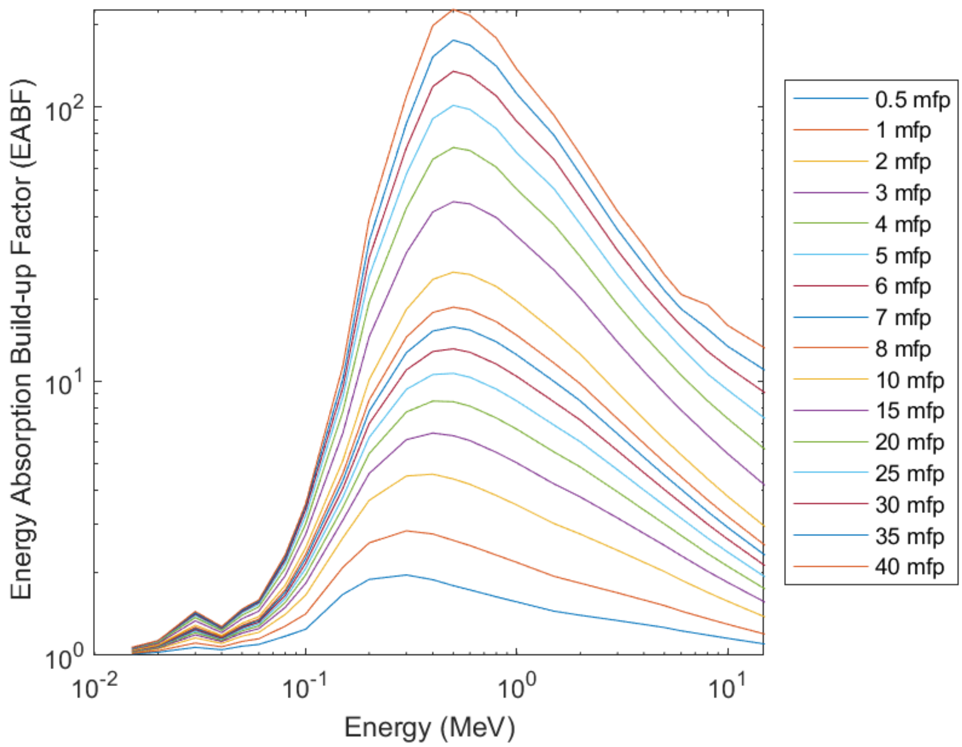

b

Figure 4.14 Variations of EBF (a) and $EABF$ (b) with photon energy at different mean free paths for S3 glass sample

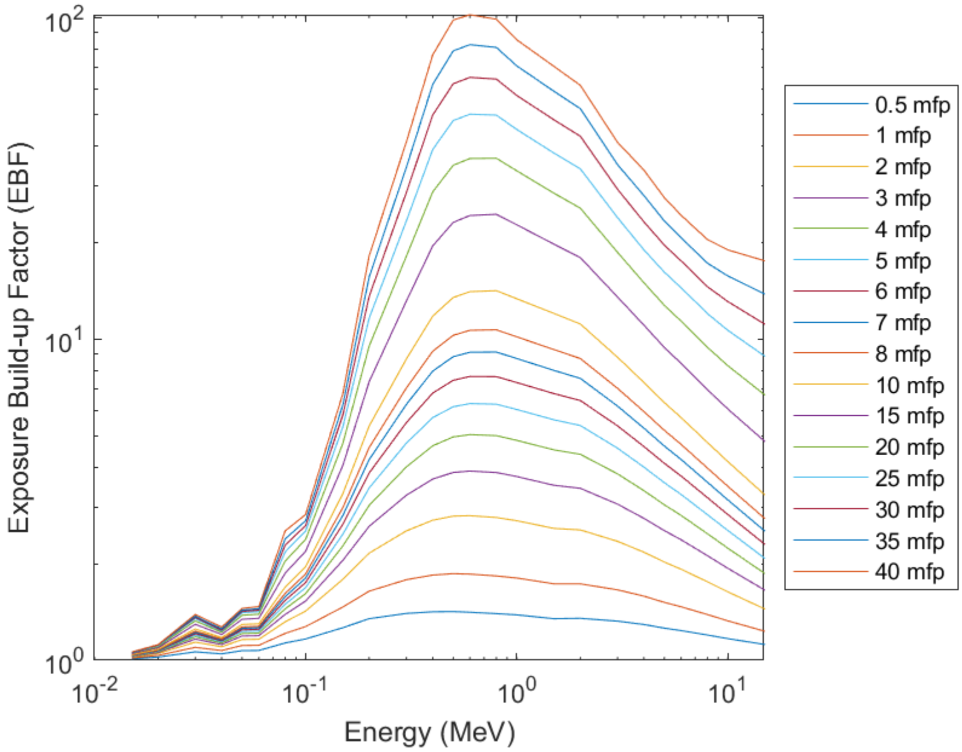

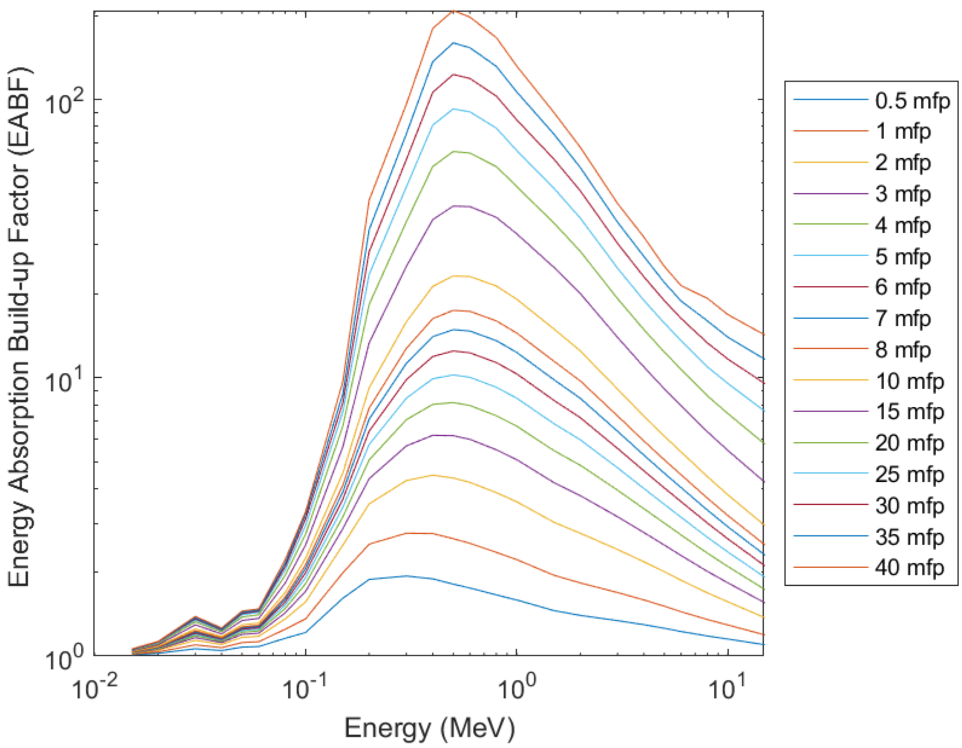

b

Figure 4.15 Variations of EBF (a) and $EABF$ (b) with photon energy at different mean free paths for S4 glass sample

EBF and $EABF$ values for four different glass samples are graphed as a function of incident photon energy at penetration depths of 0.5, 1, 2, 3, 4, 5, 6, 7, 8, 10, 15, 20, 25, 30, 35 and 40 mfp. It is observed that EBF and $EABF$ values increase with increasing mfp values for all glass samples. At higher penetration depths, photons are more difficult to escape from the material than at lower penetration depths due to the more frequent occurrence of multiple scattering events. At the same time, photons take longer to penetrate the thicker material and the number of accumulated photons increases. The high EBF and $EABF$ values obtained at high penetration depths can be attributed to these two conditions. As a result, it was found that EBF and $EABF$ values for all glass samples increased with increasing penetration depth, with the lowest EBF and $EABF$ values at 0.5 mfp penetration depth and the highest EBF and $EABF$ values at 40 mfp penetration depth.

For all glass samples, EBF and $EABF$ values have minimum values in the low energy region where the photoelectric effect is dominant, reach their maximum values in the Compton region and increase again in the very high energy region. In the region dominated by Compton interactions, multiple scattering occurs because the reenergized photons cannot be fully ejected due to Compton interactions. Therefore, the build-up of photons reaches a maximum in the Compton region. The number of photons accumulating towards higher energy regions decreases as they gradually lose their energy as a result of the interactions. Compton interactions only reduce the energy of the photon; they do not absorb it. The photoelectric interaction, however, absorbs the photon and causes it to be removed or completely absorbed.

As a result, it was observed that the EBF and $EABF$ values decreased gradually as the energy of the incident gamma photons increased and increase steadily with increasing penetration depth from 0.5 mfp to 40 mfp. It was seen that EBF and $EABF$ values, which are related to the effective atomic number (Z_{eq}), respond differently with the change in the energy of the incident photon with increasing Dy^{3+} concentration in the material. The addition of Dy^{3+} to the $23CaO - 10Al_2O_3 - (50 - x)B_2O_3 - 6BaO - 10Na_2O - xDy_2O_3$ glass system increased the shielding ability of the glass system.

5
CONCLUSION

In the context of this thesis, the changes in the nuclear properties of four different glass systems doped with varying concentrations of Dy^{3+} and formulated as $23CaO - 10Al_2O_3 - (50-x)B_2O_3 - 6BaO - 10Na_2O - xDy_2O_3$ (x=0.1, 0.3, 0.5, and 1.0% mol) were investigated and the effect of these changes on the use of the glass system as a shielding material was investigated. Glass samples are prepared with a conventional melt-quenching technique. The samples were labelled S1, S2, S3 and S4 and doped with Dy^{3+} at 0.1%, 0.3%, 0.5%, and 1.0%, respectively. Changes in the nuclear properties of the glass samples as a function of the energy of the incident photon allow the ability of the glass system to be evaluated for its ability to shield against radiation. The evaluation was performed with the radiation shielding parameters LAC, MAC, HVL, TVL, mfp, ACS, ECS, Z_{eff}, N_{eff}, C_{eff}, Z_{eq}, EBF and $EABF$, each of which is specific to the glasses. The shielding parameters were calculated and determined in the energy range of 10^{-3}-10^{5} MeV by Phy-X/PSD software. As a result of the Phy-X/PSD analyses, important findings have emerged regarding the suitability of all glass systems for use as radiation shielding materials.

Examination of the linear attenuation coefficients and mass attenuation coefficients of the glass samples at different photon energies revealed that the radiation attenuation efficiency of the system increases with increasing Dy^{3+} concentration. The S4 glass sample with the highest Dy^{3+} concentration consistently showed superior shielding performance with higher mass attenuation coefficients and lower half-value layer thicknesses. The low HVL and TVL values of the material in the high energy region indicate that it is preferred as a thin shielding material both economically and ergonomically. The decreasing HVL and TVL values with increasing Dy^{3+} concentration indicate that lower thicknesses are needed for shielding with increasing system density. At the same time, it is concluded from the inverse relationship between LAC and HVL that when evaluating the shielding properties of a material, it should not be evaluated with a single parameter. mfp value is directly related to the thickness of the material. The thickness of the shielding material increases the shielding ability of the material as it reduces the passage and scattering of the photon. mfp refers to the distance travelled by the photon in the material during interactions. It can be interpreted that the narrower this distance means that the photon will interact more and therefore will be absorbed more. When evaluated together with HVL, it can be said that the mfp results are similar to HVL and S4 glass sample with the highest Dy^{3+} concentration with low mfp value in the high energy region is a better shield than the other samples by taking LAC into account.

ACS and ECS parameters are directly related to Z_{eff}, N_{eff} and C_{eff} parameters. The effective number of atoms and electrons in the material may vary depending on the interactions of the incident photon with the material due to the photoelectric effect, Compton scattering and pair production processes. When Phy-X/PSD results for all glass systems are considered, three different energy regions where these three interactions are effective can be clearly seen in all graphs. The first region is the low energy region (≤0.1 MeV) where the photoelectric effect dominates, the second region is the medium energy region (0.1<x<1.02 MeV) where Compton scattering dominates, and the third region is the high energy region (≥1.02 MeV) where pair production dominates. The maximum values of Z_{eff}, N_{eff} and C_{eff} of all glass systems in the first region are due to the photoelectric absorption cross section aggravation. In the second region, these values are almost constant until the third region since the absorption cross section is proportional to the atomic number. In the third region, a slight increase in the values is observed with the introduction of pair production. While ACS and ECS values alone cannot be evaluated about the shielding ability of the material, the radiation shielding ability of the system increases in cases where the Z_{eff} value, which can comment on the photon-matter interaction alone and mentions the chemical properties of the material, is high. The Z_{eff} value is defined for a material consisting of different components and is related to the density and atomic number of the material, thus explaining the shielding ability of the material in terms of pure elements. In this study, compared to different glass systems, the Z_{eff} value of the system was initially increased by the inclusion of heavy metal oxides in the components of the system. Later, when the results were evaluated in response to increasing Dy^{3+} concentrations, it was concluded that an increase in the Z_{eff} value occurred and that the Z_{eff} value is related to the density and weight of the material as well as the energy. The S4 glass sample with the highest Dy^{3+} concentration showed the best shielding ability against incident photons in all energy ranges. At the same time, the glass system meets the desired properties of low mfp and high Z_{eff} values at high energies for the shielding material.

EBF and $EABF$ parameters are important parameters to evaluate the consequence of the interaction of the incident photon with the material. Since the accumulation of the photon in the material is related to its distribution and range in the material, more accurate results of the shielding capability are obtained when the EBF and $EABF$ parameters are evaluated together with the mfp parameter. For each glass sample, the change of EBF and $EABF$ parameters depending on the energy of the incident photon at different mfp values were observed. For EBF and $EABF$ values, it can be said that they show sharp peak values in the second region where Compton effect is dominant, and they are more affected by pair formation in the third energy region compared to other parameters. This is because EBF and $EABF$ parameters are directly related to the number and direction of the scattered photons. Photons, which lose their energy slowly due to the Compton effect, accumulate in the material, so both parameters show sharp peaks in the Compton region. As the mfp value increases, the number of photons accumulated in the environment increases as scattering will occur in a more widespread area as a result of interactions. Considering the relationship between the mfp value and the HVL value, it is concluded that increasing the thickness of the material will increase the number of photons accumulated and the EBF and $EABF$ values will also increase. The relationship of EBF with the Z_{eq} parameter is also remarkable. Depending on the photon-matter interactions, the dependence of EBF on the chemical composition of the material in different energy regions also changes. While minimum EBF values are observed in the sample with minimum Z_{eq} value due to the photoelectric effect, this situation is reversed with the dominance of pair formation. Since photons are under Compton effect in the medium energy region, they show changes independent of Z_{eq}. It is seen that EBF and $EABF$ parameters depend on the energy of the incident photon as well as mfp and Z_{eq} parameters and when all these factors are considered, S4 glass sample with the highest Dy^{3+} concentration among the samples shows the best shielding capability. At the same time, this glass system also satisfies the desired properties of low mfp and high Z_{eq}values at high energies for the shielding material.

This thesis is important in terms of the fact that the glass system studied for radiation shielding applications does not contain lead in its components and the properties of the system have been improved and can be further improved. The findings show that the doping of Dy^{3+} ions into the glass system matrix enhances the shielding capability of the system by increasing the radiation absorption and reducing the formation of secondary particles and shows the potential for the use of glass systems as effective, environmental and sustainable materials to reduce the harmful effects of ionizing radiation in industrial and medical applications. With this thesis study, the use of $23CaO - 10Al_2O_3 - (50 - x)B_2O_3 - 6BaO - 10Na_2O - xDy_2O_3$ (x=0.1, 0.3, 0.5, and 1.0% mol) glass system as a radiation shielding material has been proven to be a suitable, effective and good alternative.

REFERENCES

[1] D. A. Pryma, *Introduction to Nuclear Medicine*, in *Nuclear Medicine: Practical Physics, Artifacts, and Pitfalls*, Oxford University Press, 2014. [Online]. Available: https://doi.org/10.1093/med/9780199918034.003.0001

[2] A. B. Reed, "The history of radiation use in medicine," *Journal of Vascular Surgery*, vol. 53, no. 1, pp. 3S-5S, 2011. [Online]. Available: https://doi.org/10.1016/j.jvs.2010.07.024

[3] T. A. Woloshyn, Ed., *Soaking Up the Rays: Light Therapy and Visual Culture in Britain, c. 1890–1940*, Manchester University Press, 2017.

[4] V. P. Guinn, "Radioactivity," in *Encyclopedia of Physical Science and Technology*, R. A. Meyers, Ed., 3rd ed., Academic Press, 2003, pp. 661-674. [Online]. Available: https://doi.org/10.1016/B0-12-227410-5/00643-8

[5] S. D'Auria, Ed., *Introduction to Nuclear and Particle Physics*, Springer International Publishing, 2018, pp. 1-11. [Online]. Available: https://doi.org/10.1007/978-3-319-93855-4_1

[6] D. Ball, "The electromagnetic spectrum: A history," *Spectroscopy - Springfield then Eugene then Duluth*, vol. 22, pp. 14-20, 2007.

[7] N. Khan, "Radioactivity: An Introduction to Mysterious Science," *Journal of Physical Chemistry & Biophysics*, vol. 07, 2017. [Online]. Available: https://doi.org/10.4172/2161-0398.1000254

[8] "The electromagnetic spectrum. The narrow range of visible light is shown enlarged at the right," *Encyclopædia Britannica*, 2014. [Online]. Available: https://www.britannica.com/science/electromagnetic-spectrum#/media/1/183297/106806

[9] A. Del Guerra and A. Del Guerra, *Ionizing Radiation Detectors for Medical Imaging*, World Scientific Pub, 2004.

[10] O. Günay, *Farklı biyomedikal görüntüleme sistemlerinde radyasyon doz çalışması*, Unpublished PhD Thesis, Kocaeli Üniversitesi, 2022.

[11] J. T. Bushberg, J. A. Seibert, E. M. Leidholdt, and J. M. Boone, *The Essential Physics of Medical Imaging*, 3rd ed., Wolters Kluwer Health, 2011.

[12] R. L. Platzman, "What is ionizing radiation?," *Scientific American*, vol. 201, pp. 74–83, 1959. [Online]. Available: https://doi.org/10.1038/scientificamerican0959-74

[13] D. S. McGregor and J. K. Shultis, "Physical Sensors: Radiation Sensors," *Encyclopedia of Sensors and Biosensors*, vol. 1, pp. 141-160, 2023.

[14] G. F. Knoll, *Radiation Detection and Measurement*, Wiley, 2000.

[15] G. B. Saha, *Physics and Radiobiology of Nuclear Medicine*, Springer, 2013. [Online]. Available: https://doi.org/10.1007/978-1-4614-4012-3

[16] R. A. Powsner and E. R. Powsner, *Essential Nuclear Medicine Physics*, Wiley, 2008.

[17] M. L'Annunziata, *Radiation Physics and Radionuclide Decay*, in *Handbook of Radioactivity Analysis*, 3rd ed., Academic Press, 2013, pp. 1-162. [Online]. Available: https://doi.org/10.1016/B978-0-12-384873-4.00001-3

[18] J. E. Martin, *Physics for Radiation Protection*, Wiley, 2013. [Online]. Available: https://books.google.com.tr/books?id=F2lYIHAI_wIC

[19] D. L. Bailey and I. A. E. Agency, *Nuclear Medicine Physics: A Handbook for Teachers and Students*, International Atomic Energy Agency, 2015.

[20] A. Mozumder, "Chapter 2 - Interaction of Radiation with Matter: Energy Transfer from Fast Charged Particles," in *Fundamentals of Radiation Chemistry*, A. Mozumder, Ed., Academic Press, 1999, pp. 5-39. [Online]. Available: https://doi.org/10.1016/B978-012509390-3/50002-3

[21] W. R. Leo, *Techniques for Nuclear and Particle Physics Experiments: A How-to Approach*, Springer, 1994.

[22] A. Das and T. Ferbel, *Introduction to Nuclear and Particle Physics*, World Scientific, 2003.

[23] P. Sprawls, *Physical Principles of Medical Imaging*, Aspen Publishers, 1993.

[24] W. R. Fahrner, "Chapter 9 An overview of radiation-matter interactions," in *Instabilities in Silicon Devices*, vol. 3, G. Barbottin and A. Vapaille, Eds., North-Holland, 1999, pp. 553-637. [Online]. Available: https://doi.org/10.1016/S1874-5903(99)80016-0

[25] M. L'Annunziata, *Handbook of Radioactivity Analysis*, Elsevier Science, 2003.

[26] E. Seeram, "Computed Tomography: Physical Principles and Recent Technical Advances," *Journal of Medical Imaging and Radiation Sciences*, vol. 41, no. 2, pp. 87–109, 2010. [Online]. Available: https://doi.org/10.1016/j.jmir.2010.04.001

[27] M. Maqbool, *An Introduction to Medical Physics*, Springer International Publishing, 2017.

[28] T. Toth and R. Hudak, "Computed Tomography - its Development, Principle and Image Artifacts," *Acta Mechanica Slovaca*, vol. 17, pp. 40-47, 2013. [Online]. Available: https://doi.org/10.21496/ams.2013.044

[29] T. M. Buzug, "Computed Tomography," in *Springer Handbook of Medical Technology*, R. Kramme, K.-P. Hoffmann, and R. S. Pozos, Eds., Springer Berlin Heidelberg, 2011, pp. 311-342. [Online]. Available: https://doi.org/10.1007/978-3-540-74658-4_16

[30] T. Flohr, "CT Systems," *Current Radiology Reports*, vol. 1, no. 1, pp. 52-63, 2013. [Online]. Available: https://doi.org/10.1007/s40134-012-0005-5

[31] M. V. Glas, *Principles of Computerized Tomographic Imaging*, 2000.

[32] W. A. Kalender, "Principles and applications of spiral CT," *Nuclear Medicine and Biology*, vol. 21, no. 5, pp. 693–699, 1994. [Online]. Available: https://doi.org/10.1016/0969-8051(94)90039-6

[33] M. J. Martínez, S. I. Ziegler, and T. Beyer, "PET and PET/CT: basic principles and instrumentation," *Recent Results in Cancer Research*, vol. 170, pp. 1–23, 2008. [Online]. Available: https://doi.org/10.1007/978-3-540-31203-1_1

[34] M. M. Alauddin, "Positron emission tomography (PET) imaging with (18)F-based radiotracers," *American Journal of Nuclear Medicine and Molecular Imaging*, vol. 2, no. 1, pp. 55–76, 2012.

[35] D. W. Townsend, "Basic Science of PET and PET/CT," in *Positron Emission Tomography: Clinical Practice*, P. E. Valk, D. Delbeke, D. L. Bailey, D. W. Townsend, and M. N. Maisey, Eds., Springer London, 2006, pp. 1-16. [Online]. Available: https://doi.org/10.1007/1-84628-187-3_1

[36] B. H. Brown, R. H. Smallwood, D. C. Barber, P. V. Lawford, and D. R. Hose, *Medical Physics and Biomedical Engineering*, 1st ed., CRC Press, 1999. [Online]. Available: https://doi.org/10.1201/9781315275604

[37] W. Jiang, Y. Chalich, and M. J. Deen, "Sensors for Positron Emission Tomography Applications," *Sensors (Basel, Switzerland)*, vol. 19, no. 22, pp. 5019, 2019. [Online]. Available: https://doi.org/10.3390/s19225019

[38] R. L. Wahl, "PET and PET/CT Imaging in Breast Cancer," in *Positron Emission Tomography: Clinical Practice*, P. E. Valk, D. Delbeke, D. L. Bailey, D. W. Townsend, and M. N. Maisey, Eds., Springer London, 2006, pp. 197-215. [Online]. Available: https://doi.org/10.1007/1-84628-187-3_13

[39] B. F. Hutton, "The origins of SPECT and SPECT/CT," *European Journal of Nuclear Medicine and Molecular Imaging*, vol. 41, Suppl 1, pp. S3–S16, 2014. [Online]. Available: https://doi.org/10.1007/s00259-013-2606-5

[40] S. Dorbala *et al.*, "Single Photon Emission Computed Tomography (SPECT) Myocardial Perfusion Imaging Guidelines: Instrumentation, Acquisition, Processing, and Interpretation," *Journal of Nuclear Cardiology*, vol. 25, no. 5, pp. 1784-1846, 2018. [Online]. Available: https://doi.org/10.1007/s12350-018-1283-y

[41] K. Riklund, "The Role of Imaging in Nuclear Medicine: The Medical Perspective," in *Imaging in Nuclear Medicine*, A. Giussani and C. Hoeschen, Eds., Springer Berlin Heidelberg, 2013, pp. 7-18. [Online]. Available: https://doi.org/10.1007/978-3-642-31415-5_2

[42] A. Studen, "Physics of Imaging in Nuclear Medicine," in *Imaging in Nuclear Medicine*, A. Giussani and C. Hoeschen, Eds., Springer Berlin Heidelberg, 2013, pp. 19-41. [Online]. Available: https://doi.org/10.1007/978-3-642-31415-5_3

[43] E. R. McVeigh, "Emerging imaging techniques," *Circulation Research*, vol. 98, no. 7, pp. 879–886, 2006. [Online]. Available: https://doi.org/10.1161/01.RES.0000216870.73358.d9

[44] G. F. Knoll, "Single-photon emission computed tomography," *Proceedings of the IEEE*, vol. 71, no. 3, pp. 320-329, 1983. [Online]. Available: https://doi.org/10.1109/PROC.1983.12590

[45] S. R. Cherry, "In vivo molecular and genomic imaging: new challenges for imaging physics," *Physics in Medicine and Biology*, vol. 49, no. 3, pp. R13–R48, 2004. [Online]. Available: https://doi.org/10.1088/0031-9155/49/3/r01

[46] N. B. Smith and A. Webb, *Introduction to Medical Imaging: Physics, Engineering and Clinical Applications*, Cambridge University Press, 2010.

[47] W. Davros, "Fluoroscopy: basic science, optimal use, and patient/operator protection," *Techniques in Regional Anesthesia and Pain Management*, vol. 11, 2007. [Online]. Available: https://doi.org/10.1053/j.trap.2007.02.005

[48] K. Maher and J. Malone, "Digital Fluoroscopy: A New Development in Medical Imaging," *Contemporary Physics*, vol. 27, pp. 533-553, 1986. [Online]. Available: https://doi.org/10.1080/00107518608211030

[49] N. Binder, L. Matthäus, R. Burgkart, and A. Schweikard, "A robotic C-arm fluoroscope," *The International Journal of Medical Robotics + Computer Assisted Surgery: MRCAS*, vol. 1, no. 3, pp. 108–116, 2005

[50] M. Abella, C. de Molina, N. Ballesteros, A. García-Santos, Á. Martínez, I. García, and M. Desco, "Enabling tomography with low-cost C-arm systems," *PloS One*, vol. 13, no. 9, p. e0203817, 2018. [Online]. Available: https://doi.org/10.1371/journal.pone.0203817

[51] T. H. Williams, A. G. Syrett, and T. J. Brammar, "W.S.B.--a fluoroscopy C-arm communication strategy," *Injury*, vol. 40, no. 8, pp. 840-843, 2009.

[52] A. Bozbıyık, Ç. Özdemir, and H. Hancı, "Radyasyon yaralanmaları ve korunma yöntemleri," *Sürekli Tıp Eğitimi Dergisi*, vol. 11, no. 7, pp. 272–274, 2002.

[53] C. Zeyrek, "İyonize Radyasyon Uygulamaları İçin Güvenlik ve Korunmaya Yönelik Genel Kavramlar," *Süleyman Demirel Üniversitesi Fen Bilimleri Enstitüsü Dergisi*, vol. 17, 2014. [Online]. Available: https://doi.org/10.19113/sdufbed.46108

[54] B. M. Moores and D. Regulla, "A review of the scientific basis for radiation protection of the patient," *Radiation Protection Dosimetry*, vol. 147, no. 1-2, pp. 22–29, 2011. [Online]. Available: https://doi.org/10.1093/rpd/ncr262

[55] R. L. Kathren, "Guide to reducing radiation exposure to as low as reasonably achievable (ALARA)," 1980. [Online]. Available: http://inis.iaea.org/search/search.aspx?orig_q=RN:11558515

[56] K. J. Strauss and S. C. Kaste, "The ALARA (as low as reasonably achievable) concept in pediatric interventional and fluoroscopic imaging: striving to keep radiation doses as low as possible during fluoroscopy of pediatric patients--a white paper executive summary," *Pediatric Radiology*, vol. 36, Suppl 2, pp. 110–112, 2006. [Online]. Available: https://doi.org/10.1007/s00247-006-0184-4

[57] R. Donahue and A. Fassò, "Radioactivity and radiation protection," *European Physical Journal C - EUR PHYS J C*, vol. 15, pp. 186-189, 2000. [Online]. Available: https://doi.org/10.1007/BF02683421

[58] M. Alhassan, B. Khan, and J. T. Baraya, "Evaluation of 1.5mm Lead Shield for Radiological Protection and Comparison of Calculated and Measured Results of Equivalent Dose," *Journal of Applied Science and Environmental Management*, vol. 23, no. 12, 2019. [Online]. Available: https://doi.org/10.4314/jasem.v23i12.17

[59] F. A. Mettler Jr, W. Huda, T. T. Yoshizumi, and M. Mahesh, "Effective doses in radiology and diagnostic nuclear medicine: a catalog," *Radiology*, vol. 248,

no. 1, pp. 254–263, 2008. [Online]. Available: https://doi.org/10.1148/radiol.2481071451

[60] H. Issard, "Radiation protection by shielding in packages for radioactive materials," in *Safe and Secure Transport and Storage of Radioactive Materials*, K. B. Sorenson, Ed. Woodhead Publishing, 2015, pp. 123-140. [Online]. Available: https://doi.org/10.1016/B978-1-78242-309-6.00009-5

[61] ICRP, "Application of the Commission's Recommendations for the Protection of People in Emergency Exposure Situations," ICRP Publication 109, Ann. ICRP, vol. 39, no. 1, 2009.

[62] Ü. Kara and Y. Kara, "A Study on Radiation in Operating Room in Suleyman Demirel University," *Acta Physica Polonica A*, vol. 130, pp. 401-403, 2016. [Online]. Available: https://doi.org/10.12693/APhysPolA.130.401

[63] P. E. Park, J. M. Park, J. E. Kang, J. H. Cho, S. J. Cho, J. H. Kim, W. S. Sim, and Y. C. Kim, "Radiation Safety and Education in the Applicants of the Final Test for the Expert of Pain Medicine," *The Korean Journal of Pain*, vol. 25, no. 1, pp. 16-21, 2012. [Online]. Available: https://doi.org/10.3344/kjp.2012.25.1.16

[64] Y. J. Chang, A. N. Kim, I. S. Oh, N. S. Woo, H. K. Kim, and J. H. Kim, "The Radiation Exposure of Radiographer Related to the Location in C-arm Fluoroscopy-guided Pain Interventions," *The Korean Journal of Pain*, vol. 27, no. 2, pp. 162-167, 2014. [Online]. Available: https://doi.org/10.3344/kjp.2014.27.2.162

[65] W. Abuzeid, J. Abunassar, J. A. Leis, V. Tang, B. Wong, D. T. Ko, and H. C. Wijeysundera, "Radiation safety in the cardiac catheterization lab: A time series quality improvement initiative," *Cardiovascular Revascularization Medicine*, vol. 18, no. 5, Supplement 1, pp. S22-S26, 2017. [Online]. Available: https://doi.org/10.1016/j.carrev.2017.04.009

[66] Y. Xiong, Y. Wang, G. Roselle, and S. Kim, "Lead/lead-alloy as a corrosion-resistant outer layer packaging material for high level nuclear waste disposal," *Nuclear Engineering and Design*, vol. 380, p. 111294, 2021. [Online]. Available: https://doi.org/10.1016/j.nucengdes.2021.111294

[67] R. Kurtuluş and T. Kavas, "Calculation of LAC and HVL values of newly developed barium-borotellurite glass containing different heavy metal oxides using Phy-X/PSD," *Pamukkale Üniversitesi Mühendislik Bilimleri Dergisi*, vol. 28, no. 7, pp. 971-976, 2022.

[68] G. Almisned, G. Bilal, D. Sen Baykal, F. T. Ali, G. Kilic, and H. O. Tekin, "Bismuth(III) oxide and boron(III) oxide substitution in bismuth-boro-zinc glasses: A focusing in nuclear radiation shielding properties," *Optik*, vol. 272, p. 170214, 2023. [Online]. Available: https://doi.org/10.1016/j.ijleo.2022.170214

[69] R. Mirji and B. Lobo, "Radiation shielding materials: A brief review on methods, scope and significance," in *National Conference on Advances in VLSI and Microelectronics*, PC Jabin Science College, Huballi, India, 2017, pp. 96-100.

[70] M. A. H. Abdullah, R. S. M. Rashid, M. Amran, F. Hejazii, N. M. Azreen, R. Fediuk, Y. L. Voo, N. I. Vatin, and M. I. Idris, "Recent Trends in Advanced Radiation Shielding Concrete for Construction of Facilities: Materials and Properties," *Polymers*, vol. 14, no. 14, p. 2830, 2022. [Online]. Available: https://www.mdpi.com/2073-4360/14/14/2830

[71] M. G. El-Samrah, M. A. Abreu Zamora, D. R. Novog, and S. E. Chidiac, "Radiation shielding properties of modified concrete mixes and their suitability in dry storage cask," *Progress in Nuclear Energy*, vol. 148, p. 104195, 2022. [Online]. Available: https://doi.org/10.1016/j.pnucene.2022.104195

[72] B. Aygün, "High alloyed new stainless steel shielding material for gamma and fast neutron radiation," *Nuclear Engineering and Technology*, vol. 52, no. 3, pp. pp. 647-653, 2020. [Online]. Available: https://doi.org/10.1016/j.net.2019.08.017

[72] B. Aygün, "High alloyed new stainless steel shielding material for gamma and fast neutron radiation," *Nuclear Engineering and Technology*, vol. 52, no. 3, pp. 647-653, 2020. [Online]. Available: https://doi.org/10.1016/j.net.2019.08.017

[73] R. Finch, H. Smartt, and R. Haddal, "Developing Reliable Safeguards Seals for Transportation Casks to be Applied, Verified, and Removed by State Operators," Sandia National Laboratories, 2017.

[74] M. Uosif, A. M. A. Mostafa, S. Issa, H. O. Tekin, Z. Alrowaili, and O. Kilicoglu, "Structural, mechanical and radiation shielding properties of newly developed tungsten lithium borate glasses: An experimental study," *Journal of Non-Crystalline Solids*, vol. 532, 2020. [Online]. Available: https://doi.org/10.1016/j.jnoncrysol.2019.119882

[75] N. Jamal AbuAlRoos, M. N. Azman, N. A. Baharul Amin, and R. Zainon, "Tungsten-based material as promising new lead-free gamma radiation shielding material in nuclear medicine," *Physica Medica*, vol. 78, pp. 48-57, 2020. [Online]. Available: https://doi.org/10.1016/j.ejmp.2020.08.017

[76] R. D. Weaver, B. J. Gerbi, and K. E. Dusenbery, "Evaluation of eye shields made of tungsten and aluminum in high-energy electron beams," *International Journal of Radiation Oncology, Biology, Physics*, vol. 41, no. 1, pp. 233–237, 1998. [Online]. Available: https://doi.org/10.1016/s0360-3016(97)00905-x

[77] V. G. Rudychev, N. A. Azarenkov, I. O. Girka, and Y. V. Rudychev, "Optimization of radiation shields made of Fe and Pb for the spent nuclear fuel transport casks," *Nuclear Engineering and Technology*, vol. 55, no. 2, pp. 690-695, 2023. [Online]. Available: https://doi.org/10.1016/j.net.2022.10.002

[78] S. Agosteo, M. Magistris, A. Mereghetti, M. Silari, and Z. Zajacova, “Shielding data for 100–250MeV proton accelerators: Attenuation of secondary radiation in thick iron and concrete/iron shields,” *Nucl. Instrum. Methods Phys. Res. Sect. B: Beam Interact. Mater. Atoms*, vol. 266, pp. 3406-3416, 2008. [Online]. Available: https://doi.org/10.1016/j.nimb.2008.05.002.

[79] P. Glumglomchit, J. Rajagukguk, J. Kaewkhao, and K. Kirdsiri, “A Novel Radiation Shielding Material for Gamma-Ray: The Development of Lutetium Lithium Borate Glasses,” *Key Eng. Mater.*, vol. 766, pp. 246-251, 2018.

[80] N. Singh, K. Singh, K. Singh, and H. Singh, "Comparative study of lead borate and bismuth lead borate glass systems as gamma-radiation shielding materials," *Nucl. Instrum. Methods Phys. Res. Sect. B: Beam Interact. Mater. Atoms*, vol. 225, pp. 305-309, 2004. [Online]. Available: https://doi.org/10.1016/j.nimb.2004.05.016.

[81] K. A. Fetterly, D. J. Magnuson, G. M. Tannahill, M. D. Hindal, and V. Mathew, "Effective Use of Radiation Shields to Minimize Operator Dose During Invasive Cardiology Procedures," *JACC Cardiovasc. Interv.*, vol. 4, no. 10, pp. 1133-1139, 2011. [Online]. Available: https://doi.org/10.1016/j.jcin.2011.05.027.

[82] M. I. Sayyed, "Investigation of Radiation Shielding Features of Lithium Cadmium Silicate Glasses," *Silicon*, vol. 15, no. 18, pp. 7717-7723, 2023. [Online]. Available: https://doi.org/10.1007/s12633-023-02616-y.

[83] S. R. Manohara, S. M. Hanagodimath, and L. Gerward, "Photon interaction and energy absorption in glass: A transparent gamma ray shield," *J. Nucl. Mater.*, vol. 393, no. 3, pp. 465-472, 2009. [Online]. Available: https://doi.org/10.1016/j.jnucmat.2009.07.001.

[84] B. M. Alotaibi et al., "Structural, optical, and gamma-ray shielding properties of a newly fabricated P2O5–B2O3–Bi2O3–Li2O–ZrO2 glass system," *Eur. Phys. J. Plus*, vol. 136, no. 2, p. 224, 2021. [Online]. Available: https://doi.org/10.1140/epjp/s13360-020-01064-6.

[85] S. R. Manohara, S. M. Hanagodimath, L. Gerward, and K. C. Mittal, "Exposure Buildup Factors for Heavy Metal Oxide Glass: A Radiation Shield," *J. Korean Phys. Soc.*, vol. 59, pp. 2039, 2011. [Online]. Available: https://doi.org/10.3938/jkps.59.2039.

[86] A. Fukuda et al., "Nihon Hoshasen Gijutsu Gakkai zasshi," vol. 60, no. 12, pp. 1723–1729, 2004. [Online]. Available: https://doi.org/10.6009/jjrt.kj00003560637.

[87] S. Singh, A. Kumar, D. Singh, K. Thind, and G. Mudahar, "Barium–borate–flyash glasses: As radiation shielding materials," *Nucl. Instrum. Methods Phys. Res. Sect. B: Beam Interact. Mater. Atoms*, vol. 266, pp. 140-146, 2008. [Online]. Available: https://doi.org/10.1016/j.nimb.2007.10.018.

[88] P. Dararutana, J. Duchaneephet, S. Pongkrapan, N. Sirikulrat, and P. Wathanakul, "Effect of Bi2O3 content on optical and radiation shielding properties of (Na2O, K2O)-SiO2–CaO-Al2O3–B2O3 glass system," *Optoelectron. Adv. Mater. Rapid Commun.*, vol. 3, pp. 525-527, Jun. 2009.

[89] S. Kaewjaeng, J. Kaewkhao, P. Limsuwan, and U. Maghanemi, "Effect of BaO on Optical, Physical and Radiation Shielding Properties of SiO2-B2O3-Al2O3-CaO-Na2O Glasses System," *Procedia Eng.*, vol. 32, pp. 1080-1086, 2012. [Online]. Available: https://doi.org/10.1016/j.proeng.2012.02.058.

[90] S. Issa and M. Kurudirek, "Investigation of Gamma Radiation Shielding Properties of Some Zinc Tellurite Glasses," *J. Phys. Sci.*, vol. 27, pp. 97-119, 2016. [Online]. Available: https://doi.org/10.21315/jps2016.27.3.7.

[91] L. Shamshad et al., "A comparative study of gadolinium based oxide and oxyfluoride glasses as low energy radiation shielding materials," *Prog. Nucl.*

Energy, vol. 97, pp. 53-59, 2017. [Online]. Available: https://doi.org/10.1016/j.pnucene.2016.12.014.

[92] K. Kaky et al., "X-ray photoelectron spectroscopy (XPS) and gamma-ray shielding investigation of boro-silicate glasses contained alkali/alkaline modifier," *Results Phys.*, vol. 14, p. 102438, 2019. [Online]. Available: https://doi.org/10.1016/j.rinp.2019.102438.

[93] O. Agar, M. I. Sayyed, H. O. Tekin, K. M. Kaky, S. O. Baki, and I. Kityk, "An investigation on shielding properties of BaO, MoO3 and P2O5 based glasses using MCNPX code," *Results Phys.*, vol. 12, pp. 629-634, 2019. [Online]. Available: https://doi.org/10.1016/j.rinp.2018.12.003.

[94] K. Kaky, "Rare-Earth Ion Effects on Radiation Shielding Parameters of GeO2-B2O3-ZnO-P2O5-Tb2O3 Glass System," *J. Mater. Eng. Perform.*, 2023. [Online]. Available: https://doi.org/10.1007/s11665-023-08918-x.

[95] B. Gurav, G. B., D. Dinkar, A. Surzhikova, D. P., and R. Rajaramakrishna, "Instigating the Asymmetry of Dy3+ Ions Doped in Borate Glasses for Photonic Device w-LED Applications," *J. Optics Photon. Res.*, 2024. [Online]. Available: https://doi.org/10.47852/bonviewjopr42022256.

[96] H. Kaur, N. Kaur, V. Bhatia, H. Singh, D. Kumar, and S. P. Singh, "The influence of Dy3+ ions on physical, structural, optical, and thermoluminescence characteristics of Li2O – BaO – B2O3 – P2O5 glass system," *Mater. Res. Bull.*, 2023.

[97] V. P. Klyuev and B. Z. Pevzner, "Thermal Expansion and Glass Transition Temperature of Calcium Borate and Calcium Aluminoborate Glasses," *Glass Phys. Chem.*, vol. 29, no. 2, pp. 127–136, 2003. [Online]. Available: https://doi.org/10.1023/A:1023498823701.

[98] D. Wu, C. Zhu, and M. Zhang, "Ce3+ - and Dy3+ -Doped Oxyfluoride Borosilicate Glasses with Near White Luminescence," *J. Am. Ceram. Soc.*, vol. 99, no. 9, pp. 2961-2969, 2016. [Online]. Available: https://doi.org/10.1111/jace.14185.

[99] M. Murthi et al., "Dy3+ doped SiO2-B2O3-Al2O3-NaF-ZnF2 glasses: An exploration of optical and gamma radiation shielding features," *Curr. Appl. Phys.*, vol. 20, p. 100137, 2020. [Online]. Available: https://doi.org/10.1016/j.cap.2020.08.004.

[100] M. I. Sayyed, "BaO-doped B2O3-Na2O-PbO-SiO2 glasses: Improved radiation shielding properties for protection applications," *Silicon*, 2024. [Online]. Available: https://doi.org/10.1007/s12633-024-02863-7.

[101] M. Al-Buriahi, C. Sriwunkum, H. Arslan, B. T. Tonguc, and M. Bourham, "Investigation of barium borate glasses for radiation shielding applications," *Appl. Phys. A*, vol. 126, p. 222, 2020. [Online]. Available: https://doi.org/10.1007/s00339-019-3254-9.

[102] M. Bengisu, "Borate glasses for scientific and industrial applications: a review," *J. Mater. Sci.*, vol. 51, no. 5, pp. 2199-2242, 2016. [Online]. Available: https://doi.org/10.1007/s10853-015-9537-4.

[103] S. Algarni et al., "Physical, Optical, and Radiation Shielding Features of Yttrium Lithium Borate Glasses," *J. Inorg. Organomet. Polym. Mater.*, vol. 32, p. 9, 2022. [Online]. Available: https://doi.org/10.1007/s10904-022-02321-0.

[104] S. A. Hussein, R. Roshdy, M. S. A. El-sadek, and M. Ezzeldien, "Effect of Al2O3 on the structural, optical and mechanical properties of B2O3- CaO-SiO2-P2O5-Na2O glass system," *Optik*, vol. 250, p. 168281, 2022. [Online]. Available: https://doi.org/10.1016/j.ijleo.2021.168281.

[105] Ö. H. Andersson et al., "In vivo behaviour of glasses in the SiO2-Na2O-CaO-P2O5-Al2O3-B2O3 system," *J. Mater. Sci.: Mater. Med.*, vol. 1, no. 4, pp. 219–227, 1990. [Online]. Available: https://doi.org/10.1007/BF00701080.

[106] M. Khoeini, S. Hesaraki, and A. Kolahi, "Effect of BaO substitution for CaO on the structural and thermal properties of SiO2–B2O3–Al2O3–CaO–Na2O–P2O5 bioactive glass system used for implant coating applications," *Ceram. Int.*, vol. 47, no. 22, pp. 31666–31680, 2021. [Online]. Available: https://doi.org/10.1016/j.ceramint.2021.08.046.

[107] M. I. Sayyed et al., "Experimental and Theoretical Study of Radiation Shielding Features of CaO-K2O-Na2O-P2O5 Glass Systems," *Materials*, vol. 14, no. 14, p. 3772, 2021. [Online]. Available: https://doi.org/10.3390/ma14143772.

[108] L. Luo, Z. Li, Q. Wang, K. Lan, and W. Jiang, "Effect of CaO on Phase Separation and Properties in Na2O-CaO-SiO2-P2O5 Opaque Glass," *IOP Conf. Ser.: Mater. Sci. Eng.*, vol. 562, no. 1, p. 012118, 2019. [Online]. Available: https://doi.org/10.1088/1757-899X/562/1/012118.

[109] S. Yang et al., "Effect of CaO doping on the properties and crystallization behavior of Y2O3–Al2O3–SiO2 glass," *Ceram. Int.*, vol. 49, no. 20, pp. 33188–33196, 2023. [Online]. Available: https://doi.org/10.1016/j.ceramint.2023.08.022.

[110] E. H. Abdel-Gawad, M. I. Sayyed, T. A. Hanafy, and M. Elsafi, "Experimental investigation of radiation shielding competence of B2O3-Na2O-Al2O3-BaO-CaO glass system," *Sci. Rep.*, vol. 14, no. 1, p. 14891, 2024. [Online]. Available: https://doi.org/10.1038/s41598-024-63329-9.

[111] I. El-Abdouni and S. Krimi, "Effect of CaO on the structure, durability and bioactivity properties of phosphate Na2O–SrO–TiO2–P2O5 glasses," *Mater. Today: Proc.*, vol. 62, pp. 6305–6311, 2022. [Online]. Available: https://doi.org/10.1016/j.matpr.2022.04.180.

[112] M. Tijaria, Y. Sharma, V. Kumar, S. Dahiya, and J. Dalal, "Effect of Na2O on physical, structural and electrical properties of borate glasses," *Mater. Today: Proc.*, vol. 45, pp. 3722–3725, 2021. [Online]. Available: https://doi.org/10.1016/j.matpr.2020.12.688.

[113] K. I. Hussein et al., "The Effect of ZnO, MgO, TiO2, and Na2O Modifiers on the Physical, Optical, and Radiation Shielding Properties of a TeTaNb Glass System," *Materials (Basel, Switzerland)*, vol. 15, no. 5, p. 1844, 2022. [Online]. Available: https://doi.org/10.3390/ma15051844.

[114] K. Kashif and A. Ratep, "Effect of Addition of Dysprosium Oxide on Spectroscopic Properties and Judd–Ofelt Analysis of Lithium Borosilicate

Glass System," *Silicon*, vol. 15, p. 10217, 2022. [Online]. Available: https://doi.org/10.1007/s12633-022-02249-7.

[115] G. Sathiyapriya et al., "An investigation on physical, structural and gamma ray shielding features of Dy3+ ions doped Telluroborate glasses," *J. Non-Cryst. Solids*, vol. 522, p. 119574, 2019. [Online]. Available: https://doi.org/10.1016/j.jnoncrysol.2019.119574.

[116] M. Uçar, H. Kayiran, and A. Korkmaz, "Gamma-ray-shielding parameters of carbon–aramid epoxy composites," *Emerg. Mater. Res.*, vol. 11, pp. 1–7, 2022. [Online]. Available: https://doi.org/10.1680/jemmr.22.00072.

[117] M. A. Zeed, A. Saeed, R. M. El Shazly, H. M. El- Mallah, and E. Elesh, "Double effect of glass former B2O3 and intermediate Pb3O4 augmentation on the structural, thermal, and optical properties of borate network," *Optik*, vol. 272, p. 170368, 2023. [Online]. Available: https://doi.org/10.1016/j.ijleo.2022.170368.

[118] E. Şakar, Ö. F. Özpolat, B. Alım, M. I. Sayyed, and M. Kurudirek, "Phy-X / PSD: Development of a user friendly online software for calculation of parameters relevant to radiation shielding and dosimetry," *Radiat. Phys. Chem.*, vol. 166, p. 108496, 2020. [Online]. Available: https://doi.org/10.1016/j.radphyschem.2019.108496.

[119] H. Singh, K. Singh, G. Sharma, R. Nathuram, and H. S. Sahota, "Photon Interaction Studies with Some Glasses and Building Materials," *Nucl. Sci. Eng.*, vol. 142, no. 3, pp. 342–348, 2002. [Online]. Available: https://doi.org/10.13182/NSE02-A2312.

[120] N. Karpuz, "Radiation shielding properties of glass composition," *J. Radiat. Res. Appl. Sci.*, vol. 16, p. 100689, 2023. [Online]. Available: https://doi.org/10.1016/j.jrras.2023.100689.

[121] H. Zahran et al., "Radiation attenuation properties of the quaternary semiconducting compounds Cu2CoGe[S, Se, Te]4," *Results Phys.*, vol. 37, p. 105488, 2022. [Online]. Available: https://doi.org/10.1016/j.rinp.2022.105488.

[122] N. Arpac and M. Aygun, "Determination of Radiation Shielding Parameters of CoCrFeNiTiX Alloys by Using Recently Developed Phy-X/PSD and EPIXS Softwares," *J. Amasya Univ. Inst. Sci. Technol.*, vol. 3, 2022. [Online]. Available: https://doi.org/10.54559/jauist.1075966.

[123] Z. Aygun and M. Aygun, "A Theoretical Study on Radiation Shielding Characteristics of Magnetic Shielding Alloys, Ni80Fe15Mo5 and Ni77Fe14Cu5Mo4, by Determining the Photon Attenuation Parameters in the Energy Range of 15keV-100GeV," *Karaelmas Fen ve Mühendislik Dergisi*, vol. 11, no. 2, pp. 165–173, 2021. [Online]. Available: https://doi.org/10.7212/karaelmasfen.900452.

[124] E. S. A. Waly, G. S. Al-Qous, and M. A. Bourham, "Shielding properties of glasses with different heavy elements additives for radiation shielding in the energy range 15–300 keV," *Radiat. Phys. Chem.*, vol. 150, pp. 120–124, 2018. [Online]. Available: https://doi.org/10.1016/j.radphyschem.2018.04.029.

[125] A. Mosleh, A. Abdelghany, H. Diab, and F. Ezz-Eldin, “Inspection of Radiation Shielding Proficiency and Effect of Gamma-Ray on ESR, Thermal, and FTIR Properties of Modified Borate Bioglasses by CuO,” *Preprint*. [Online]. Available: https://doi.org/10.21203/rs.3.rs-1279683/v1.

PUBLICATIONS FROM THE THESIS

Conference Papers

1. A. Kutuk and O. Gunay, "Half-Value Layer and Tenth-Value Layer Parameters of Lithium Barium Borophosphate Glass Samples Doped with Dy3+ Ions," presented at the 6th International Conference on Natural and Applied Science and Engineering (ICNASEN-2024), Online, Turkey, May 24-26, 2024.

2. A. Kutuk, F. E. Onat, and O. Gunay, "Linear Attenuation Coefficient and Mass Attenuation Coefficient Parameters of Lithium Barium Borophosphate Glass Samples Doped with Dy3+ Ions," presented at the 7th International Conference on Sustainable Sciences and Technology (ICSuSaT-2024), İstanbul, Turkey, July 12-14, 2024.